Aerodynamic Design Integration of Strut Braced Wings

MSc Thesis Aerospace Engineering

Pranav Zinjarde

Delft University of Technology

TU Delft

Aerodynamic Design Integration of Strut Braced Wings

MSc Thesis Aerospace Engineering

by

Pranav Zinjarde

to obtain the degree of Master of Science
at the Delft University of Technology,
to be defended publicly on Friday September 29, 2023 at 09:30 AM.

Student number:	5542596	
Project duration:	December, 2022 – September, 2023	
Thesis committee:	Dr. ir. G. la Rocca	TU Delft, Chair
	Dr. ir. M.F.M (Maurice) Hoogreef	TU Delft, Supervisor
	Dr. ir. D.M.J (Daniël) Peeters	TU Delft, Examiner

TU Delft

Preface

It is an overwhelming feeling to see this thesis write the final chapter of my master's journey at TU Delft. The past two years have been intense with many ups and downs, but an exponential growth. Looking back, I'm filled with pride at how far TU Delft has propelled me, both in terms of personal development and academic achievement. My gratitude toward this institution knows no bounds.

I would like to express my immense gratitude to my supervisor, Dr.ir. M.F.M. (Maurice) Hoogreef, whose guidance has played a phenomenal role in my learning curve during my thesis. He has been an excellent mentor and I am genuinely thankful for his unwavering support and understanding during the most challenging moments. I would also like to thank my committee members, Dr.ir. G. la Roccaa and Dr.ir. D.M.J (Daniel) Peeters for investing their time and expertise in evaluating my thesis.

It would have been impossible to complete my thesis on time without the continuous intellectual and mental support from my dear friends and colleagues in my thesis room, NB 1.09. I extend a special thanks to Egon Beyne and Lukas Müller, whose insights significantly contributed to the quality of my thesis.

Above all, my deepest appreciation goes to my family, the unwavering pillars of strength and motivation throughout my master's journey. Lastly, but certainly not least, I want to express my gratitude to Isha and my close friends, who have consistently believed in me and stood by me during the most challenging times.

आचार्यात् पादमादत्ते पादम् शिष्यः स्वमेधया।
कालेन पादमादत्ते पादम् सब्रह्मचारिभिः।।

Pranav Zinjarde
Delft, September 2023

Summary

Due to the high aspect ratio and low induced drag of aircraft with strut-braced wings, they are being extensively studied due to their fuel-saving potential. This thesis aims to expand the fundamental knowledge in the design of aircraft with Strut Braced Wings (SBW) by achieving the following objectives.

The objectives of this thesis are twofold, with their primary focus on evaluating the effect of changing the typical design variables for an SBW, such as the wing span, root chord, spanwise strut attachment location, wing taper ratio, wing sweep and engine location on the aerodynamics, weights and performance of an SBW. The first objective was to evaluate the significance of including the propeller slipstream effects in the preliminary stage design optimisation of a low-speed, short-range SBW. This aligned with the hypothesis that the performance of an SBW could be enhanced by using swirl recovery. The second objective of this thesis was to investigate the sensitivity of various design variables to the aircraft's fuel burn and other performance metrics at the optimum SBW design.

A Design of Experiments (DOE) approach was used to explore the design space involving the typical influential SBW design parameters. The geometry and mesh files were created using OpenVSP for every DOE point. This was followed by the aerodynamic analysis in a panel method-based software called Flightstream, which could capture the relevant aerodynamic flow phenomena with reasonable accuracy. The aerodynamic analysis was performed twice- first without considering slipstream effects and second by simulating them. Regression-based analytical equations, particularly designed for the weight estimation of the wing and strut, were used from the literature. Empirical equations from FLOPS were used for the rest of the aircraft components. The performance of the SBW was calculated iteratively using the Breguet range equation along with a few modifications. All the SBW designs were constrained by a maximum wing loading criterion.

From two sets of the DOE results (with and without propeller effects), it was observed that the two optimum SBW designs were identical in terms of external geometry and performance. A deeper investigation revealed that the variation in the spanwise engine positioning (to maximise the swirl recovery) resulted in a marginal change of the induced drag (less than two drag counts). It was concluded that the propeller slipstream effects could be excluded from the preliminary stage, design optimisation of a propeller-powered, short-range SBW to reduce computational expense. However, the results should be treated with a pinch of salt due to the limitations of panel methods. Moreover, the SBW was optimised only for cruise, not for other flight phases such as take-off and climb, which may benefit from swirl recovery.

Finally, a sensitivity analysis was performed to evaluate the trends in the performance metrics, such as fuel burn, lift-to-drag ratio, wing loading and maximum take-off weight when subjected to variations in the design variables at the optimum. The impact of the fuel burn was quantified, while the other performance metrics were qualitatively answered. The research findings revealed that certain design variables had a greater influence on fuel burn than others when varied by $\pm$10% w.r.t their optimum value. The wing root chord had the highest sensitivity with an impact of 11.6% of total mission fuel mass, followed by the normalised strut location and wing span with less than 2.3% impact. The wing thickness to chord ratio, taper ratio, sweep, spanwise engine location and strut chord had the least impact on fuel burn of less than 1%. Subsequent SBW designs can leverage these findings when making modifications after the preliminary design phases. Evaluating the impact of design variables on fuel burn allows for informed decisions on whether optimisation should be reconsidered for the modified SBW design. However, it must be noted that the sensitivity study may not be generalised, and the impact on fuel burn can vary depending on the optimum configuration.

Contents

List of Figures

List of Tables

Nomenclature

Abbreviations

Abbreviation	Definition
AOA	Angle Of Attack
AOI	Angle Of Incidence
ALBATROS	Aile Laminaire hauBAnée à Traînée Réduite par Optimisation multidiSciplinaire
ALD	Actual Lift Distribution
AGILE	Aircraft Generation multi-disciplinary optimisation for Innovative collaboration of heterogeneous teams of Experts
AR	Aspect Ratio (of wing)
CFRP	Carbon Fibre Reinforced Plastic
CFD	Computational Fluid Dynamics
CROR	Counter Rotatory Open Rotor
DOC	Direct Operating Costs
DOE	Design Of Experiments
DOE	Design Of Experiments
ELD	Elliptical Lift Distribution
FrEAC's	Future Enhanced Aircraft Configurations
ICAO	International Civil Aviation Organization
MDO	Multi-Disciplinary Optimisation
MRB	Modified RHEA Baseline
MTOW	Maximum Take Off Weight
MTOM	Maximum Take Off Mass
NLF	Natural Laminar Flow
OEW	Operating Empty Weight
OEI	One Engine Inoperative
RANS	Reynold's Averaged Navier Stokes
RHEA	Robust-and sustainable-by-design ultra-high aspect ratio wing and Airframe
SBW	Strut Braced Wing aircraft
SFC	Specific Fuel Consumption
SR	Short
SR	Short Range
SUGAR	Subsonic Ultra Green Aircraft Research
TLAR	Top Level Aircraft Requirements
TOM	Take Off Mass
TOGW	Take Off Gross Weight
USW	Unswept
WER	Weight Estimation Relationships

Symbols

Symbol	Definition	Unit
α	Angle of attack	deg
η_{engine}	Normalized spanwise location of engine attachment location w.r.t wing	-
η_{fold}	Normalised location of wing folding mechanism w.r.t wing span	-
η_{strut}	Normalized spanwise location of strut attachment location w.r.t wing	-
η_j	Propulsive efficiency	-
b	Wing span	m
C_{Di}	Induced Drag coefficient	-
C_{Do}	Frictional Drag coefficient	-
C_D	Total drag coefficient	-
C_L	Total lift coefficient	-
$C_{l,\alpha}$	Sectional lift coefficient slope	$m^{-1}deg^{-1}$
C_l	Sectional lift coefficient	m^{-1}
C	Chord length	m
C_s/C_w	Ratio of strut chord to wing chord	-
C_{MAC}	Mean Aerodynamic Chord	m
$C_{T,fs}$	Thrust coefficient Flightstream	m
D	Drag force	N
D_p	Diameter of propeller	m
f	Fuel mass fraction	-
γ	Local change in angle of attack due to swirl	deg
J	Advance ratio	-
k_e	Engine relief factor	-
l_r	Lift per unit span at wing root	N/m
l	Tail moment arm	m
L	Lift force	N
L_{des}	Lift at design point	N
L_{ht}	Lift produced by horizontal tail	N
M_{covers}	Mass of the covers	kg
M_{fold}	Mass of the folding mechanism	kg
$M_{spars,ribs}$	Structural weight of the aircraft	kg
N	Rotational speed of propeller	RPM
N_z	Load factor	-
$\frac{P}{W}$	Power to weight ratio	W/kg
ρ	Density of air	kg/m^3
R	Range	m
S	Area	m^2
S_{ref}	Wing reference area	m^2
t/c	Thickness to chord ratio	-
T	Thrust	N
V	Cruise speed	m/s
V'	Speed of air downstream of propeller	rad/s
V_T	Tail volume coefficient	-
W	Swirl velocity in slipstream	m/s
W	Wing loading (MTOW/S_{ref})	kg/m^2
W_{des}	Weight of the aircraft at design point	N
W_{des}	Weight of the aircraft at design point	N
W_{engine}	Mass of the engines	N
W_{fuel}	Mission fuel mass	N
W_{fuel}	Mission fuel mass	N

$W_{payload}$	Payload weight of the aircraft	N
ω	Rotational speed of propeller	rad/s
y	Spanwise position	m

1

Introduction

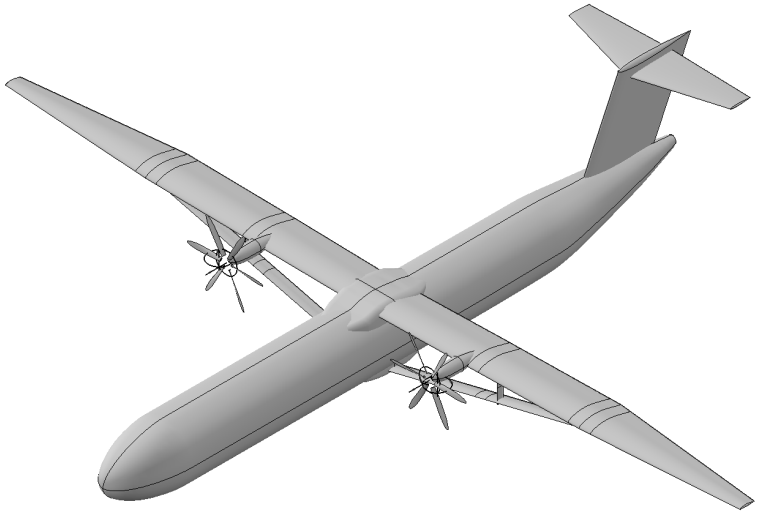

Figure 1.1: Typical design of an SBW

In an attempt to meet the ICAO climate-neutral aviation goals by 2050, unconventional aircraft designs such as the flying-V, blended wing body aircraft, SBW, Prandtl Box wing concept and twin-fuselage aircraft may stand out over the conventional tube and wing configuration[1]. This study focuses on the design of an SBW. An SBW is typically designed with high aspect ratio wings that benefit from a lower induced drag. However, this results in a significant increase in the bending moment at the root. Consequently, it results in a heavier wing structure that can negate the fuel-saving benefits. Thus, a structural supporting member (strut) connecting the wing and the fuselage is used. In some designs, an additional structural member called a jury is present between the strut and the wing. This jury is incorporated to increase the strut's buckling resistance during negative 'g' loads like landing. The strut and the jury are illustrated in Figure 1.2.

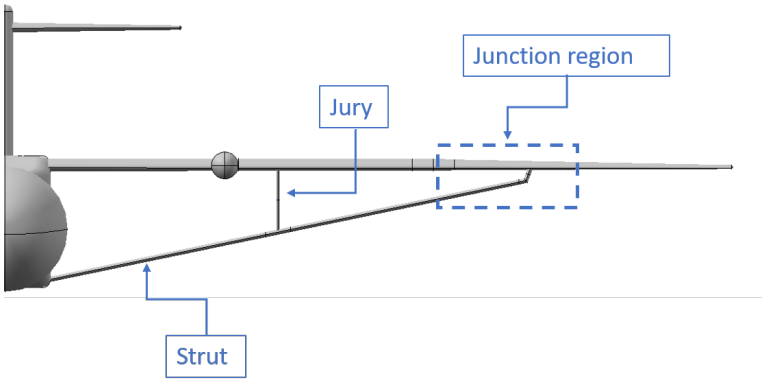

Figure 1.2: Schematic of an SBW

However, the additional strut comes at the price of an increased frictional and interference drag. Moreover, wave drag and shock-induced flow separation in the junction region that is formed between the wing and strut can further deteriorate the performance of an SBW[2], typically at higher Mach numbers as illustrated in Figure 1.3. Thus, an SBW must be carefully designed to ensure that the overall performance is not compromised due to the abovementioned effects. The fuel-saving potential of an SBW has been confirmed by multiple research projects[1], [3]–[5].

In this chapter, section 1.1 provides an overview of the state of the art in the design of an SBW. Based on the literature, the research gaps are identified in section 1.2. The corresponding research questions are framed in section 1.3 and the significance of the research outcome is explained in section 1.4

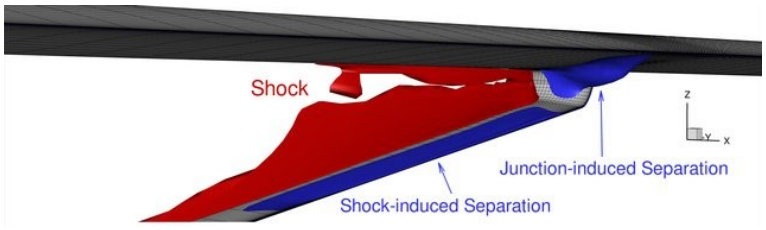

Figure 1.3: Shock waves and shock-induced separation in the junction region[2]

1.1. Previous work

Owing to the fuel-saving potential of an SBW, it has gained prominence, driving substantial research into SBW design over the past couple of decades. Exhaustive research on the SBW has been done under the SUGAR project[6]–[12]. Additionally, a notable contribution to SBW research has been made by projects like FrEACs[1], ALBATROS[3], AGILE[4] and RHEA[5]. Multiple individual research works have investigated the detailed design aspects of SBWs.

1.1.1. Conceptual design of an SBW

In the conceptual design stage, Natural Laminar Flow (NLF) on the wings was believed to further lower the fuel consumption due to the reduced frictional drag[1], [3], [4], [6], [13]. The use of NLF, however, can have several limitations due to practical reasons like vibrations, insects/dust sticking to the wings, propeller slipstream (if present), etc., let alone the relatively higher Mach regimes (approximately 0.7) as assumed in the projects mentioned above. Moreover, a few also investigated using an unducted fan in a counter-rotating architecture for the engines, as seen in Figure 1.4. Using Counter Rotatory Open Rotor (CROR), engines resulted in additional fuel savings [7] primarily due to the higher bypass ratio of the engines. Due to this reason, CROR engines were also assumed by Moerland, Pfeiffer, Böhnke, *et al.* [1]. However, CRORs are infamous for their higher noise levels and complexity. This can create problems with airport noise regulations and maintenance-related costs, respectively. Engines mounted at the rear of the fuselage Figure 1.4b were preferred in a few designs in an attempt to preserve the

Natural Laminar Flow (NLF) over the wings[1][3][13]. However, the aft shifting of the Center of Gravity (CG) due to the rear fuselage-mounted engines results in a shorter tail arm. The tail size has to increase to maintain the required tail volume coefficient, resulting in added weight and skin friction drag. Due to the higher efficiency of propellers at lower speeds, a turboprop engine was considered by RHEA[5]. Given the complexity, weight and noise issues of a CROR engine, they were not considered as a possible alternative. In the case of rear fuselage-mounted engines, the wake from the wing was expected to create a non-uniform loading on the propellers[5]. This could result in higher vibrations and fatigue-related issues, because of which RHEA decided to go with wing-mounted turboprop engines.

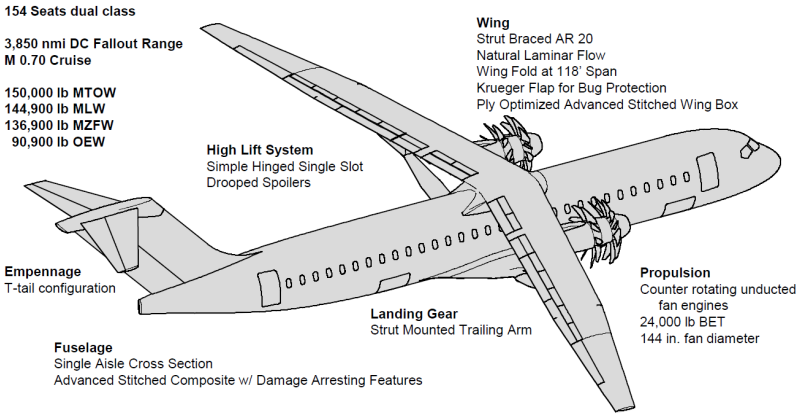

(a) SUGAR High-unducted variant [7]

(b) FrEACS SBW [1]

Figure 1.4: CROR engines used in SUGAR High and FrEACs SBW

1.1.2. Analysis tools

Pinho Chiozzotto [13] used a vortex lattice method (AVL) to perform the aerodynamic analysis for the preliminary sizing of the SBW. To capture the aeroelastic deformations of the SBW, Torrigiani, Bussemaker, Ciampa, *et al.* [4] used a flexible body analysis tool called AMLoad[14]. These panel method-based methods cannot resolve complex aerodynamic phenomena such as interference drag, compressibility effects and shock-induced flow separation, which are likely to be present in the junction region[2] (Figure 1.3), thereby overpredicting the performance of an SBW. Moerland, Pfeiffer, Böhnke, *et al.* [1] and RHEA[5] used multi-level fidelity methods for their analysis. Although the higher fidelity methods can capture the complex aerodynamic effects, the decision-making was based on lower fidelity methods, which may not always capture all the relevant effects, leaving the possibility of overlooking a few SBW designs. Bradley, Droney, and Allen [7] and Secco and Martins [2] used RANS-based CFD solvers in their SBW design process. Similarly, Liu and Yu [15] and Duggirala, Roy, and Schetz [16] also performed RANS simulations to evaluate the aerodynamic effects in the junction region of an SBW. For the weight estimation, Carrier, Atinault, Dequand, *et al.* [3] used modified empirical equations to account for the bending moment relief from the strut. However, this can reduce the fidelity of the results

due to numerous structural complications in an SBW, such as the bucking of the strut during landing and the aeroelastic effects. Bradley, Droney, and Allen [7] used a quasi-steady structural analysis tool for their weight estimation. Pinho Chiozzotto [13], Taflan, Smith, and Loughlan [17], and Locatelli, Riggins, Kapania, *et al.* [18] newly developed the physics-based analysis methods specifically for the structural sizing of an SBW.

1.1.3. Design space exploration approach

The wing span (b), Aspect Ratio (AR), sweep (Λ), taper ratio (λ), Normalized spanwise location of strut attachment location w.r.t wing (η_{strut}), number of juries, thickness to chord ratio (t/c) and strut chord to wing chord ratio (C_s/C_w) were the typical design parameters relevant for an SBW [1], [3], [7], [13]. Moerland, Pfeiffer, Böhnke, *et al.* [1] and Torrigiani, Bussemaker, Ciampa, *et al.* [4] performed a Design Of Experiments (DOE) study to evaluate the effect of these design parameters on the performance of an SBW. This was followed by creating a surrogate model using the DOE results to run optimisations/sensitivity studies. Bradley, Droney, and Allen [7] performed a full (Multi-Disciplinary Optimisation) MDO in which they considered the abovementioned typical design variables. Carrier, Atinault, Dequand, *et al.* [3] used a one-shot initial sizing model for their design, whereas Pinho Chiozzotto [13] used a simple optimisation algorithm to perform the initial sizing of the SBW. Ma, Karpuk, and Elham [5] used SUAVE for the initial sizing of their SBW.

1.1.4. Results from previous SBW designs

The value of the normalised strut location, η_{strut} of around 0.5-0.7 resulted in a good compromise between bending moment relief and frictional drag[1], [3], [5], [7]. Bradley, Droney, and Allen [7] analysed the effect of increasing the number of juries and concluded that a single jury in between the wing and the strut was sufficient to increase the buckling strength of the strut. Adding a second jury did not result in significant performance changes. In the junction region, flow acceleration initially resulted in shock waves and flow separation[10][2]. After performing an aerodynamic twist optimisation, it was observed that the optimiser provided a negative twist to invert the suction peaks. This resulted in a negatively lifting strut[10][2] as seen in Figure 1.5.

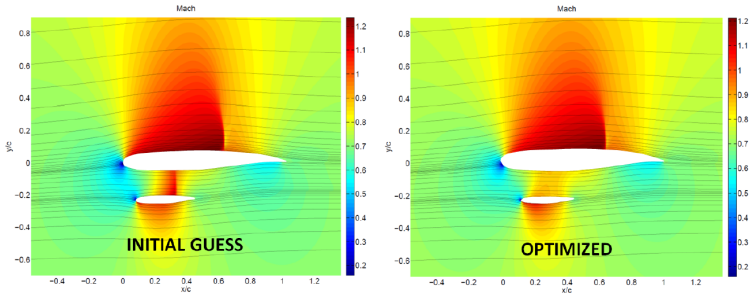

Figure 1.5: Inverted suction peaks on the strut to reduce flow acceleration in the junction region[10]

On the contrary, the strut twist angle increased for the regions close to the wing as seen in Figure 1.6. This was done to reduce the flow acceleration caused by the air's converging passage between the wing and the strut due to the rotation of the strut chord.

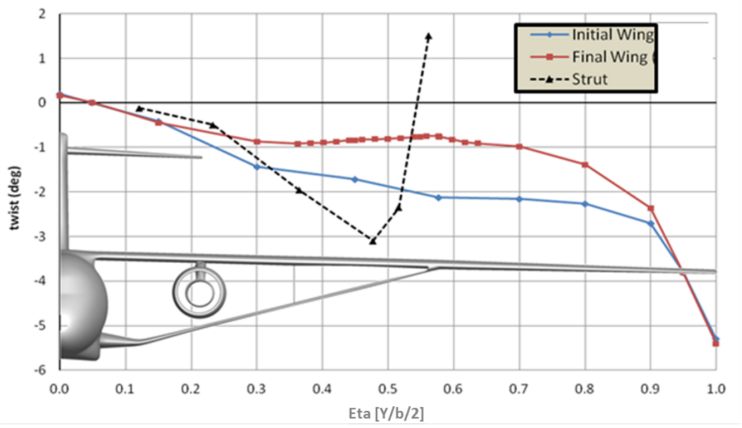

Figure 1.6: Twist distribution of SUGAR High[10]

Moreover, Droney, Sclafani, Harrison, *et al.* [10] also performed a study to investigate the effect of using a lifting strut. It was concluded that the induced drag of the aircraft did not change as long as the combined (wing and strut) lift distribution was elliptical. However, a lifting strut was more promising when implemented on SBWs operating at higher cruise Mach numbers (~0.8). This was due to the reduced wing's compressibility drag due to the lower aerodynamic loading. [11]. Pinho Chiozzotto [13] designed an SBW for a Boeing 737-type mission profile that featured two rear-mounted turbofan engines. An initial sensitivity study was performed to evaluate the effects of normalised strut location, wing aspect ratio, strut chord to wing chord ratio (C_s/C_w) and wing sweep. A simple optimisation algorithm was included to evaluate the final performance parameters such as Direct Operating Costs (DOC), Lift to Drag ratio (L/D), and Maximum Take Off Weight (MTOW). The results from the study are listed below.

1. Strut-Span station (η_{strut}) trade w.r.t constant aspect ratio:

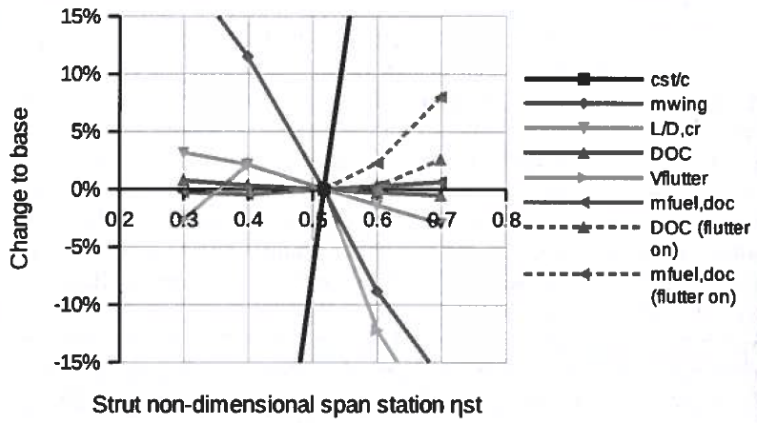

Figure 1.7: Sensitivity of η_{strut} [13]

   From Figure 1.7, it observed that increasing the value of η_{strut} resulted in a reduced weight of the aircraft since the bending moment relief of the strut was provided over a larger moment arm. Due to the longer strut, it was more prone to buckling, and as a countermeasure, the thickness of the strut relative to the wing was increased. Due to the addition of frictional drag, the overall L/D ratio decreased. As expected, the wing weight and L/D values are higher for lower η_{strut} values. From the perspective of aeroelasticity, the flutter margin was reduced since the optimised wing with a lower bending moment had a lower stiffness.
2. Aspect ratio trade w.r.t a constant η_{strut}:

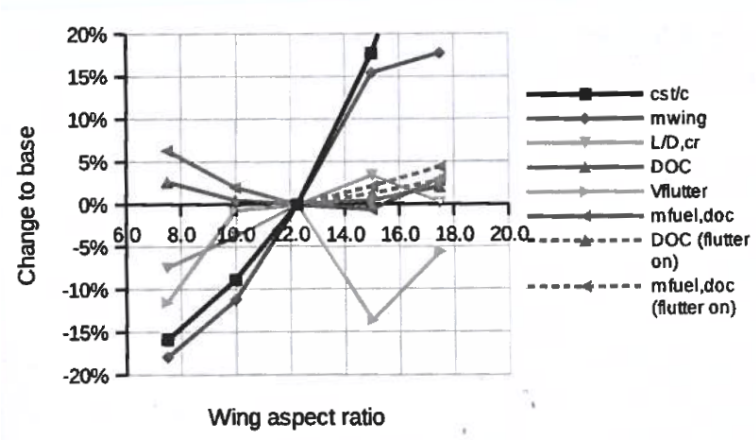

Figure 1.8: Sensitivity of aspect ratio [13]

From Figure 1.8, it was observed that increasing the aspect ratio resulted in a better L/D ratio but higher wing weight. However, the net result of these two increased DOC. For a constant value of η_{strut}, the t/c of the wing has to increase to counter the high bending loads. This higher t/c was beneficial from a flutter margin point of view due to the higher stiffness of the resulting wing.

3. Strut chord to Wing chord ratio (C_s/C_w): Increasing C_s/C_w resulted in a strut that was more resistant to buckling and could thus be slightly lighter. Over most of the range, the effect of the strut chord ratio was more or less constant. However, the strut weight exponentially increased due to the heavier internal structure needed to counter the buckling loads. This increased the DOC.
4. Wing sweep trade: For the reasonably high cruise Mach number (0.78) for an SBW, transonic drag had to be taken care of. Reducing the sweep requires a wing with lower thickness to minimise wave drag, which would otherwise be avoided with wing sweep. The wing structural weight had to increase to support the wing loading with a lower t/c. Since the optimiser would converge at the lowest DOC, the resulting design was the best combination of aerodynamics and weights. For this low value of t/c, a heavier wing was required, which was traded by the optimiser for a lower aspect ratio to ensure a lower bending moment.

The abovementioned results provided valuable insights into the sensitivity of the design variables to the DOC. However, the sensitivity of other aircraft parameters such as wing span, root chord (C_r), t/c and taper ratio was not evaluated. Although the effect of wing span, root chord and taper ratio was encompassed in aspect ratio, their independent effects were not investigated. Furthermore, AVL was used for the aerodynamic analysis, which may not accurately predict the relevant aerodynamic effects, such as compressibility drag, for an SBW designed for high subsonic speeds. This can reduce the fidelity of the results.

1.2. Research gap

Before framing the research questions, the research gap was identified and is explained below. Most of the abovementioned research was done for a B737/A320 type aircraft mission corresponding to a Mach regime of around 0.7 to 0.8 and 150 passengers. The exception was the RHEA project[5] wherein a comparison was performed between an SBW and a Twin Fuselage aircraft configuration for short, medium and long-range mission profiles. It was proved that an SBW had a superior performance for a Short Range (SR) mission, revealing its potential to be used for that mission profile. With emerging companies like Heart Aerospace planning to use an SBW and operate on battery-powered engines, the research on propeller-powered, low-speed SBW is becoming more crucial. Additionally, many more variants of existing aircraft that intend to increase the lift-to-drag ratio in the future are likely to incorporate a strut in their designs. This makes the research on short-range SBW designs significant.

The propeller slipstream effects were never included in the design of an SBW by any previous research works. Evaluating these effects might be crucial for an SBW due to potential problems like shock waves

that can be formed in the junction due to flow acceleration. On the contrary, it was hypothesised that the wing-strut-jury combination could also maximise the swirl recovery from the propeller slipstream, thereby reducing the drag. These two phenomena are illustrated in Figure 1.9. The lack of research done on this aspect creates the first research gap. The research work under the RHEA SR-SBW provided valuable insights into the design of low-speed SBW based on an ATR 72-600 type mission profile. Nonetheless, their work exhibited certain imperfections. To illustrate, their weight estimation method relied on a few assumptions related to planform, kink location, thickness to chord ratio distribution, etc., that were not completely adhered to. Moreover, the aircraft was designed using an initial sizing tool and was not fully optimised. This may result in a misprediction of the performance of an SBW. Lastly, the sensitivity of different design variables to the performance metrics, such as fuel burn, MTOW and wing loading, was unknown. The significance of knowing these design trends is explained in section 1.4. These gaps led to the formulation of the research questions in section 1.3.

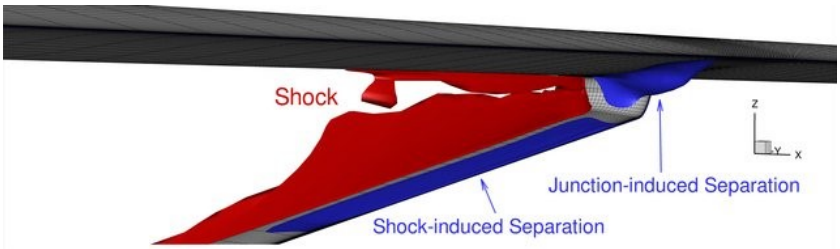

(a) Susceptibility of junction region to compressibility and interference drag[2]

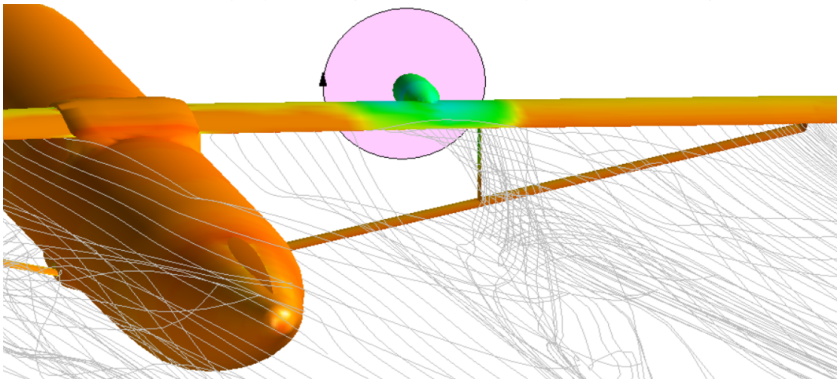

(b) Possibility of swirl recovery from the wing-strut-jury combination

Figure 1.9: Significance of considering propeller slipstream effects in an SBW

1.3. Research questions

This thesis was built up on the initial work done by RHEA[5] on the design of a low-speed, SR-SBW. Based on the research gap, the research question and sub-questions were formulated below.

What is the effect of changing the expected influential design parameters, such as wing span, wing root chord, thickness, sweep angle, taper ratio, normalised strut location and strut chord, on the performance of a short-range, propeller-powered Strut Braced Wing aircraft while considering propeller slipstream effects?

1. **To what extent are the two optimised SBW designs-one with, and the other without considering propeller slipstream effects, different from one another in terms of external design and performance?**
2. **If they are distinctly different, what design variables are crucial when designing an SBW considering slipstream effects?**
3. **To what extent is the performance of the optimised SBW better w.r.t the initially sized RHEA-SR SBW?**
4. **What is the sensitivity of different design variables to the fuel burn and other performance metrics of the optimised SBW configuration?**

1.4. Significance of research outcome

The key differences in the design of an SBW optimised with and without propeller slipstream effects would be understood, and the design variables with a higher sensitivity to slipstream effects would be known. This knowledge can be used to set up preliminary design rules for designing an SBW without considering aerodynamic slipstream effects in an optimisation.

Moreover, the possibility that the optimised SBW design could be a local optimum was indicated by Bradley, Droney, and Allen [7]. Using the outcome of this thesis, an initial guess about the optimum design configuration for a short-range, low-speed SBW design would be known with the propeller slipstream effects included. This can be used as a quick check for future SBW projects to confirm whether a converged MDO design will likely be a local or global optimum.

Finally, the outcome of the thesis would be helpful to get insights into the influence of the different design variables on the performance of short-range, low-speed SBW. These trends can be useful when the preliminary design has to be modified during the detailed design stage in some cases. For instance, this was observed in the case of SUGAR High[7] wherein an entire MDO had to be re-run after a few design parameters had to be modified in the detailed design stage. This can often be very computationally expensive, and could be beneficial if this stage can be avoided. With the insights obtained from this thesis, one can get a preliminary idea about the influence of the design variables (that have to be modified at a later stage) on the aircraft performance. Accordingly, a decision can be made if it is worth running an MDO.

In this way, the thesis outcome can be used to increase the fundamental knowledge in the design of an SBW.

1.5. Report structure

In chapter 2, a comprehensive overview of the process used to evaluate the performance of the SBW is provided. This includes the geometry modeller (section 2.2) used to generate the meshes for Flightstream aerodynamic analysis (section 2.3). Furthermore, the methods used for weight estimation of different components of the SBW are explained in section 2.4. The working of the performance model, which utilised the aerodynamic analysis and weight estimation tool outputs, is expatiated in section 2.5. section 2.6 provides the motivation and the design details about the baseline SBW model used for this thesis. Finally, the design space exploration approach details are provided in section 2.7.

The chapter 3 provides an exhaustive overview of the results and discussions. section 3.1 explains results obtained from the initial sensitivity. These results were used to decide the bounds of the DOE study. The results and explanations relevant to the research questions are provided in section 3.2 and section 3.3. The final sensitivity analysis results are explained in section 3.4. Finally, the conclusions and potential avenues for future research are explained in chapter 4.

2

Methodology

2.1. Research approach

To answer the research questions, the design space exploration was done using a DOE approach to evaluate the performance of different SBW designs. Each DOE point contained information about a unique combination of design variables. The geometry and mesh files were generated for these DOE points using OpenVSP.This mesh was used to perform the aerodynamic analysis in Flightstream. The weight estimation of the SBW design was done parallelly using empirical equations applicable to an SBW. The performance metrics such as mission fuel mass, maximum take-off weight, empty weight, lift-to-drag ratio and thrust coefficient were estimated iteratively by the Performance model using the output from the aerodynamic analysis and the weight estimation. The abovementioned process provides a simplified explanation for the overall framework of the thesis and can be seen in Figure 2.1. A Python code was implemented which could provide the data transfer and run various operations.

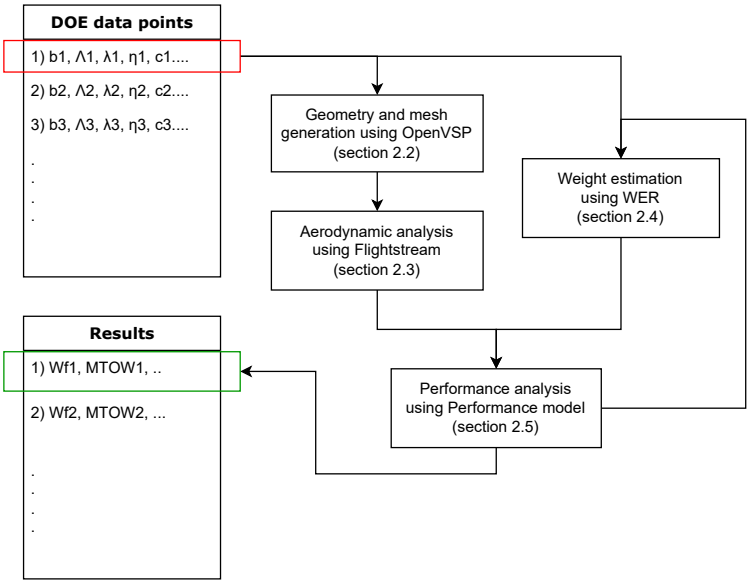

Figure 2.1: Overall framework

In the above figure, the variables bear their usual meanings as defined previously. Moreover, the above process was carried out for the propeller on and off conditions, and the results were stored separately. The iterative nature of the performance model is indicated by the second arrow in Figure 2.1, which goes from the performance analysis to the weight estimation.

2.2. Geometry modeller

This section explains the details about the functionality of OpenVSP pertinent to this thesis.

To facilitate the quick generation of different SBW designs, a scriptable parametric geometry modelling software that could generate the mesh files was required. For this purpose, OpenVSP was selected. It contains predefined components, such as the wing, fuselage and propeller, that can be modified as required.

OpenVSP can export mesh files such as Cart3D, PLOT3D and Gmsh. Moreover, additional sections with more tesselations can be added to different components for mesh refinement, as seen in Figure 2.2. By default, the software uses a structured mesh, which would also be used for the thesis.

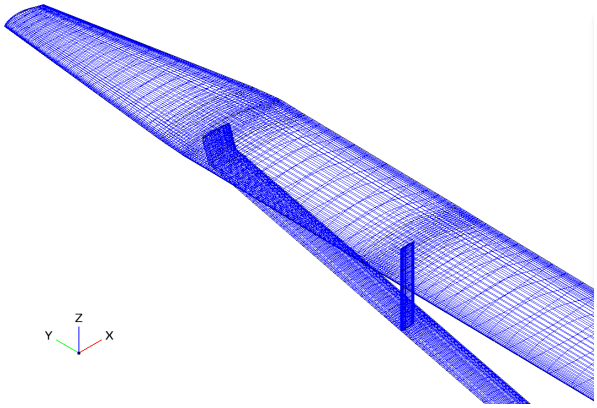

(a) Illustration of a refined mesh in OpenVSP

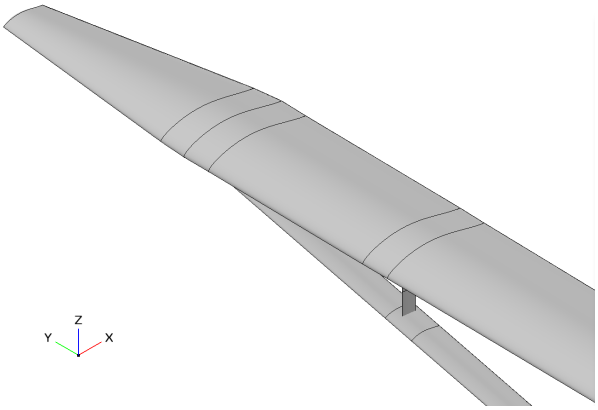

(b) Illustration of the sections added for mesh refinement

Figure 2.2: Mesh refinement using OpenVSP

Moreover, OpenVSP allows users to use a script to perform the abovementioned operations. The scripting process could be done in three ways (that were identified).

1. VSP script method: In this method, the user can write step-by-step instructions corresponding to the operations that could be done in the Graphical User Interface (GUI). These have to be written in a text file (.vspscript) in a C++ format.
2. Application Program Interface (API) method: This approach uses a Python/MATLAB wrapper to convert the commands from Python/MATLAB to C++ equivalent using the API.
3. Design variable approach: A simple text file can modify an existing baseline geometry. The design parameters that need to be modified must be initially saved in the '.des' file. For instance, these baseline values can be modified using a programming language. OpenVSP can read the file with the updated values to reflect the changes. This approach was considered the most suitable for a DOE study and was implemented.

Figure 2.3 illustrates a few SBW designs that were created using this approach

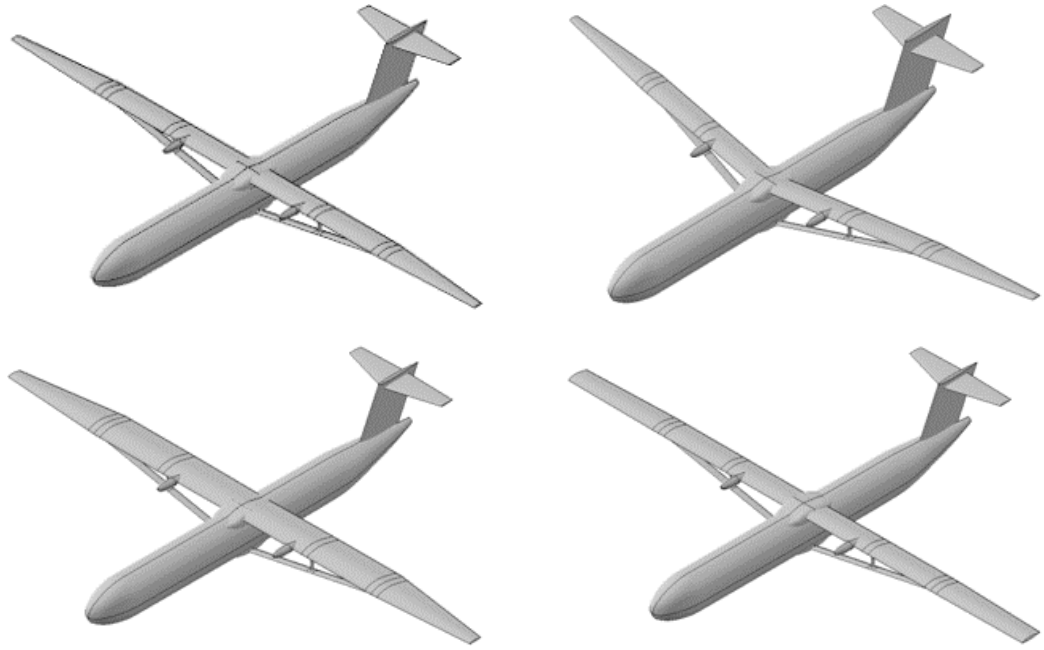

Figure 2.3: Different geometries created using OpenVSP script

The parametrization of the SBW used for this thesis is shown in Figure 2.4. The wing sweep angle is defined w.r.t the quarter chord length as seen in Figure 2.15 and is consistent with the definition in the Weight Estimating Relationships (WER) that are explained in section 2.4.

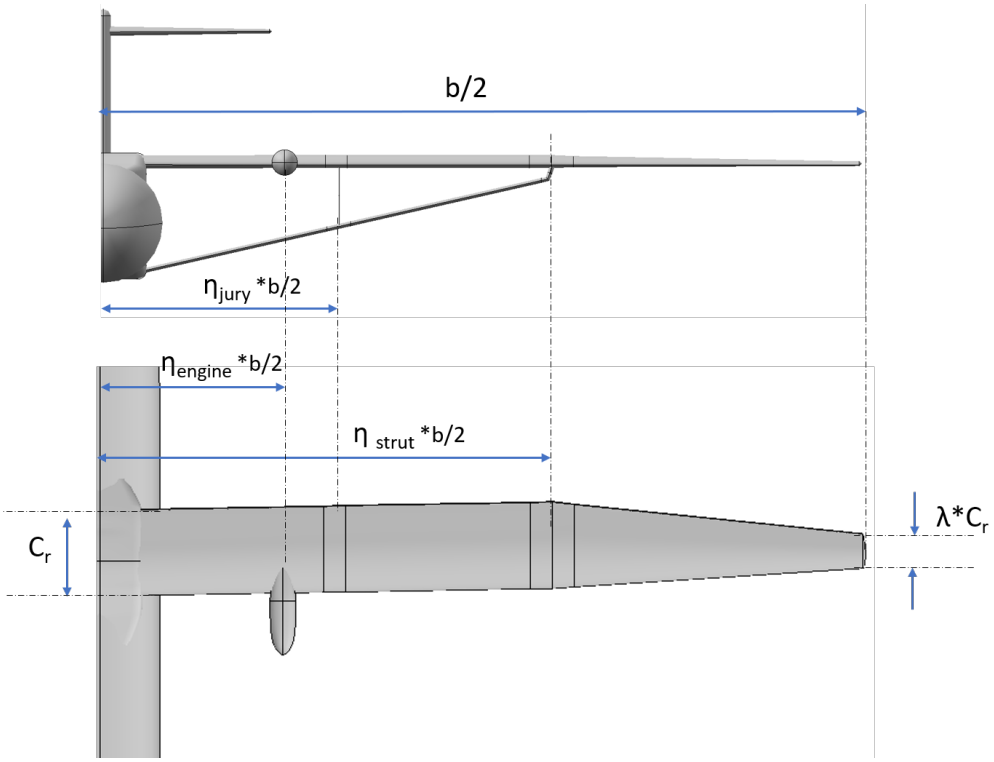

Figure 2.4: Parametrization of SBW

2.3. Aerodynamic analysis

A comparative analysis of the two analysis tools considered for this thesis is provided in subsection 2.3.1. Due to the better accuracy of Flightstrem for capturing the effects relevant to this thesis, it was finalised after running CFD validation cases provided in subsection 2.3.2. Finally, the Flightstream setup for performing the aerodynamic simulations is discussed in subsection 2.3.3.

2.3.1. Comparative study of aerodynamic analysis tools

Low to mid-fidelity software that could provide the right compromise between fidelity and computational time was required to sweep a larger design space. For this purpose, two-panel method-based aerodynamic analysis tools were considered, namely VSPAero[19] and Flightstream[20]. Reasonable accuracy in the prediction of polars and slipstream effects in complicated geometries like the SBW was expected from the aerodynamic analysis tool. Since the reference data for all these requirements together was unavailable, the validation was addressed individually and is mentioned in the subsequent subsections.

Polars

For comparing the accuracy in predicting the polars, wind tunnel reference data from Sinnige, Arnhem, Stokkermans, *et al.* [21] was used. The Model 2, with a modular cambered wing and wing-tip mounted propellers, was used to compare the polars. The measurements were taken for an advance ratio (J) of 0.7 at a freestream velocity of 40m/s. The setup used can be seen in Figure 2.5a.

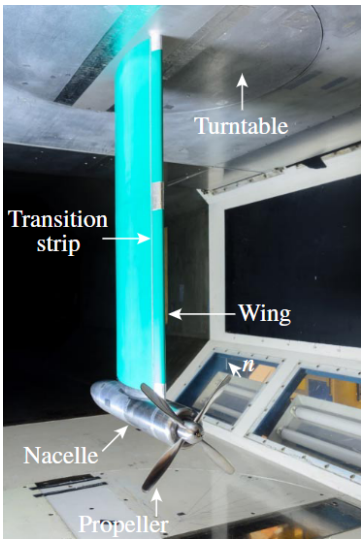

(a) Model 2- used for comparison of polars[21]

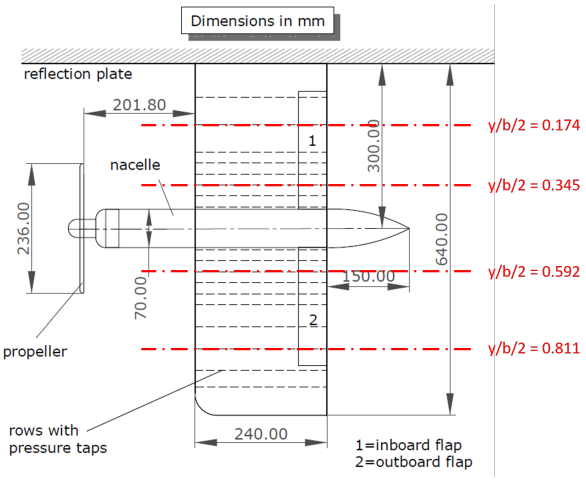

(b) PROWIM- used for comparison of lift distribution[22]. Note: figure has been modified to indicate spanwise sections

Figure 2.5: Wind tunnel models from Sinnige, Arnhem, Stokkermans, *et al.* [21] and Veldhuis [22]

A reasonably accurate prediction of the lift polars was obtained by both the software and can be seen in Figure 2.6a. Although VSPaero better predicted the slope of the lift curve, Flightstream could better capture the flow effects close to separation. The drag polars from VSPaero had better accuracy over the range of AOA, especially at higher advance ratios. However, Flightstream was slightly more accurate even at lower advance ratios as long as the Angle Of Attack (AOA) was restricted to smaller values.

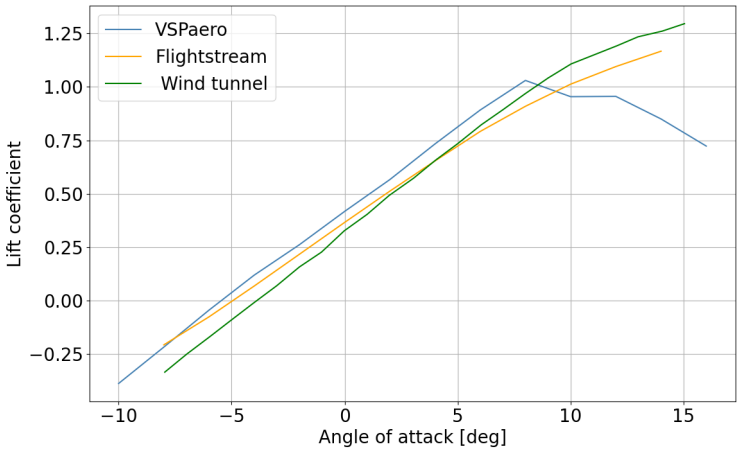

(a) Lift polar comparison

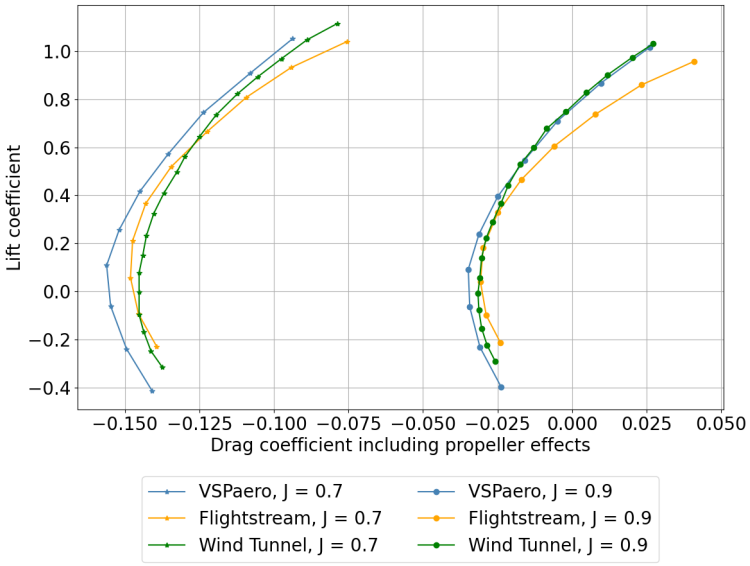

(b) Drag polar comparison

Figure 2.6: Comparison of VSPaero and Flightstream results with wind tunnel data for model 2-conventional configuration[21].

Lift distribution

Wind tunnel measurement data from Veldhuis [22] was used to compare the lift distribution. The model used here was the PROWIM, a wing with symmetric airfoils in a conventional nacelle configuration as seen in Figure 2.5b. Similar flow conditions with a freestream velocity of 40m/s and an J of 0.7, as before were used in this setup.

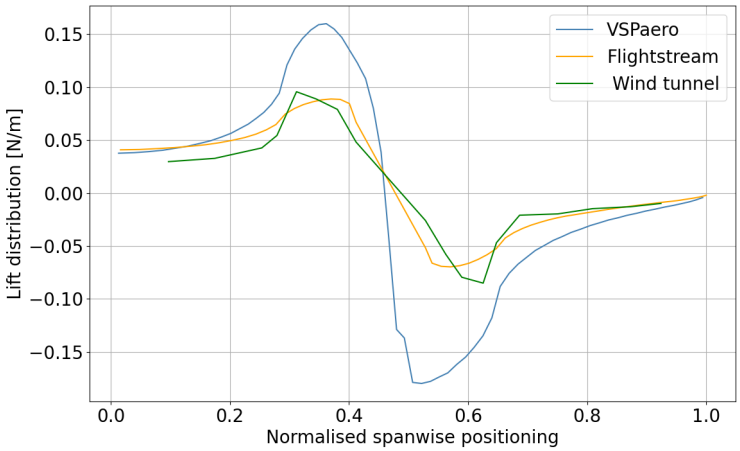

(a) Lift distribution at 0^0 AOA

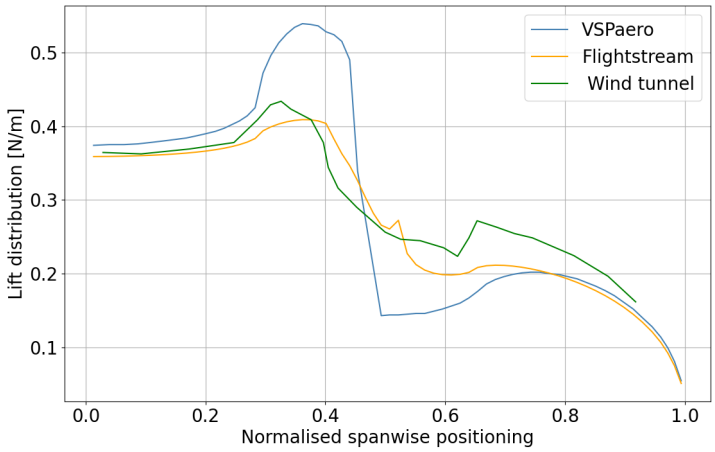

(b) Lift distribution at 4^0 AOA

Figure 2.7: Comparison of VSPaero and Flightstream results with reference[22]

The lift distribution was better predicted by Flightstream compared to VSPaero as seen in Figure 2.7a and Figure 2.7b for both the AOA. In Figure 2.7b, the error in the lift prediction was around 5% for Flightstream and 15% for VSPaero. From these results, it was understood that Flightstream had better overall predictions for polars and lift distribution than VSPaero. Hence, VSPaero was discarded, and additional simulations were run to validate Flightstream.

Pressure coefficient distribution

A comparison of the sectional pressure coefficient (C_P) prediction for different chordwise sections w.r.t wind tunnel measurements is shown in Figure 2.8. The wind tunnel data was recorded by Veldhuis [23] and was based on the same wind tunnel model (Figure 2.5b) and test conditions in [22].

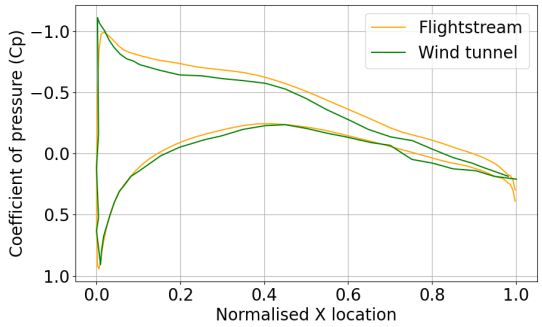

(a) y/b/2 = 0.174 (outside slipstream, near the root)

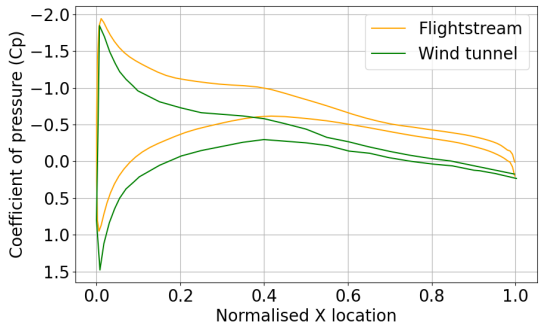

(b) y/b/2 = 0.345 (inside slipstream, near the root)

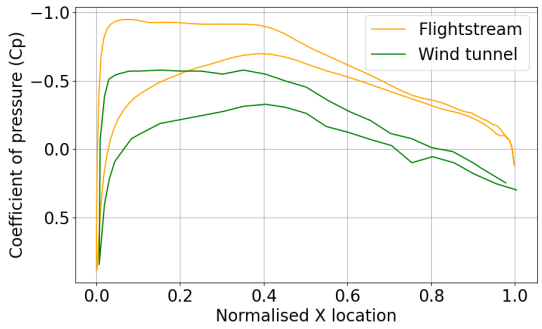

(c) y/b/2 = 0.592 (inside slipstream, near the tip)

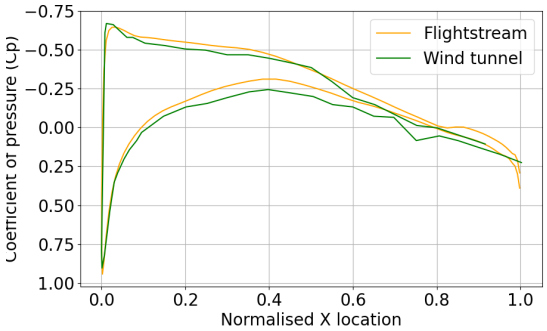

(d) y/b/2 = 0.811 (outside slipstream, near the tip)

Figure 2.8: Comparison of C_P vs. x plots between Flightstream and Wind tunnel measurement[23]

From Figure 2.8a and Figure 2.8b, it can be observed that the sectional pressure distributions are well predicted outside of the slipstream region. The slipstream region experiences an increase in the flow velocity and the addition of a swirl component to the flow. The former causes a vertical shift in the C_P vs. x plot (towards the suction side), while the latter causes a change in the local angle of attack as

seen by the downstram wing sections. On the upgoing side of the propeller, the wing experiences a local increase in the AOA, while the downgoing side reduces the local AOA on the wing. This results in a C_P vs. x distribution that is different from the one outside the slipstream region. From Figure 2.8b and Figure 2.8c, it was observed that the axial velocity increase in the slipstream is slightly overpredicted by Flightstream (as seen from the higher offset compared to wind tunnel measurements). In contrast, the local change in the AOA was well captured (as seen from the similar pressure distribution patterns).

2.3.2. CFD Validation

Since the previous validation studies were for considerably low-speed (approximately Ma 0.1) wind tunnel data and a simple wing, they were not fully representative of the actual phenomena that would be observed in the case of an SBW at higher speeds. At higher Mach numbers, panel methods can deviate from reality due to the compressibility effects. This can be crucial, particularly in the junction region where it is combined with interference drag effects. Hence, another validation study was performed using the data from Secco and Martins [2].

SBW geometry- PADRI Mach 0.7

PADRI SBW (Figure 2.9a) is a B737 or A320 type aircraft designed for a cruise speed of Mach 0.7. Secco and Martins [2] performed a RANS-based aerodynamic twist optimisation of PADRI SBW and compared the data of the optimised PADRI SBW with the unoptimised one. Since the PADRI unoptimised SBW geometry was open source, the geometry file was used to perform an analysis in Flightstream for comparison.

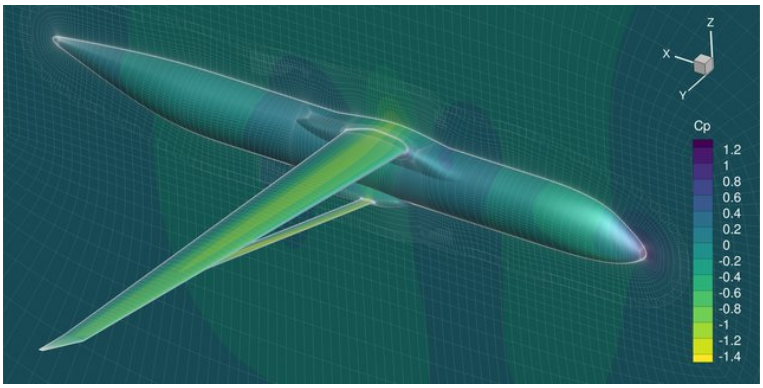

(a) PADRI SBW CFD [2]

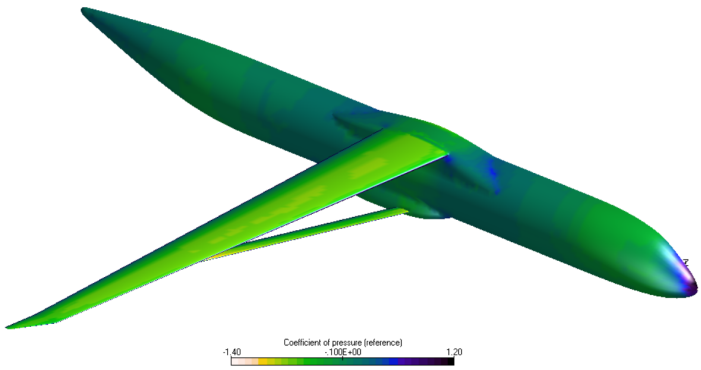

(b) PADRI SBW Flightstream

Figure 2.9: Comparison of pressure coefficients between CFD and Flightstream

From Figure 2.9, it can be seen that the overall prediction from Flightstream is reasonably good. However, the complex aerodynamics in the junction region were not accurately captured by Flightstream.

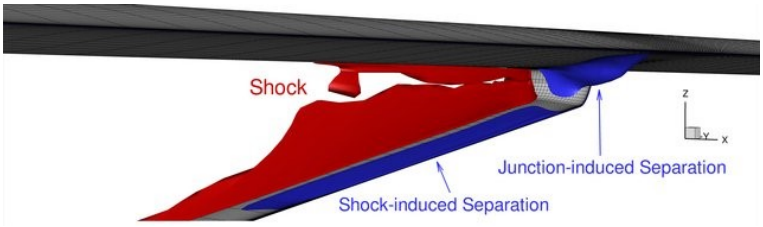

(a) Shock waves and flow separation- CFD prediction[2]

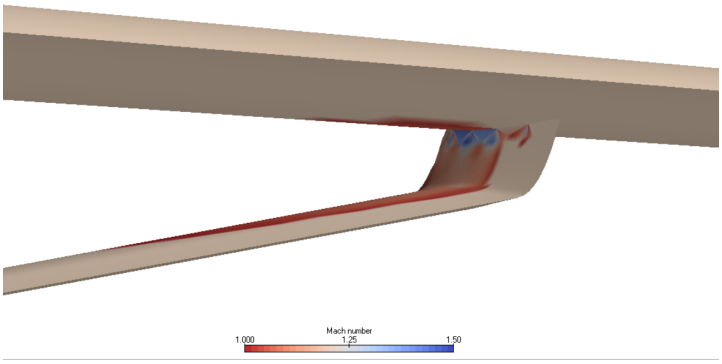

(b) Supersonic flow- Flightstream prediction

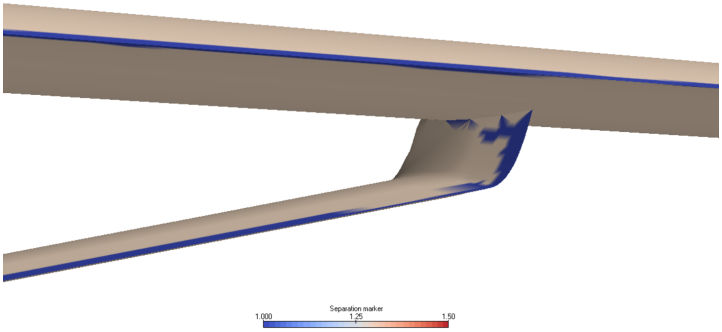

(c) Flow separation- Flightstream prediction

Figure 2.10: Comparison of aerodynamic effects in PADRI junction region as predicted by CFD and Flightstream

From Figure 2.10b and Figure 2.10a, it was observed that the presence of sonic flow due to the flow acceleration in the junction region was reasonably well captured on the upper surface of the strut and the lower surface of the wing. However, the shock-induced flow separation regions (marked in blue) in Figure 2.10c could not be well predicted compared to Figure 2.10a due to the limitations of panel methods. This resulted in an increased lift prediction and the induced drag, which offset the drag rise due to shock waves and separation. Due to this reason, there was a 9% over-prediction in the lift coefficient and a 7% over-prediction in the drag coefficient.

SBW geometry- PADRI Mach 0.42

Since the abovementioned phenomena are not expected to be present in the case of an ATR 72 type, low-speed (Ma 0.42) aircraft, a CFD simulation was performed for the same aircraft using ANSYS Fluent. The entire procedure, including the set-up and running of the CFD simulation, was performed by a colleague working on a similar research topic on SBW. The work could not be cited since the research was not yet published, but the author gives full credit for the work. The meshing was done locally in Fluent, which had around 28 million cells and a y+ value between 30-50 for the wing and strut (Figure A.8). Since the the prediction of the complex boundary layer phenomena, such as boundary layer transition was not of interest here, it was decided to proceed with this relatively coarse mesh. The convergence tolerance for the residuals was 1e-3, which was slightly higher but resulted in a reasonably accurate prediction of lift and drag coefficients with errors less than 1%. The turbulence model used

was Spalart-Allmaras. Before performing a simulation for Mach 0.42, a simulation for Mach 0.7 was performed to verify the CFD setup, and the results were compared with PADRI[2].

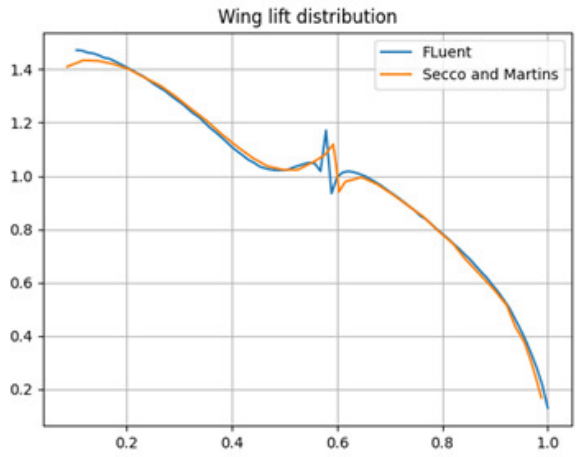

Figure 2.11: Comparison of lift distribution plot between Secco and Martins [2] and Fluent

From Figure 2.11, a good accordance between the lift distribution plots was observed. The spikes in the lift distribution correspond to the location of the strut attachment point where the lift changes suddenly due to the flow acceleration in the junction. However, the lift and drag coefficient error was less than 1%, even with the relatively coarse mesh. The same setup as above was replicated for a lower Mach number of 0.42 to resemble the behaviour of an ATR-72-type SBW aircraft. The resulting lift distribution is plotted in Figure 2.12.

(a) Wing lift distribution comparison

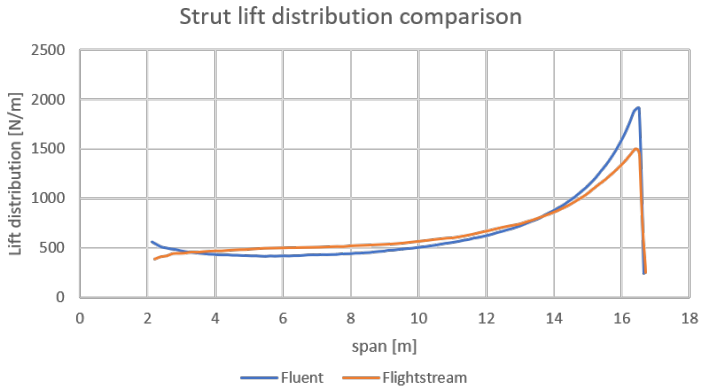

(b) Strut lift distribution comparison

Figure 2.12: Comparison of results from Fluent and Flightstream for Mach 0.42

From Figure 2.12a, an unusual drop in the lift prediction from Fluent was observed at the wing-strut junction. Although a slight wing lift reduction is expected in the junction region due to the flow acceleration on the wing's lower surface, the lift reduction's magnitude was unreasonably high. This lift deficit extended until the wing root, which was also not expected. This unexpected drop was not observed in the case of Flightstream, and hence, the lift prediction of the wing-strut combined was lower by 10%. The primary reason behind this behaviour was unknown, and the difference in lift prediction is not indicative of the accuracy of Flightstream. However, the lift distribution over the strut as predicted by Flightstream, was very close to that of Fluent (Figure 2.12b). The overall difference in the drag coefficient was less than 2.5%. However, this value cannot be trusted due to the possible error in the CFD simulation. Nevertheless, it was decided to go ahead with Flightstream for the aerodynamic analysis.

2.3.3. Flightstream set up

Flightstream is a surface vorticity-based inviscid flow solver that can predict viscous effects using viscous coupling and flow separation models[24]. The propeller slipstream effects can either be modelled by an actuator disc or by performing an unsteady simulation of the propeller geometry. It can also account for compressibility effects using corrections. The computational time can be reduced to less than half by using X-Z symmetry.

Parameter	Setting	Effect
X-Z symmetry	Enable	Reduced computational time. Propeller slipstream effects restricted to counter-rotating engines
Viscous boundary layer type	Turbulent	Forces flow to be turbulent since capturing effects of NLF was not intended
Viscous coupling	Enable	Non-linear viscous effects are captured as long as flow is attached
Flow separation	Enable	For modelling flows with separation using Stratford's criterion to identify separated regions and semi-empirical model for post-separation pressure values
Flow separation model	Axial	Used for standard airplane and marine applications
Compressible flow	Enable	Use corrections to account for compressibility effects
Convergence tolerance	1e-4	Get a good compromise between simulation time and accuracy. Error in drag prediction by an order of 1 count was considered acceptable

Table 2.1: Flightstream settings used based on guidelines[25]

As mentioned in section 1.1, preserving NLF over the wings can be challenging, because of which a turbulent boundary layer was simulated in this thesis. Due to the higher skin friction drag of a turbulent boundary layer compared to a laminar one, the results are expected to be conservative. The propeller slipstream effects were simulated using an actuator disc instead of an unsteady simulation to lower the computational time. The actuator disc was assumed to have an inboard-up rotation sense. Finally, the cruise speed and atmospheric conditions were used from the Top Level Aircraft Requirements (TLARs) of RHEA as seen in Figure A.12. Table 2.1 explains the Flightstream set up with

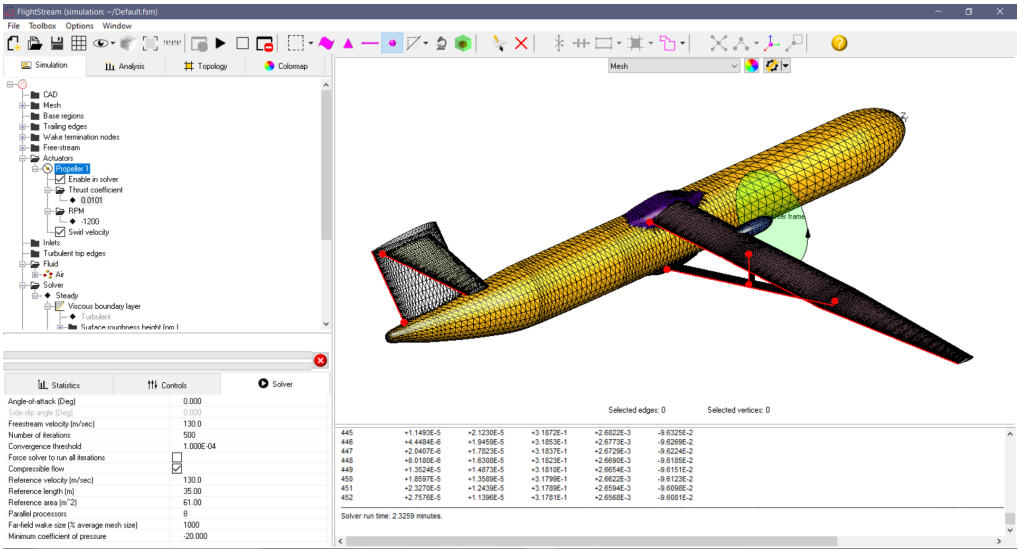

(a) Mesh set up in Flightstream

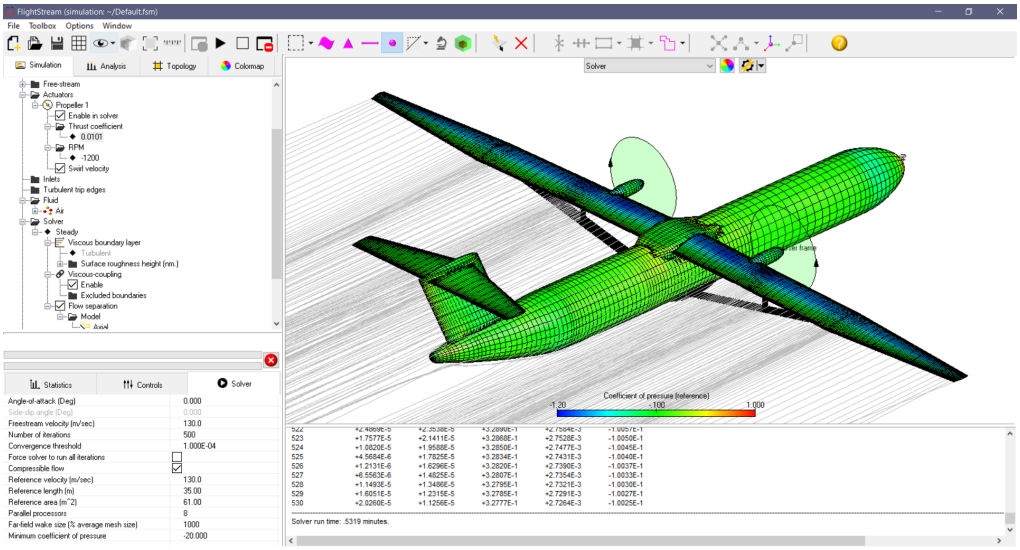

(b) Solver set up in Flightstream

Figure 2.13: Flightstream set up

Meshing

A PLOT3D format mesh file was exported from OpenVSP (section 2.2) for analysis in Flightstream. Moreover, a mesh sensitivity study was performed to determine the appropriate mesh size for the wing. The chordwise tesselations were increased to study the effect on the aerodynamic coefficients for a reasonable spanwise distribution of the panels. The appropriate mesh size was identified when the relative error between the two was less than 2%. After determining the chordwise tesselations, a similar study was performed for the spanwise direction. The above process was repeated for the horizontal tail. The details can be found in section A.1.

Additionally, mesh refinement was provided to the wing-strut, wing-jury and strut-jury junction regions to achieve better meshing at the intersections as seen in Figure 2.14a. This was primarily done to avoid solver divergence issues due to incorrect mesh at the junctions and to minimise the numerical error. Moreover, a generic wing-body and strut-body fairing was created in OpenVSP and can be seen in Figure 2.14b.

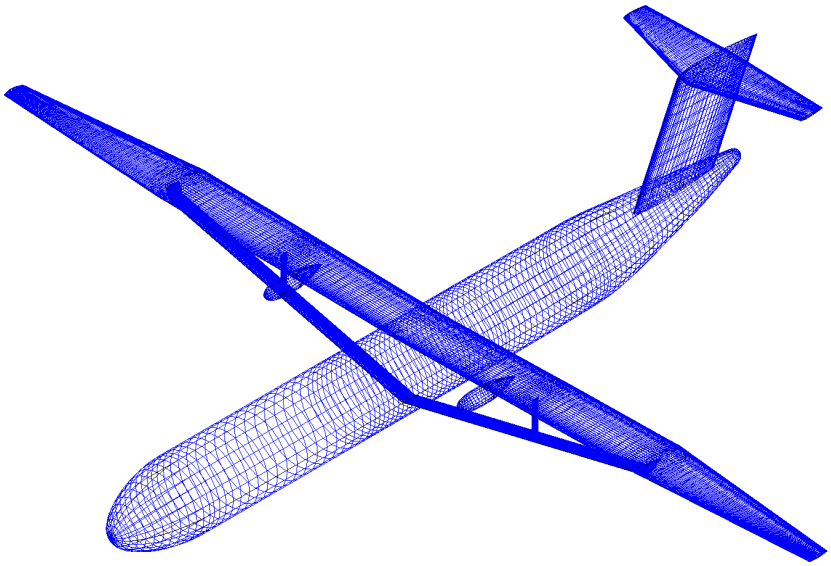

(a) An instance of the mesh used for analysis in Flightstream

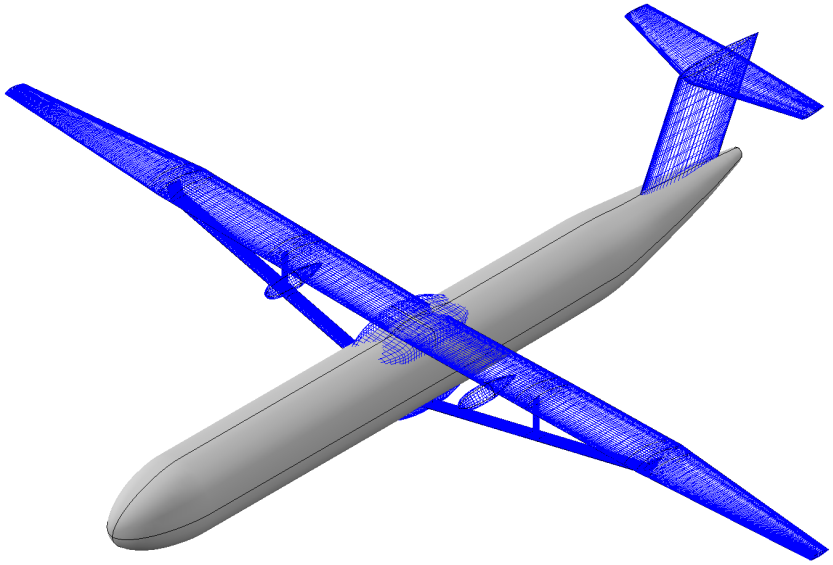

(b) Mesh with wing body and strut body fairing

Figure 2.14: Mesh files from OpenVSP

2.4. Weight estimation

In this section, the details about the weight estimation methods used for the different aircraft components are provided. The weight estimation of the wing and strut was done using regression-based, analytical equations (subsection 2.4.2) that were developed using a physics-based method explained in subsection 2.4.1.

Due to the absence of any existing unconventional aircraft configurations like the SBW, empirical methods that largely rely on statistical aircraft data are not fully accurate[17]. Although a few of them, such as Torenbeek[26] and FLOPS[27] use correction factors to account for the strut, they have their own limitations. For instance, a 'bending moment relief factor' can be provided in FLOPS; however, this does not directly scale with η_{strut}. The correlation between the two may not be known beforehand, limiting the tool's straightforward implementation.

For this reason, multiple physics-based methods have been developed[13], [17], [18]. Pinho Chiozzotto [13] went a bit further and developed Weight Estimating Relationships (WER), which were simple analytical regression-based equations to predict the weight of the wing and strut. After defining the design variables and their ranges, Pinho Chiozzotto [13] performed a DOE sampling to fill the design space with different SBW configurations. The physics-based analysis method was run for these DOE points, and a linear regression analysis was used to develop the WER.

2.4.1. Overview of physics-based method

The physics-based method aimed to develop a Level 1 method for wing weight estimation considering the static aeroelastic effects. Moreover, the method was designed to apply to unconventional aircraft configurations like the SBW. The physics-based method used a simplified aeroelasticity model, which considered static aeroelastic effects such as deviations in load distributions and lift cure slope, aileron efficiency and static divergence. The wing and the strut were sized for thirteen load cases, such as low-speed and high-speed manoeuvre, positive gust, negative gust, landing loads, etc. Although the physics-based method featured considerable flexibility in the choice of the lift distribution, materials, engine location, sweep angle, planform of the wing and strut, etc., they were based on a few assumptions listed below.

Assumptions of the physics-based method

1. The planform of the SBW was assumed to be a semi-tapered one with the kink location being at the η_{strut} position as seen in Figure 2.15
2. The planform of the strut was assumed to be rectangular with the chord length defined w.r.t that of the wing (C_s/C_w).
3. The front and rear spars of the wing were assumed to pass through 12% and 60% of the chord length, respectively for the untapered section. For the tip section, the front spar was assumed to pass through 28% of the chord length as seen in Figure 2.15. The load reference axis passed through the centerline of the wing box.
4. The jury's- chord, airfoil t/c, wing box dimensions, and thickness of the covers and webs were half as that of the strut.

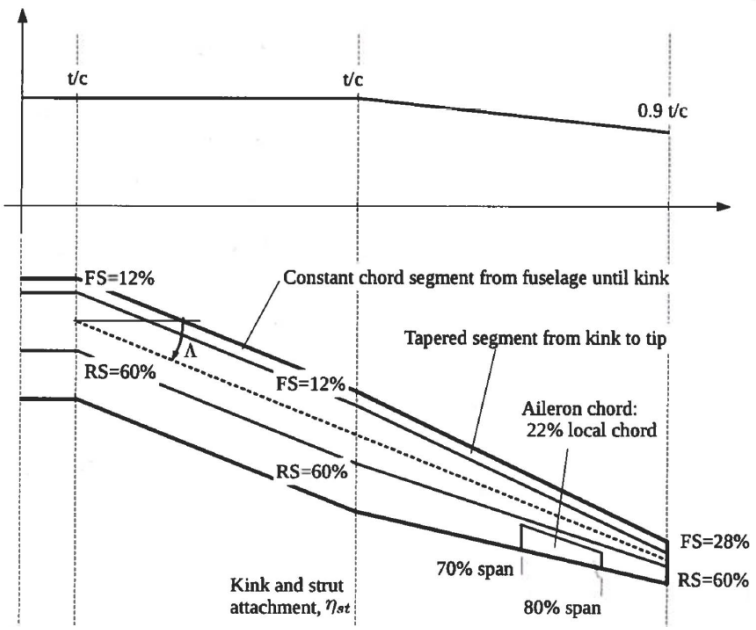

Figure 2.15: Schematic of the SBW planform assumed by Pinho Chiozzotto [13]

2.4.2. Overview of Weight Estimating Relationships

Along with the abovementioned assumptions (subsection 2.4.1), the WER required further simplifications and were hence based on additional assumptions. This was done to reduce the number of variables and data points for the DOE study. A few of the relevant assumptions are mentioned below

Assumptions of the WER

1. The strut was attached to the front spar of the wing.
2. The box width of the strut was 30% of its chord length
3. The t/c of the strut was calculated using the t/c of the wing as follows

$$t/c_{strut} = t/c_{wing} + \frac{0.05}{cos\Lambda} \tag{2.1}$$

4. The sweep of the strut was equal to that of the wing measured at the quarter chord location.
5. The strut was made of Carbon Fibre Reinforced Plastic (CFRP) material.
6. A jury was placed in between the strut and the wing.
7. The limit load factors of +2.5g and -1g were considered.
8. An elliptical lift distribution for the wing was assumed.
9. The t/c of the wing was assumed to be constant over the untapered region and equal to that at the root. Within the kink and the tip, it was assumed to linearly reduce to 90% of the value at the tip as seen in Figure 2.15
10. The bending moment relief due to the engine (k_e) was equal to one (no relief) for the engine locations inboard of the η_{strut} location and a correction factor could be applied otherwise.
11. The fuselage dimensions, maximum zero fuel Weight and maximum landing weight were a function of MTOW.
12. The sizing of the internal structure, such as the minimum thickness of the covers and skin, rib spacing and the pitch of the stringers, was based on a few design rules.

In addition to the abovementioned assumptions, a few others (irrelevant to this thesis) have not been listed here, and additional details can be found in Chapter 5 of [13].

Pinho Chiozzotto [13] clasified the WER according to the type of material used and the wing sweep. An SBW designed for a futuristic time frame is likely to make partial use of lighter materials like the

CFRP as seen in SUGAR High[6] and RHEA[5]. Since the baseline aircraft for this thesis was the ATR 72-600, the wing sweep was expected to be very low. Hence, it was decided to use the WER applicable to an unswept (USW), CFRP-based SBW. The regression-based method for the CFRP USW SBW had an R^2 value of 0.983, an average error of 4.24% and a maximum error of 25% compared to the physics-based method. The plot of the regression accuracy can be found in Figure A.9 in the Appendix.

The WER used for the weight estimation of the wing were divided into the weight of the covers (Equation 2.2), the weight of the spars and ribs (Equation 2.3), the weight of the strut and jury combined (Equation 2.4), and the mass of the secondary structure like flaps, fairings, pylon attachments, slats, spoilers, paint etc.(Equation 2.5).

$$M_{covers} = k_e \cdot C_1 \cdot MTOM^{a1} \cdot (W/S)^{b1} \cdot AR^{c1} \cdot cos(\Lambda)^{d1} \cdot (t/c)^{e1} \cdot V^{f1} \cdot (1+\lambda)^{g1} \cdot (1-\eta_{strut})^{h1} \quad (2.2)$$

$$M_{spars,ribs} = C_2 \cdot MTOM^{a2} \cdot (W/S)^{b2} \cdot AR^{c2} \cdot cos(\Lambda)^{d2} \cdot (t/c)^{e2} \cdot V^{f2} \cdot (1+\lambda)^{g2} \cdot (1-\eta_{strut})^{h2} \quad (2.3)$$

$$M_{strut} = C_3 \cdot MTOM^{a3} \cdot (W/S)^{b3} \cdot AR^{c3} \cdot cos(\Lambda)^{d3} \cdot (t/c)^{e3} \cdot V^{f3} \cdot (1+\lambda)^{g3} \cdot (1-\eta_{strut})^{h3} \cdot P_s^{i3} \quad (2.4)$$

$$M_{sec} = 0.0443 \cdot MTOM \quad (2.5)$$

where k_e is the engine relief factor, which is equal to one for engine location inboard of η_{strut}, $MTOM$ is the Maximum Take Off Mass, W/S is the wing loading(N/m^2), AR is the aspect ratio, V is the cruise speed(m/s) and P_s is a factor given by

$$P_s = 1 - \frac{(C_s/C_w)^{0.5} \cdot \eta_{strut}^2}{AR^{0.5}} \quad (2.6)$$

The values of the corresponding exponents are mentioned in Table 2.2

Parameter	C	a	b	c	d	e	f	g	h	i
Covers (1)	3.86E-3	1.374	-0.69	1.157	-0.826	-0.853	-0.048	0.829	1.393	-
Spar,rib (2)	0.617	1.414	-0.98	0.066	-0.325	0.389	0.065	0.369	0.624	-
Strut (3)	8.67E-4	1.471	-1.293	0.831	-4.785	-0.53	0.584	1.425	-5.577	69.9

Table 2.2: WER coefficients for CFRP USW SBW aircraft[13]

Pinho Chiozzotto [13] considered the following design variable ranges for the DOE study (Table 2.3).

Parameter	MTOM (kg)	W/S (N/m^2)	AR	Sweep deg	t/c	V m/s	taper ratio	Normalised strut location	Strut chord ratio
Lower Bound	20000	3000	10	0	0.08	130	0.1	0.3	0.1
Upper bound	250000	8000	20	10	0.18	200	0.5	0.7	0.3

Table 2.3: WER bounds for CFRP USW SBW aircraft[13]

Due to the easy implementation of these equations and their suitability for SBW configurations, the WER were used in this thesis for estimating the weight of the wing and strut. It must be noted that RHEA used similar empirical equations, also from Pinho Chiozzotto[28] in their research. However, the difference between the WER from [28]and [13] was that the former developed dedicated WER called CFRP USW for lower sweep values ($< 10^0$) in the regression analysis, whereas the latter considered sweep values within a broader range ($0^0 - 40^0$). Due to this reason, the latter ones were less accurate at lower values of sweep and were not used for this thesis. Another difference was regarding the inclusion of the load factor (N_z). The former assumed a maximum load factor of 2.5g, while the latter included it in the design variables. The bounds for the WER ([28]) used by RHEA are given in the table below.

Parameter	MTOM kg	W/S N/m^2	AR	Sweep deg	t/c	V m/s	taper ratio	Normalised strut location	Strut chord ratio	N_z
Lower Bound	20000	3000	10	0	0.08	130	0.1	0.25	0.1	2.0
Upper bound	250000	8000	20	40	0.18	200	0.5	0.75	0.3	3.0

Table 2.4: Bounds of the WER[28] used by RHEA

2.4.3. Validation

The physics-based method was validated by Pinho Chiozzotto [13] against the high fidelity results from SUGAR High[7]. Moreover, the prediction of the WER was also compared, and the results can be seen in Table 2.5

Component	SUGAR High (kg)	Physics-based method prediction		WER prediction	
		Abs value	% error	Abs value	% error
Wing	8046	6979	-13.3	6748	-16.1
Strut	7562	6379	-15.6	6029	-20.3
Wing+Strut	484	600	23.8	719	48.4

Table 2.5: Validation of physics-based method and WER[13]

The error in the prediction by the physics-based method was within 10-20%, which is reasonable for an unconventional aircraft configuration with additional uncertainty in the results from the high fidelity methods[13]. Multiple assumptions and simplifications related to the materials, structure and geometry as explained in subsection 2.4.2 had to be implemented for developing the WER. Due to this reason, the error was even higher for the WER. However, the relative error between the physics-based method and the WER was quite low, reflecting the regression-based method's accuracy.

2.4.4. Weight estimation of other aircraft components

Configuration		HLFC (Percentage of laminar flow area on the wing and tailplane)	Load alleviation (max. load factors)	Advanced materials & structures
Short-range	SBW	65%	+1.5 g and -0.5 g	20% structural weight reduction
	TF	70%		
Mid-range	SBW	50%	+1.5 g and -0.5 g	20% structural weight reduction
	TF	55%		
Long-range	SBW	50%	+1.5 g and -0.5 g	20% structural weight reduction
	TF	55%		

Figure 2.16: Advanced technologies assumed by RHEA SR-SBW[5]

For the rest of the aircraft components like fuselage, empennage, landing gear, etc., empirical equations from FLOPS[27] were used. Moreover, the structural weight of the components other than the weight of the wing and strut (since they already assumed advanced materials like CFRP in their construction) was reduced by 20%, similar to the assumptions in the advanced technologies by RHEA (Figure 2.16). The weight contribution due to the aircraft paint, systems and nacelles was retained from RHEA (Figure A.10)

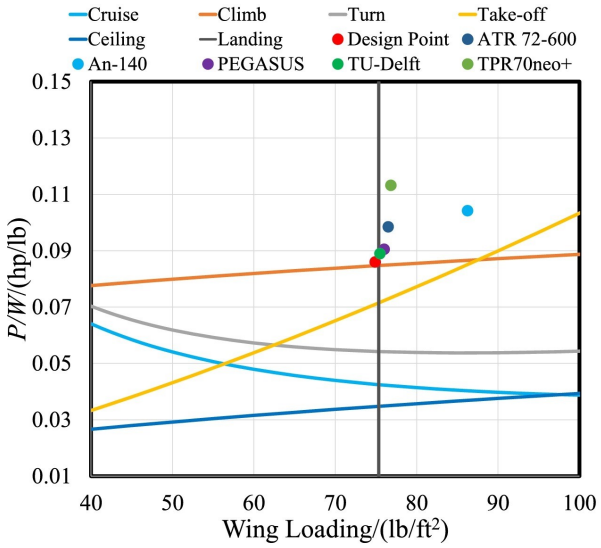

a) SR-SBW

Figure 2.17: Constraint diagram for RHEA SR-SBW [5]. *all marked points other than 'Design Point' are irrelevant for this thesis

The weight of the engines was estimated based on the power requirement of the aircraft. For this thesis, the SBW designs were constrained by a maximum wing loading constraint corresponding to the landing constraint in Figure 2.17. The design points of other reference aircraft considered by Ma, Karpuk, and Elham [5] can be seen in the legend of Figure 2.17 and can be ignored for this thesis. This is further explained in section 2.7. From the constraint diagram (Figure 2.17), the $\frac{P}{W}$ ratio corresponding to the wing loading of the aircraft at the climb constraint was evaluated. The engine's weight was calculated under the assumption of a constant power-to-weight ratio of the engine. This value was taken from the engine specifications of the PW127 engine [29], which powers the ATR 72-600. Thus, the weight of the engines was given by Equation 2.7.

$$W_{engines} = \frac{(\frac{P}{W})_{aircraft} \cdot MTOW}{(\frac{P}{W})_{engine}} \tag{2.7}$$

To fully utilize the potential of an SBW by maximising the span, the use of a wing folding mechanism is often considered to comply with the airport gate sizes[6][5]. To estimate the weight of this mechanism, an empirical equation (Equation 2.8) from [30] was used for this thesis wherever applicable.

$$M_{fold} = 0.07 * MTOM * 0.5 * (1 - \frac{2}{\pi}\eta_{fold} * \sqrt{1 - \eta_{fold}^2} - \frac{2}{\pi} sin^{-1}\eta_{fold}) \tag{2.8}$$

where η_{fold} is the normalised location of the wing folding hinge w.r.t the wing span.

2.5. Performance model

In this section, the details about the Performance model that was used to evaluate the different performance metrics such as fuel burn (W_{fuel}), Maximum Take-Off Weight (MTOW), Operating Empty Weight (OEW) and Lift to Drag ratio (L/D) are explained.

The performance model incorporated the geometry modeller section 2.2, weight estimation tool (section 2.4) and used the results from the aerodynamic analysis (section 2.3). Evaluation of the aircraft performance for the flight phases other than cruise was beyond the scope of this thesis. Due to the complex inter-dependencies between the performance parameters, they have to be often evaluated using an iterative process. To illustrate, the WER used to calculate the structural weight (W_{str}) of the aircraft are a function of MTOW, and the MTOW is the sum of the W_{str}, payload and W_{fuel}. Hence, an initial value of MTOW had to be assumed, and the final value was obtained by iterating.

The performance model consisted of three iterative loops as shown in Figure 2.18. The outermost loop was used to modify the twist distribution and maintain an Elliptical Lift Distribution (ELD). This was done to comply with the assumptions of the WER stated in subsection 2.4.1. The second loop was used to converge for MTOW, and the innermost loop corresponded to an equilibrium condition at cruise. It must be noted that the constraints were evaluated in section 2.7 and not in the performance model. The procedure followed in Figure 2.18 is explained below.

1. For a given SBW configuration as defined by the DOE points, the external geometry and mesh (PLOT3D) files were created using OpenVSP (section 2.2). Initially, the geometry assumed a predefined twist distribution for the wing, which was likely to produce an ELD. The twist distribution could later be modified if required in step 9.
2. After using a suitable initial guess for MTOW ($MTOW_{guess}$), the structural weight of the aircraft was calculated.
3. The aerodynamic analysis was used to generate the lift and drag polars using Flightstream. These polars were used as surrogates for predicting the lift coefficient and the L/D for different AOA to reduce the computational time. An initial guess for the Angle Of Incidence (AOI) was used, and C_L and L/D values corresponding to the AOI were evaluated. In addition, the lift distribution plots were exported to be used later in step 9.
4. In the next step, W_{fuel} is evaluated using the Breguet range equation:

$$W_{fuel} = [1 - f \cdot exp(\frac{SFC}{\eta_j} \cdot \frac{-R}{L/D})] \cdot MTOW \tag{2.9}$$

   where R is the range of the aircraft, SFC is the Specific Fuel Consumption, η_j is the propulsive efficiency and the factor f accounts for the fuel fractions used outside of cruise. The values of R, SFC η_j are provided in Table A.1. The fraction f was reverse calculated using the data from RHEA with the explanation provided in subsection A.3.1. Thus, W_{fuel} is a function of L/D and MTOW of the SBW.
5. In the next step, the weight of the aircraft at the design point (W_{des}, which was assumed to be at mid-cruise) was calculated using the following equation:

$$W_{des} = \sqrt{MTOW(MTOW - W_{fuel})} \tag{2.10}$$

6. The lift produced by the aircraft at the assumed AOI in step 3 is compared with W_{des}, and an update to the AOI is provided (from the polars) if the convergence criterion is not met. This step was included in determining the AOI of the wing, which would result in a wing lift (L_{des}) that was equal to W_{des}. it must be noted that the polars in Flightstream were calculated by increasing the AOA of the entire aircraft and not by changing the AOI of the wing. This was done to reduce the time required to generate a new geometry, initialise it and run the solver. Due to other lifting surfaces, such as the strut and the horizontal tail, their effects on the polars had to be decoupled. This was done by decomposing the total lift at each AOA into the lift generated by the individual components. The lift produced by the wing ($C_{Lw,(AOA)}$) at different AOA was added to the

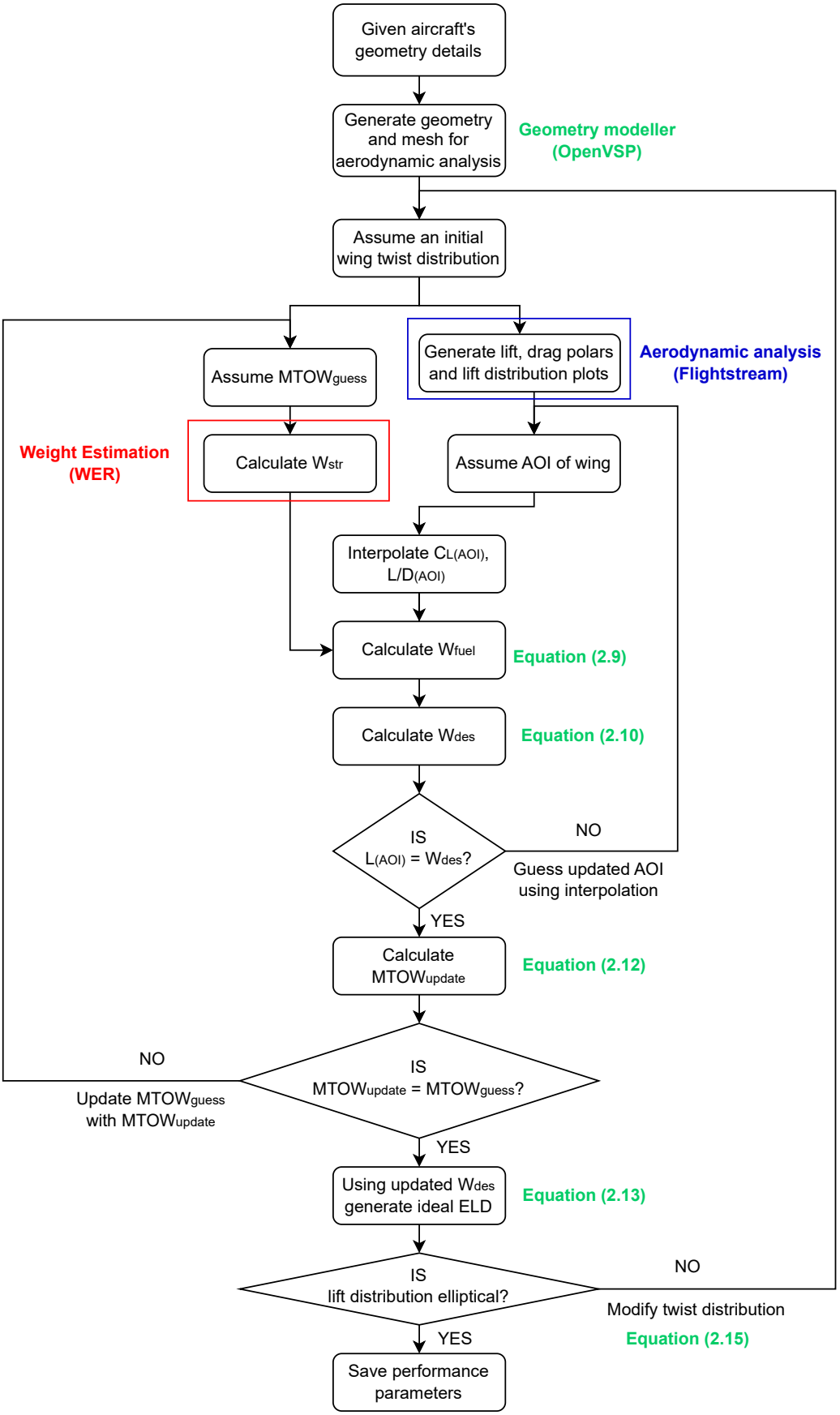

Figure 2.18: Performance model flowchart

baseline (at 0^0 AOA) value of the lift produced ($C_{L,const}$) by the rest of the aircraft. This can be mathematically explained in Equation 2.11.

$$C_{L,(AOA)} = C_{Lw,(AOA)} + CL_{const} \tag{2.11}$$

This was based on the assumption that the effect of the strut on the wing lift was negligible. This can be justified due to the considerable separation between the wing and the strut over most of the wing span, except near the junction region. In the ideal case scenario, the SBW should be analysed with the wing mounted at the AOI required to sustain an equilibrium condition. The above procedure should be repeated until the AOI of the wing is equal to the prediction from the polars. However, this would require creating multiple geometry and mesh files, which must be initialised multiple times before running the simulations in Flightstream. This can significantly increase the computational time. However, the AOI of the wing was changed only if the elliptical lift distribution criterion exceeded the threshold, and the twist in the wing's geometry (and hence the Geometry modeller process) had to be modified anyway.

7. Once the AOI loop was converged, the MTOW was recalculated using the most recent values of W_{fuel} and W_{str} using the following equation

$$MTOW_{update} = W_{fuel} + W_{str} + W_{payload} \tag{2.12}$$

where $W_{payload}$ (= 7976kg) accounts for the payload mass along with the weight of the operating items as used by RHEA[5](Figure A.10).

8. If MTOW was not converged, the process was repeated until convergence. Once done, the ELD [N/m] required to produce a lift equal to the updated value of W_{des} is evaluated using

$$ELD = l_r * \sqrt{1 - \frac{y^2}{(b/2)^2}} \tag{2.13}$$

where y is the normalised spanwise length, and l_r is the lift per unit span required to be produced at the wing root and is given by

$$l_r = 2 * \frac{(L_{des} + L_{ht})}{\pi S_{ref}} \tag{2.14}$$

where L_{des} is the lift corresponding to W_{des}, L_{ht} is the lift produced by the horizontal tail and S_{ref} is the reference area of the wing. The above equation was derived by equating W_{des} to the area under the curve of a half ellipse with the semi-major axis equal to the wing span. The negative lift contribution from the horizontal tail was also taken into account.

9. As mentioned in step 3, the lift distribution plots for different Angles Of Attack (AOA) were saved in addition to the polars. A comparison of ELD with the lift distribution at the required AOI was done by interpolating. The twist distribution was updated if the tolerance criterion was not satisfied. The updated twist distribution was provided by calculating the difference between ELD and the Actual Lift Distribution (ALD). This difference in the lift was converted to an equivalent change in the twist angle using the lift curve slope. This lift curve slope is evaluated separately for each spanwise position using the lift distribution plots. The change in twist angle (θ) for a given spanwise position, 'y', is given by

$$\theta_{(y)} = \frac{ELD_{(y)} - ALD_{(y)}}{C_{l\alpha(y)}} \tag{2.15}$$

where the numerator is the difference in the sectional lift at 'y', which has to be compensated by adjusting the twist ($\theta_{(y)}$) and $C_l\alpha(y)$ is given by

$$C_{l\alpha(y)} = \frac{C_{l(y)_{\alpha_2}} - C_{l(y)_{\alpha_1}}}{\alpha_2 - \alpha_1} \tag{2.16}$$

where α_2 and α_1 are the AOA corresponding to the two lift distribution plots considered for interpolation.

The wing was divided into different sections depending upon the required mesh refinement as shown in (Figure 2.2b). Each section could be assigned a value of the twist angle as calculated from Equation 2.15.

The results from the above process are illustrated in Figure 2.19. It can be observed that the initial twist (Figure 2.19a)distribution, as assumed in step 1, loosely resembled an ELD with an error of 9.5%. After executing step 9, the final twist better matched the ELD with an error of 7%. The slight distortion in the plot at approximately 10m is possibly due to the flow acceleration in the junction region.

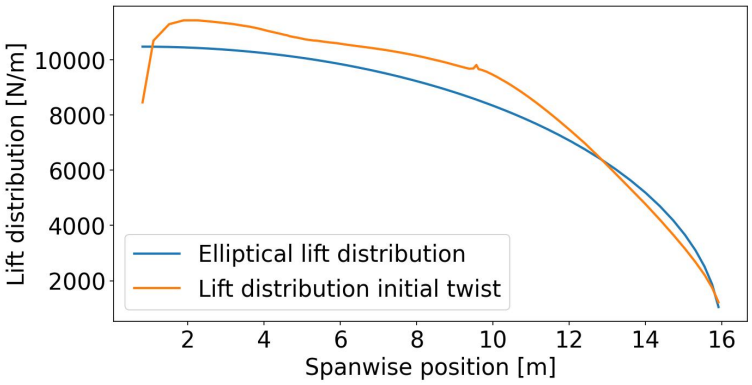

(a) Lift distribution corresponding to the initially guessed twist distribution (step 1)

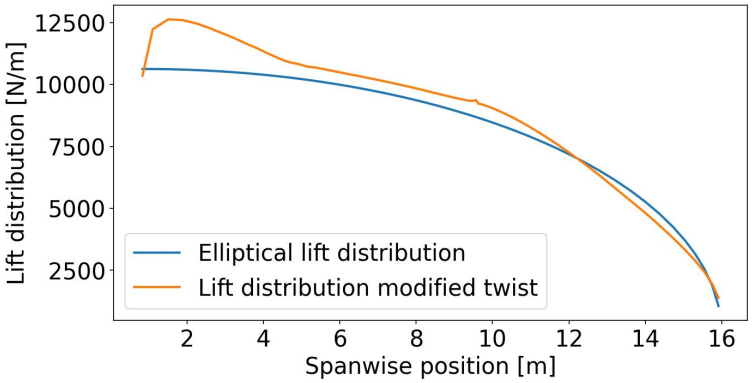

(b) Lift distribution corresponding to the final twist distribution (step 9)

Figure 2.19: PADRI SBW

Due to the discrete nature of the wing sections (Figure 2.2b), the twist angle was defined within the root and the tip of a local wing section. Typically near the root of the wing, this resulted in a bulge as seen in Figure 2.19b. Nevertheless, the overall lift distribution was still better than the initial one, as seen in Figure 2.19a.

10. The process was terminated when the resulting lift distribution was elliptical and the performance parameters were saved. The details about the constraints are covered in section 2.7.

The performance model discarded the DOE point if either one of the following conditions was encountered.

1. The required lift at the design point (L_{des}) was more than the lift which the wing could produce within the AOA range of the polars considered. This meant that a wing with an angle of incidence higher than 6^o (which was the upper limit of AOA for the polars) could still not generate the required lift at cruise.
2. The given combination of aerodynamic performance (L/D) and structural weight (W_{str}) resulted in an infeasible design. This corresponded to a failure in the MTOW loop (Equation 2.12).

3. The twist angle suggested by Equation 2.15 was unreasonably high ($> 10^o$). This occurred when the twist angles suggested by Equation 2.15 were mathematically correct but practically infeasible.
4. The number of iterations required for any of the abovementioned loops exceeded their threshold value.

2.6. Baseline SBW aircraft

The details about the design and performance of the equivalent baseline model that was developed for this thesis along with its purpose is explained in this section.

As mentioned in section 1.3, this thesis was aimed at the design of a short-range, low-speed SBW aircraft. Moreover, this research was built on the work done under the RHEA[5] project while aiming to enhance certain aspects of their research. The initially sized RHEA SR-SBW could not be directly used as the baseline for this thesis since the design violated a few assumptions of the WER[28] implemented by them. Table 2.6 compares the assumptions of the WER with their actual implementation in RHEA.

Parameter	WER assumptions	RHEA implementation
Planform	Semi-tapered (subsection 2.4.1)	Tapered
Load factor	Valid between 2-3 (Table 2.4)	Used for N_z = 1.5 (Figure 2.16)
Normalised strut location	Kink of planform (subsection 2.4.1)	Independent
Wing t/c distribution	Constant within untapered section, linearly decreasing to 90% of root t/c for tapered section (subsection 2.4.1)	Linearly reducing from root to tip
Lift distribution	Elliptical (subsection 2.4.2)	Did not mention the use of any method to achieve Elliptical Lift Distribution (ELD)
Strut planform	Constant chord (subsection 2.4.1)	Tapered
Strut sweep	Same as wing sweep (subsection 2.4.2)	Independent
Presence of jury	1 jury present (subsection 2.4.1)	No jury considered
Wing aspect ratio	Valid for value < 20 (Table 2.4)	Used for AR as high as 25

Table 2.6: Comparison of WER assumptions with their actual implementation in RHEA

Since the initially sized SR-SBW aircraft from RHEA featured a partially incorrect geometry (Table 2.6), a modified equivalent baseline model that fully complied with the assumptions was developed. It was designated as the Modified RHEA Baseline (MRB). The following changes were made to the RHEA SR-SBW design:

1. As mentioned in Table 2.6, the AR of RHEA-SR SBW was more than the limit for which the WER[28] were validated. Hence, the AR was reduced to 20 (which was the upper bound of the WER as shown in Table 2.4). The wing span was calculated using the updated aspect ratio and the same wing area as the RHEA SR-SBW. Similarly, the taper ratio from RHEA was preserved. Finally, the location of the kink of the semi-tapered planform was fixed at the η_{strut} location of the RHEA SR-SBW.
2. For the strut, the linearly tapered planform was converted to a constant chord one using the average chord length value. Moreover, the sweep of the strut was kept the same as that of the wing as per the assumptions explained in Table 2.6
3. Finally, a jury was added between the strut and the wing. The exact location of the jury, as assumed by the WER, was not explicitly provided by Pinho Chiozzotto [13]. The dimensions of the jury were half of the strut as explained in subsection 2.4.1. Hence, the impact of the jury on the overall aerodynamics was expected to be less significant, and its exact positioning was not considered crucial. The non-dimensional location of the jury w.r.t the wing was kept constant and equal to that of SUGAR[7].

Table 2.7 and Figure 2.20 shows the initial RHEA-SR SBW geometry and MRB comparison. The MRB was used as the baseline SBW for this thesis.

Component	RHEA baseline	Modified RHEA Baseline	Unit
Wing span	39	35	m
Wing root chord	2.3	2	m
Wing aspect ratio	25	20	-
Wing area	61	61	m^2
Wing taper ratio	0.4	0.4	-
Wing sweep	1	1	deg
Wing root t/c, tip t/c	0.18, 0.13	0.15	-
Wing airfoil family	NACA 65 series	NACA 65 series	-
Normalised strut location	0.6	0.6	-
Strut root chord, tip chord	0.66, 0.46	0.56, 0.56	m
Strut sweep	0	1	deg
Strut root t/c, tip t/c	0.2, 0.2	0.2, 0.2	-
Strut airfoil family	NACA 65 series	NACA 65 series	-
Jury chord	Absent	0.28	m
Jury t/c	Absent	0.1	-
Jury airfoil	Absent	NACA 4 series	-

Table 2.7: Comparison of RHEA SR-SBW and MRB design parameters

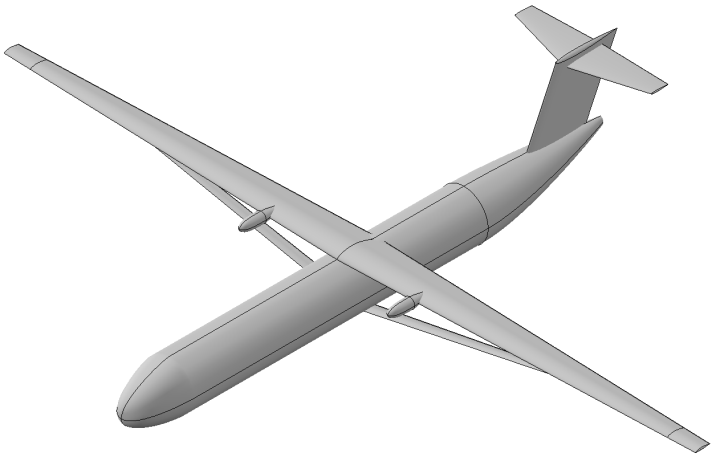

(a) Original RHEA-SR SBW[5]

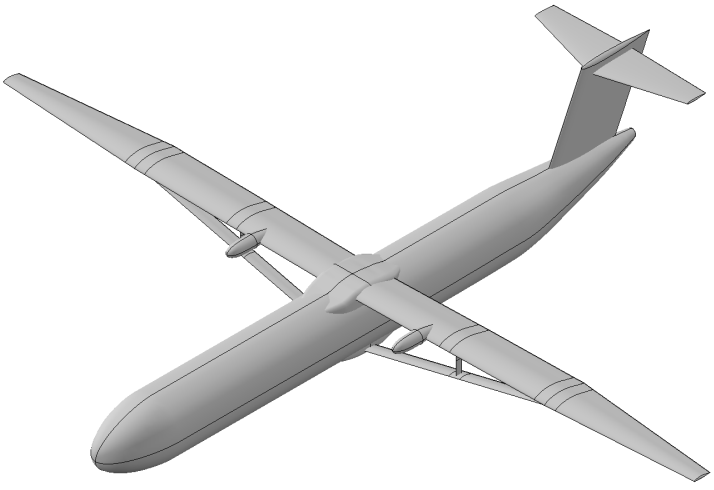

(b) MRB

Figure 2.20: External geometry comparison of RHEA-SR-SBW and MRB

Table 2.8 compares the performance and the weight breakdown of the RHEA and MRB. A reasonable

agreement between the structural weight breakdown can be seen in the table.

Parameter	RHEA value	MRB value	Unit	Difference (%)
Fuel mass	1432	1777	kg	24.1
Maximum take-off mass	22229	22240	kg	0.05
Empty mass	14321	12487	kg	-12.8
Lift-to-drag ratio	26	19.5	-	-25
Wing loading	364	361	$kg/m2$	-0.82
Wing-strut-jury mass	2103	2089	kg	-0.7
Fuselage mass	2497	2717	kg	8.8
Propulsion system mass	1288	1331	kg	3.3
Landing gear	643	659	kg	2.5
Horizontal tail	201	365	kg	81.6
Vertical tail	312	385	kg	23.4

Table 2.8: Comparison of performance and weight breakdown of RHEA[5] and MRB

From Table 2.8, the fuel burn was around 27% higher for MRB compared to RHEA. This is due to the lower aspect ratio and the induced drag of MRB compared to that of RHEA. Since NLF on the wings and the empennage were not assumed, the skin friction drag was higher than RHEA, further reducing the lift-to-drag ratio. Due to the partially incorrect implementation of the WER to predict the wing-strut mass, the prediction was expected to be optimistic. Due to this, the wing-strut mass for RHEA and MRB were quite similar despite the considerably different geometries. The mass of the fuselage, landing gear and propulsion system matched reasonably well, as seen in Table 2.8. The difference in the empennage mass was likely due to the difference in the empirical equations used for the predictions. The weight estimation in RHEA was performed using SUAVE, which relies on empirical equations from FLOPS and Raymer, whereas the equations used in this thesis were restricted to FLOPS only. The overall differences in the mass predictions cancelled out because of which the maximum take-off mass was quite similar. Since the wing area was kept the same, the wing loading was also similar for RHEA and MRB.

2.7. Design Space Exploration

This section covers the details of the design space exploration approach used to answer the research questions. subsection 2.7.1 explains the overall design process, including the preliminary sizing of different components, constraint analysis and the performance evaluation of the SBW for prop-off and prop-on conditions. The details about the set up of the DOE matrix are explained in subsection 2.7.2

The design space exploration was performed using a DOE approach similar to that of FrEACs[1] or AGILE[4] with the MRB as the baseline geometry. Based on the investigation performed by FrEACs[1], SUGAR[7] and RHEA[13], the influential design parameters were identified. These were typically the wing span, wing aspect ratio, normalised strut location, strut depth, strut chord, thickness to chord ratio, number of juries, etc. Since the WER from Pinho Chiozzotto [13] were used for the weight estimation in this thesis (section 2.4), it implied that the design variables were limited to those in the WER equations, e.g. Equation 2.2. Thus, the possible design variables had to be chosen from W_{TO}, W/S, AR, Λ, t/c, V, λ, (C_s/C_w) and η_{strut}. Out of these, the independent geometry-related design variables were identified. These were the wing span, root chord, t/c, η_{strut}, taper ratio and sweep. The corresponding dependent variables were W_{TO}, AR and W/S. The cruise velocity was not the focus of this study and was kept equal to that of RHEA (Figure A.12). The NACA 65 series airfoil family used by RHEA was carried forward. Evaluating the performance of the SBW for different airfoil families was beyond the scope of this thesis.

Since it was hypothesized that an outboard engine positioning could help in propeller slipstream recovery and enhance the aerodynamic performance of the wing, the normalised location of the engine (η_{engine}) was added to the list of design variables. An outboard engine position can reduce the bending moment of the wing, thereby reducing the wing-box structural mass[17] and further improving the performance of the SBW. In his WER, Pinho Chiozzotto [13] assumed that this weight reduction could be neglected in the preliminary design stage as far as the engine was placed inboard of the strut. For engines located outboard of η_{strut}, an engine relief factor was used as discussed previously in subsection 2.4.2. In this thesis, engine positions outboard of the strut location are irrelevant and only the engine positions inboard of the strut were considered. Hence, the WER could not capture the impact of engine placement on the wing weight reduction. However, an outboard engine positioning requires a larger size of the vertical tail and the rudder to provide sufficient lateral stability in case of One Engine Inoperative (OEI) conditions[26]. This can increase the weight of the vertical tail and the drag for an outboard engine positioning, thereby lowering the performance of the SBW. For this thesis, the effect of engine positioning was studied from a purely aerodynamic perspective. Nevertheless, its impact on the overall performance of the SBW is likely less significant, given the opposing effects of a slightly outboard engine positioning. The setup of the DOE matrix is covered in subsection 2.7.2.

2.7.1. Execution procedure

The overall design process can be summarized using the flowchart in Figure 2.21.

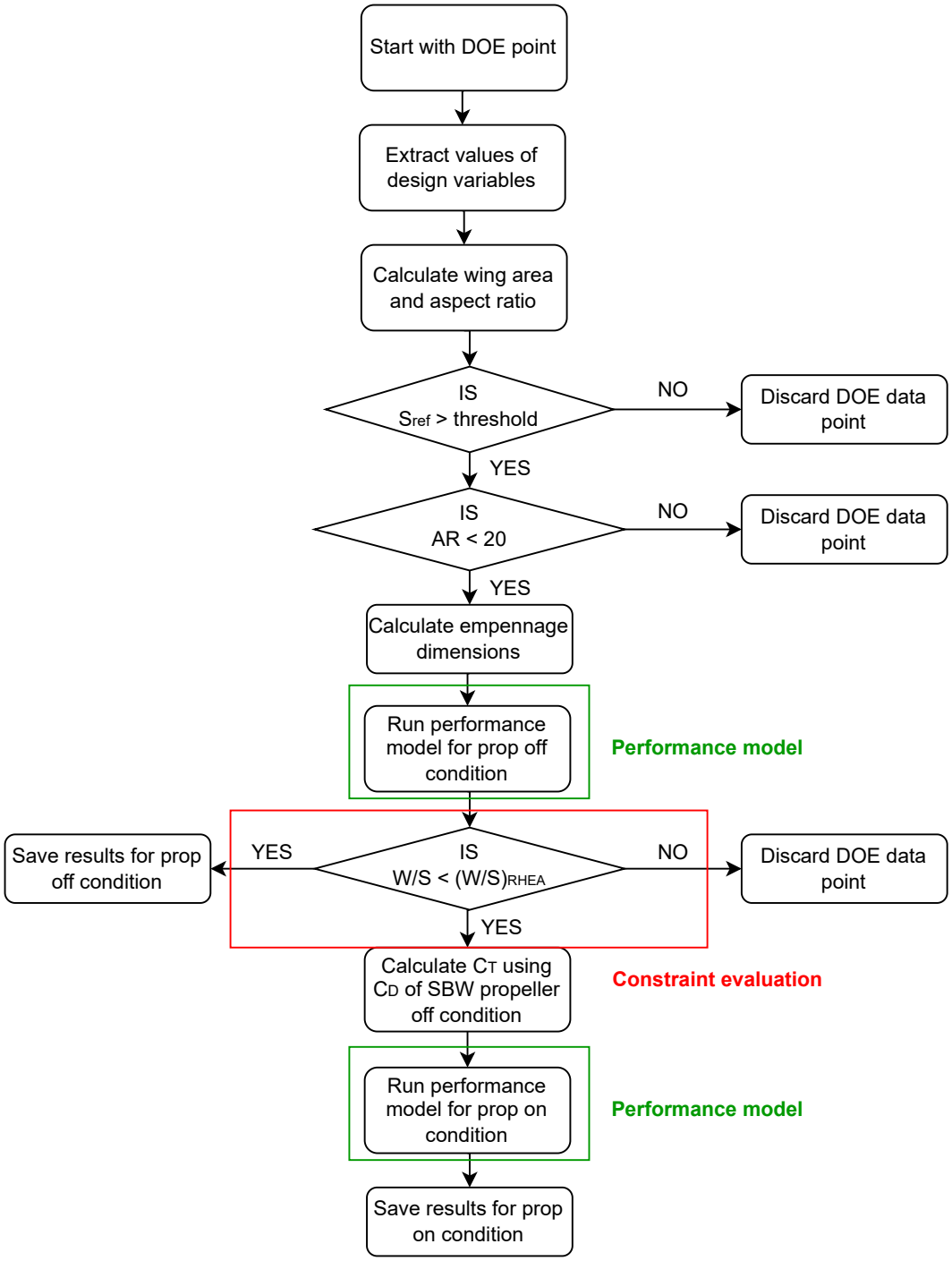

Figure 2.21: Design space exploration flowchart

A step-by-step explanation of Figure 2.21 is provided below.

1. Each DOE data point corresponds to a combination of design variables such as wing span, taper ratio, sweep, etc. The first step fed these values into the design space exploration model.
2. In the next step, the wing area was calculated. After performing a few preliminary investigations, it was observed that aircraft with wing areas lower than $55m^2$ typically exceeded the maximum wing loading constraint. To avoid spending computational resources on the DOE points likely to violate this constraint, a condition was imposed to remove data points with wing areas lower than this threshold.

3. Similarly, another condition was imposed for the aspect ratio. As discussed in Table 2.6, the WER were validated only for AR lower than 20. Thus, no simulations were run for the DOE points, resulting in aspect ratio values higher than 20.
4. Once the above two conditions were satisfied, the tail sizing was performed. The vertical and horizontal tail arms corresponding to the wing dimensions were calculated for each DOE point. This was used to estimate the horizontal and vertical tail dimensions corresponding to the tail volume coefficients using Equation 2.17 and Equation 2.18. The tail volume coefficients and the aspect ratio of the horizontal and vertical tails were assumed to be constant and equal to that of RHEA-SR SBW.

$$S_{ht} = \frac{VC_{ht} * S_{ref} * C_{MAC}}{l_h} \tag{2.17}$$

$$S_{vt} = \frac{VC_{vt} * S_{ref} * b}{l_v} \tag{2.18}$$

where C_{MAC} is the mean aerodynamic chord of the wing, S is the area, VC is the volume coefficient, l is the moment arm, and the subscripts 'ht' and 'vt' represent the horizontal and vertical tails. The mean aerodynamic chord was approximated by the mean geometric chord and is calculated for a semi-tapered wing using Equation 2.19[31]

$$C_{MAC} = \frac{2}{3}(\frac{3\eta_{strut} + (1-\eta_{strut})(1+\lambda+\lambda^2)}{1+\eta_{strut}+\lambda(1-\eta_{strut})}) \tag{2.19}$$

5. In the subsequent step, the performance model (section 2.5) was run for the propeller off condition, and the results of the different performance parameters such as the W_{fuel}, MTOW, L/D and W/S were stored.
6. In the next step, the constraints were evaluated, and the DOE points were discarded if the wing loading exceeded the maximum value of 364 kg/m^2 (from the landing constraint in Figure 2.17). It must be noted here that all the SBW designs with a lower wing loading were considered valid. Although designs with similar wing loadings are desired to make a fair comparison, it was not possible in this case due to the overconstrained nature of this problem. This was because the values of the design variables fixed the wing area, and the MTOW was a function of the weight and aerodynamics (Equation 2.9), both of which were functions of the SBW design.
7. If the wing loading constraint was satisfied for the propeller off condition, the geometry with the updated twist (if applicable) was run with the propeller on condition. The required thrust coefficient ($C_{T,fs}$) as per the definition in Flightstream was calculated by equating it to the total drag of the aircraft at cruise to simulate an unaccelerated flight.

$$T = \frac{1}{2}\rho V^2 C_D S_{ref} \tag{2.20}$$

where T is the total thrust requirement of the SBW.

$$C_{T,fs} = \frac{T/2}{\rho\pi(\omega(D_p/2))^2} \tag{2.21}$$

where the numerator is halved to account for two engines, ω represents the rotational speed, which was 126 rad/s [29]), and D_p is the propeller diameter. For this thesis, the diameter was not varied and was kept equal to that of the ATR 72-600 (and also RHEA-SR SBW). A larger diameter can increase the propeller tip speeds, hence the corresponding noise. Moreover, a smaller diameter may result in a lower bypass ratio, reducing engine efficiency. Hence, it was not considered as a design variable. The values of cruise speed from Figure A.12, rotational speed (N) and the diameter of the propeller (D_p) resulted in an advance ratio (J) of approximately 1.65.

$$J = \frac{V}{N * D_p} \tag{2.22}$$

8. Finally, the results of the propeller on condition were saved. After running a few simulations, it was observed that the wing loading did not change significantly when the slipstream effects were included. Hence, the constraints were not re-evaluated for results with slipstream effects.

In addition to the wing loading constraint, the fuel tank volume constraint is often considered. This requires the aircraft to be able to carry the required mission fuel in the fuel tanks situated in its wings. Given the higher wing span, shorter range and better fuel efficiency of the SBW compared to a conventional aircraft, an active fuel tank volume constraint was not implemented. Instead, the mission fuel volume requirement was calculated and compared to the fuel tank volume of the optimum design. It was estimated that the volume available in the fuel tanks was twice what the optimised design required. Even for the least fuel-efficient aircraft encountered during the DOE study, the available volume was 40% more than the required fuel volume. A detailed procedure behind these calculations is documented in subsection A.4.1

2.7.2. DOE matrix

As mentioned in the previous section, the design variables included the wing span, root chord, wing thickness, taper ratio, strut location, wing sweep, strut chord ratio and engine location. An initial sensitivity study was performed before determining the population, levels (number of intermediate values assigned to a design variable) and bounds of the design variables. The results can be found in Figure 3.1.

Based on the observations in Figure 3.1 Table 2.9 was developed. The intermediate values were equally spaced depending on the number of levels.

Parameter	Lower bound	Upper bound	Unit	Number of levels
Wing span	32	39	m	4
Wing root chord	1.5	2.4	m	4
Wing t/c	0.08	0.15	-	3
Normalised strut location	0.5	0.7	-	3
Taper ratio	0.15	0.5	-	3
Normalised engine location	0.2	0.4	-	3

Table 2.9: Bounds and levels considered for DOE study

The justification for the bounds and levels in Table 2.9 is provided below

1. As seen in Figure 3.1a, the fuel-saving benefits of an SBW are typically seen within the range of 32-38m. However, the span limit was extended a bit further than that of RHEA SR SBW. Due to the higher impact on fuel burn, it was decided to allot four levels for the wing span.
2. Despite the violation of the wing loading constraint and aspect ratio criterion in Figure 3.1b, it was nevertheless decided to cover a broader range for the root chord. This was due to the possibility of not violating them for values of wing span, taper ratio and η_{strut} other than the baseline considered in Figure 3.1. Due to the higher sensitivity of the root chord to fuel burn, four levels were assigned to it.
3. The fuel burn for the t/c in Figure 3.1c was observed to be the lowest within a range of 0.08 - 0.15. Due to the relatively lower sensitivity on fuel burn, three levels were considered.
4. As discussed in section 1.1, a typical $\eta strut$ value of 0.5-0.6 resulted in the optimum performance for an SBW. Nevertheless, the upper limit was extended to 0.7 to include η_{strut} values higher than the baseline. Due to the relatively linear trend of the graph in Figure 3.1d, it was decided to allot three levels for η_{strut}.
5. Due to the relatively chaotic nature of the fuel burn trend in Figure 3.1e, the bounds were kept the same as before with three levels.
6. It was observed in Figure 3.1f that there were no potential gains of increasing the sweep angle beyond 2^o. Furthermore, the lower sensitivity to fuel burn at values below 2^o was removed from the design variables list and kept constant at 1.5^o.
7. The engine location was varied between 0.2 and 0.4 with three levels due to its lower effect on fuel burn as seen in Figure 3.1g. Due to the diminishing benefits of swirl recovery beyond η_{engine} value of 0.37, as well as the exclusion of tail sizing based on OEI condition, the upper bound was restricted.

8. From Figure 3.1h, it was observed that increasing the C_s/C_w value had a clear benefit on reducing fuel burn and MTOW. Hence, it was decided not to include it as a design variable, and it was kept constant at 0.3 for the design space exploration.

Assuming a full factorial design, the number of levels and design variables in Table 2.9 corresponds to 1296 DOE points. However, as explained in Figure 2.21, the aspect ratio and wing area criteria ensured that the simulations were not performed for the infeasible points. Additionally, some DOE points were discarded due to the failure in the performance model (explained in section 2.5, last paragraph) and a few more due to occasional divergence in the Flighstream solver. Due to the above reasons, the final number of DOE points was reduced to around 390, which was still sufficient.

3

Results

This section is divided into four parts. section 3.1 explains the results and discussions from the initial sensitivity analysis used to set the bounds and levels in subsection 2.7.2. The results and discussion for the first and second research sub-questions (section 1.3) are explained in section 3.2. Similarly, those for the third and fourth research questions are summarised in section 3.3 and section 3.4 respectively.

3.1. Initial sensitivity study

As mentioned in section 2.7, an initial sensitivity analysis was performed to understand the trends in fuel burn for different design variables (Figure 3.1). The baseline geometry considered for this study was the MRB. Despite the violation (if applicable) of the aspect ratio criterion or the wing loading constraint as discussed in section 2.7, the results were generated but would be treated cautiously.

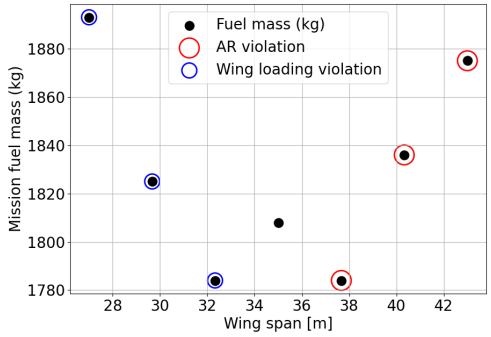

(a) Sensitivity of wing span to fuel burn

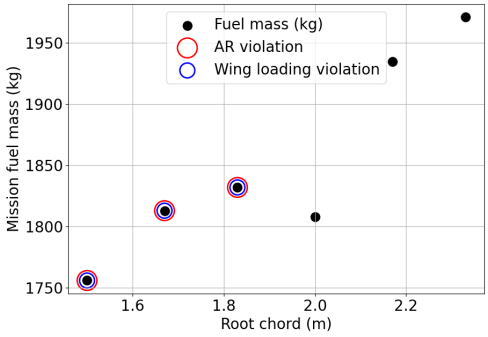

(b) Sensitivity of wing root chord length to fuel burn

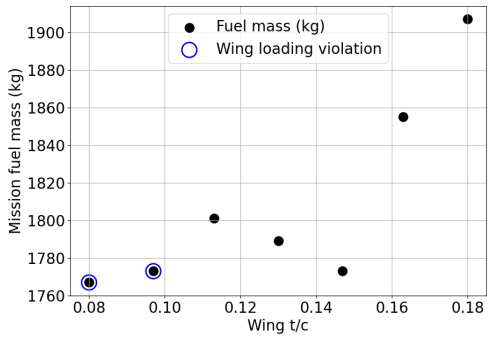

(c) Sensitivity of wing t/c to fuel burn

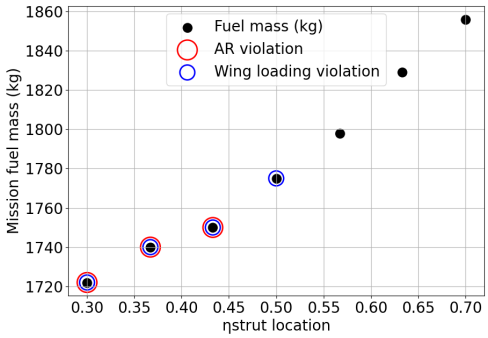

(d) Sensitivity of η_{strut} to fuel burn

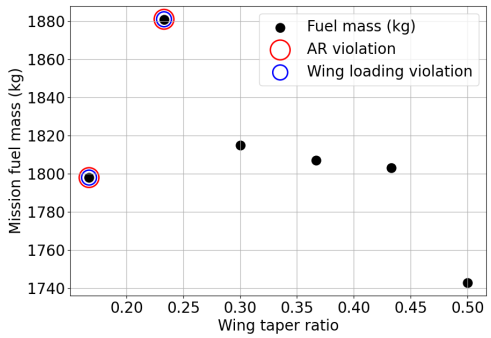

(e) Sensitivity of wing taper ratio to fuel burn

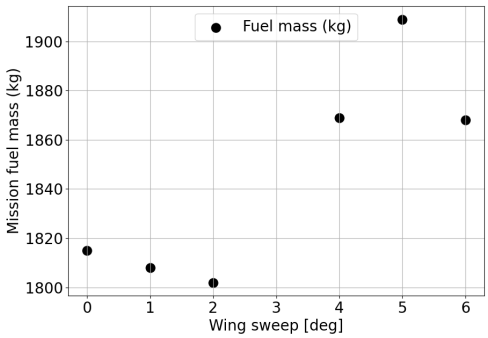

(f) Sensitivity of wing sweep to fuel burn

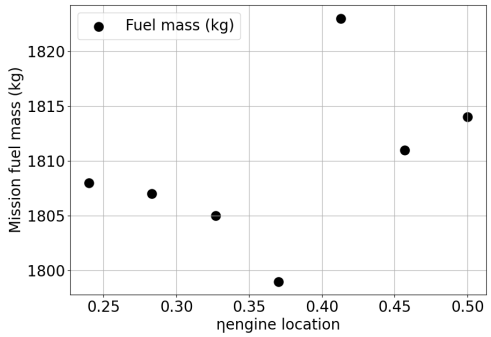

(g) Sensitivity of η_{engine} to fuel burn

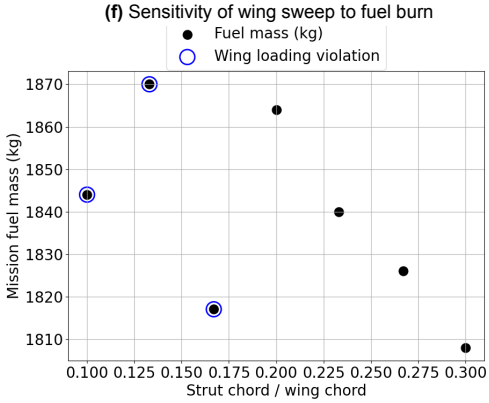

(h) Sensitivity of C_s/C_w to fuel burn

Figure 3.1: Initial sensitivity analysis results

The following observations were made from the results in Figure 3.1. Before analysing the trends,

it must be noted that the results for every DOE point may not be entirely accurate. This was because the meshing performed in OpenVSP occasionally resulted in a few highly skewed cells near the intersections despite the refinement provided. This was beyond the user's control and caused unexpected results in Flightstream. While the residuals usually diverged to infinity and could be easily spotted, sometimes they were stabilised by the solver but contained inaccurate results. These points would be marked as 'anomalies' in the rest of the report.

1. **Wing span:**
   The lowest value of wing span in Figure 3.1a corresponds to that of an ATR 72-600, while the upper bound was 10% higher than that of RHEA. It was observed that increasing the wing span resulted in the violation of the aspect ratio criterion. Hence, it must be noted that the results for these values may not be fully accurate due to the lack of WER validation. For lower values of wing span, the wing loading criterion gets violated primarily due to a lower wing area. Due to the higher aspect ratio of the wings with longer wing spans, the L/D ratio of the aircraft increases. However, the increase in the MTOW of the aircraft negates the gains after approximately 32m. The cause behind the sudden drop in the fuel burn at 35m was likely an anomaly.

2. **Wing root chord:**
   For lower values of the root chord length, the aspect ratio and the wing loading criteria were violated due to the reduction in wing area as seen in Figure 3.1b. With increasing chord length, the mass of the wing was expected to reduce due to the lower aspect ratio. This was because the major contribution to the wing mass was from the covers (Equation 2.2), which was directly proportional to the aspect ratio. Although a lower structural mass could improve the performance, the lower L/D of the low aspect ratio wings resulted in a higher fuel burn, as seen in Figure 3.1b. The slight drop in the fuel burn at 2m was possibly an anomaly.

3. **Wing t/c:**
   The t/c range in Figure 3.1c was based on the bounds for which the WER were valid as shown in Table 2.3. The increased MTOW violated the wing loading criterion for lower values of t/c due to the higher structural strengthening required to support a thinner wing and strut. Due to the lower t/c, the pressure drag of the wing was reduced, and the fuel burn was minimised. However, increasing the t/c resulted in a lighter structure but a higher drag. Although a single local minimum was expected here, the reason behind the two minima at 0.08 and 0.15 was not identified. For t/c values higher than 0.15, the increase in drag negated the benefits of having a lighter wing structure.

4. **Normalised strut location:**
   Similar to the previous case, the range for η_{strut} was based on the validity of the WER. Here, it must be noted that the effect of η_{strut} was not only restricted to the bending moment relief but also indirectly influenced the wing planform. This was because the kink of the semi-tapered planform was a function of the η_{strut} as stated in subsection 2.4.2. Due to the lower wing area at lower values of η_{strut}, the aspect ratio and wing loading criteria were violated, as seen in Figure 3.1d. A linearly increasing trend was observed in fuel burn with increasing η_{strut}; however, the results for the lower values cannot be trusted fully due to the violation of the aspect ratio constraint. The L/D ratio of the designs primarily governed the fuel burn due to the relatively constant value of MTOW over the range. Lower values of η_{strut} resulted in a smaller wing area and a larger lift coefficient, increasing the induced drag. The parasitic drag was effectively constant over the entire range. The net effect of these trends resulted in a decreasing value of L/D, thereby explaining the increase in the fuel burn.

5. **Wing taper ratio:**
   The limits for the taper ratio plot in Figure 3.1e were also based on the validity range of the WER. Lower values of the taper ratio resulted in a lower wing area and violated the aspect ratio and wing loading constraints. Increasing the taper ratio did not significantly change the fuel burn except at the upper bound. The sudden increase in the fuel burn at a taper ratio of 0.25 was suspected to be an anomaly. At the maximum value investigated, the fuel consumption dropped considerably.

However, the exact reason behind the sudden drop was unknown.

6. **Wing sweep:**
   From Figure 3.1f, it was observed that the fuel consumption was minimal for a sweep angle between 1-2 degrees, which possibly corresponded to the best compromise between a lower drag and reasonably weight wing weight penalty. At higher sweep angles, the MTOW increased due to the higher weight of the aft swept wings. This was due to the increased length of the spars for the same wing span. Additionally, the longer spars are weaker in torsion, requiring additional structural strengthening, further increasing the wing weight. The reason why the fuel consumption dropped at a sweep angle of 6 degrees was not understood. However, this was less likely to be an anomaly because a similar trend was observed in the fuel burn in the final sensitivity analysis (Figure 3.10f). Nevertheless, the low-speed SBW was not expected to have higher sweep angles and was not investigated further.

7. **Normalised engine location:**
   As hypothesized in section 1.3, the effect of changing the engine positioning did change the fuel burn of the SBW, although the effect was less significant. This was primarily due to the change in the induced drag of the SBW. As the value of η_{engine} increases, the swirl recovery from the wing-strut jury combination increases. The swirl recovery reduces after an η_{engine} value of around 0.37, possibly due to the larger separation between the jury and the slipstream. The sudden increase in the fuel burn at η_{sngine} value of 0.41 was unknown and possibly due to an anomaly.

8. **Strut chord ratio**
   The range for the C_s/C_w values was based upon the validity of the WER. For lower values of C_s/C_w (0.2-0.3), the mass of the strut increases exponentially, thereby increasing the MTOW and violating the wing loading constraint. This increase in the strut's mass was due to the additional structural strengthening required for the smaller strut to counter buckling loads. The higher MTOW results in an increase in the lift coefficient and the induced drag. On the contrary, the skin friction drag of the strut reduces due to the smaller wetted area. The sudden reduction of the fuel burn for C_s/C_w value of approximately 0.1 and 0.16 were unexpected and could be anomalies. Nevertheless, the fuel burn showed a clear trend towards favouring a higher value of C_s/C_w due to the lower MTOW and induced drag.

3.2. Effect of propeller slipstream on the optimum designs

The performance optimisation of the SBW was performed with and without considering slipstream effects in the aerodynamic analysis. From the results of the DOE, the two designs optimised for minimum fuel burn are compared in terms of external geometry (Table 3.1) and performance (Table 3.2).

Parameter	MRB value	Prop off optimised	Prop on optimised	Unit
Wing span	35	34.3	34.3	m
Wing root chord	2	2.1	2.1	m
Wing t/c	0.15	0.08	0.08	-
Normalised strut location	0.6	0.7	0.7	-
Wing taper ratio	0.4	0.3	0.3	-
Normalised engine location	0.25	0.25	0.3	-
Wing area	61	64.5	64.5	m^2
Wing aspect ratio	20	18.3	18.3	-

Table 3.1: External design comparison of the SBW optimised with and without propeller slipstream effects

Parameter	MRB value	Prop off optimised	Prop on optimised	Unit	% change w.r.t MRB
Fuel mass	1777	1654	1654	kg	-7
Maximum take-off mass	22240	22309	22309	kg	0.3
Empty mass	12487	12679	12679	kg	1.5
Lift to drag ratio	19.5	21.4	21.4	-	9.7
Wing loading	361	345	345	$kg/m2$	-4.4
Lift coefficient	0.615	0.589	0.589	-	-4.2
Drag coefficient	314	274	274	counts	-12
Frictional drag coefficient	221	192	193	counts	-13
Induced drag coefficient	93	82	81	counts	-11
Wing strut mass	2089	2246	2246	kg	7.5
Fuselage mass	2718	2718	2718	kg	0
Empennage mass	727	789	789	kg	0.2
Engine mass	1332	1322	1322	kg	-0.8

Table 3.2: Performance and mass breakdown comparison of the SBW designs optimised with and without propeller slipstream effects

From Table 3.1, it was observed that the two designs were quite similar in terms of external geometry except for the slight difference in the engine location. The performance of the two SBW designs was also identical w.r.t each other as seen in Table 3.2 apart from the slight difference in the drag breakdown. Due to this similarity, the percentage change in the performance metrics (Table 3.2) of the optimised design w.r.t the MRB is only evaluated for the one with slipstream effects.

The similarity between the two optimised designs indicates that the effect of changing the normalised engine positioning in combination with η_{strut}, wing span and root chord was negligible on the performance of the SBW. Two possible reasons behind this observation were speculated.

1. The swirl component in the propeller slipstream was small for cruise conditions with a relatively higher advance ratio and a lower thrust coefficient. Hence, maximising swirl recovery from the wing-strut-jury combination by optimally positioning the engine did not result in any significant benefits
2. The swirl could not be significantly recovered from the slipstream, given that they can be effectively captured by the aerodynamic analysis tool. The ability of Flightstream to capture these effects can be evaluated as follows. As seen in Figure 3.2, the propeller slipstream causes a change in the local angle of attack and can change the pressure coefficient distribution on the downstream wing section. This change in the pressure coefficient distribution can be used as a quick check to evaluate if Flightstream can effectively capture the slipstream effects. It was observed in Figure 2.3.1 that Flightstream could predict the local AOA changes reasonably well, although the axially induced velocity was slightly overpredicted.

Before the above two phenomena are investigated, the concept of swirl recovery is briefly explained here. The propeller slipstream increases the freestream velocity from V to V' due to the induced axial velocity component. Moreover, the propeller rotation induces a vertical velocity component to the flow (W), which is responsible for the change in the local AOA as seen by the downstream wing element. On the upgoing side of the propeller, this causes an increase in the AOA and a decrease on the downgoing side. This can be explained using Figure 3.2

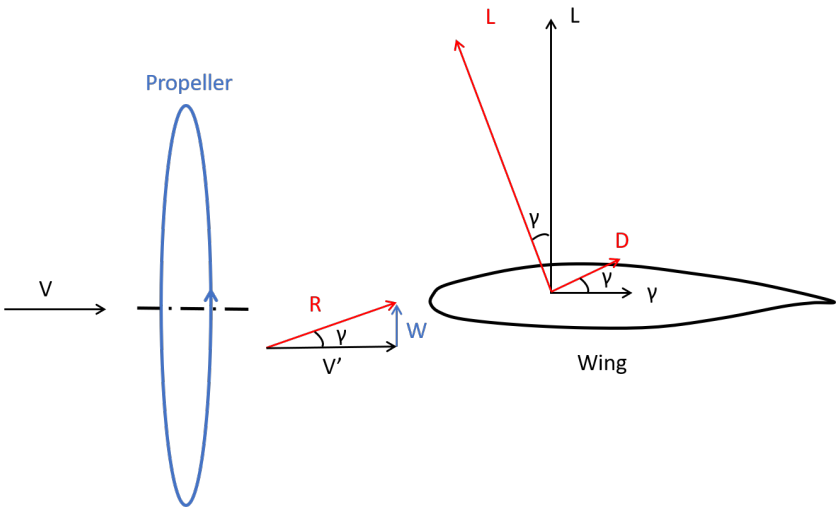

Figure 3.2: Swirl recovery schematic for the upgoing side of the propeller

The resultant (R) of V' and V' is inclined at an angle (γ) w.r.t the freestream velocity. This causes a local tilting of the lift and drag vectors. The X-component of the lift gets aligned in the direction of thrust, which lowers the effective drag of the wing section. Moreover, the drag component in the X direction is also reduced. Thus, the local upwash induced by the propeller swirl reduces the wing's induced drag, which is called the effect of swirl recovery [32]. In contrast, the downgoing side of the wing experiences the opposite effects, with a reduction in the wing lift and an increase in the drag. However, the gradient in the lift distribution between the inboard and the outboard sections can be used to harness a net non-zero benefit from swirl recovery.

3.2.1. Presence of significant swirl in slipstream

The swirl component in the slipstream can cause local changes in the AOA as seen in Figure 2.8. Thus, the chordwise pressure coefficients were plotted for the wing, strut and jury sections at the locations indicated in Figure 3.3 to check for any effects of the local AOA change.

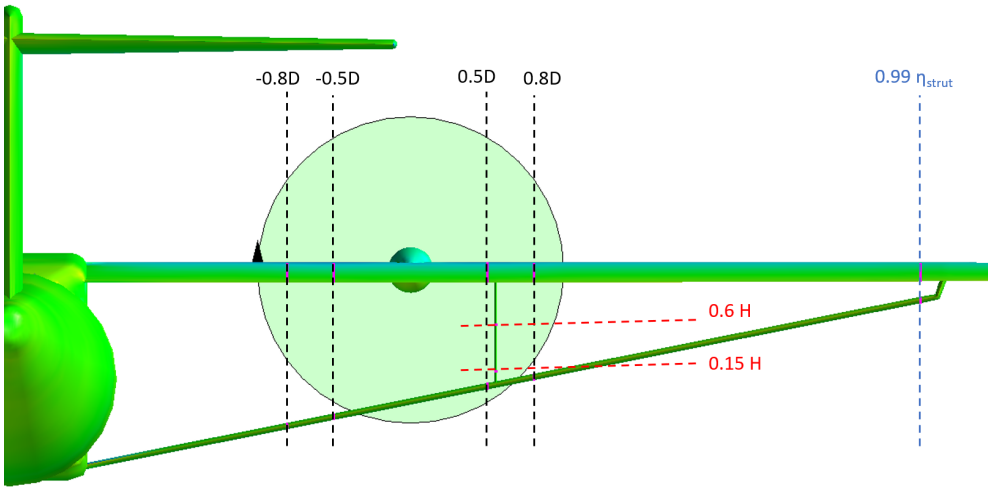

Figure 3.3: Schematic of the cross sections at which pressure coefficients were plotted

In the above figure, 0.5D indicates a spanwise distance of half the propeller diameter (3.96m) measured from the centre of rotation (5.15m from the fuselage centreline) towards the wing tip. Similarly, -0.5D indicates a position towards the wing root.

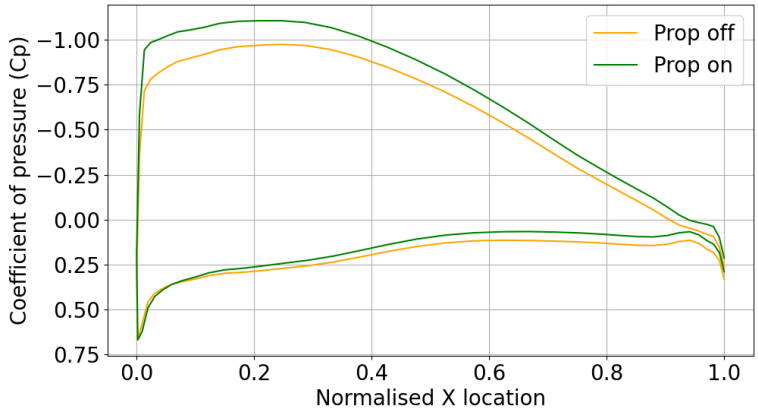

(a) C_P vs x for -0.5D

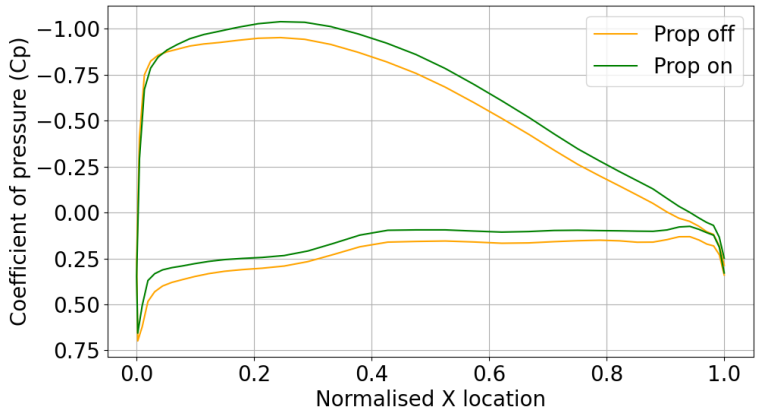

(b) C_P vs x for 0.5D

Figure 3.4: Pressure coefficient plots for wing under the influence of propeller slipstream

From Figure 3.4, it can be seen that the C_P vs. x plot is slightly shifted upwards due to the increase in the dynamic thrust over the wing. Although small changes in the shape of the pressure distribution can be observed, they were not significant. This could either be due to a lower swirl component in the slipstream or due to the characteristics of the airfoil in general. To further investigate the presence of swirl, the lift and drag distribution graphs were plotted in Figure 3.5

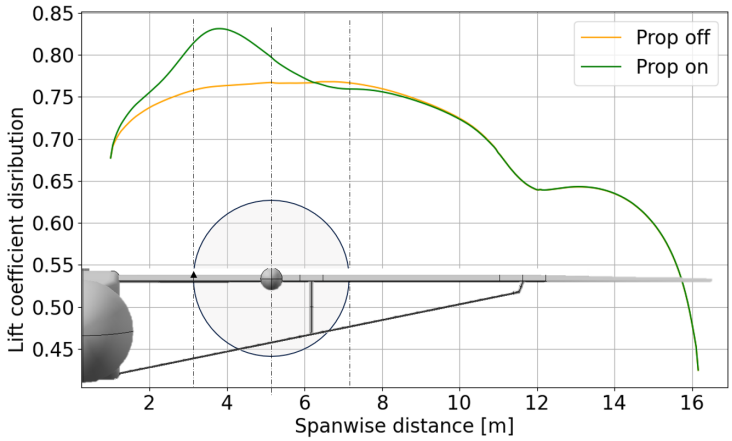

(a) Lift distribution with comparison

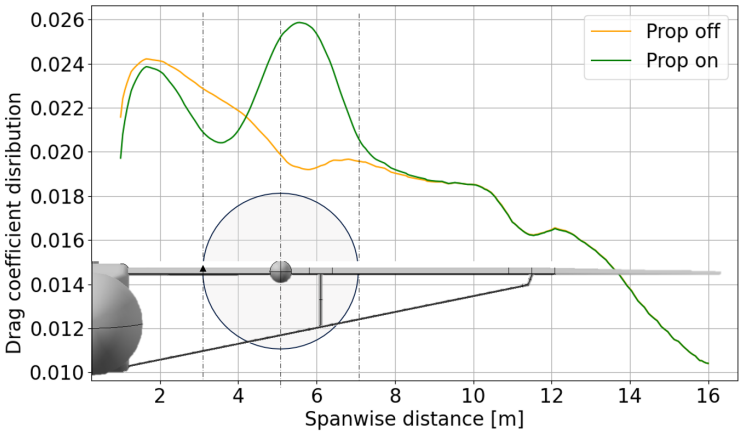

(b) Induced drag distribution with comparison

Figure 3.5: Comparison of the lift and induced drag distributions

Due to the local increase in the AOA on the upgoing side and a decrease on the downgoing side of the propeller, the lift and drag distributions were altered compared to the prop off condition as seen in Figure 3.5. Schematic of the wing, strut and propeller are added to get a perspective of their relative location w.r.t the distributions. The increase in the AOA on the upgoing side increases the lift produced on that side of the propeller. This increase in the AOA also causes tilting of the lift vector in the thrust direction, thereby reducing the wing's induced drag on the upgoing side as explained in Figure 3.2. On the contrary, the lower local AOA on the downgoing side reduces the wing lift. As explained in Figure 3.2. This also causes an increase in the induced drag. Due to the distinct changes in the plots compared to the prop-off condition, a non-negligible swirl in the slipstream was confirmed. Moreover, it can be seen in Figure 3.3 that the majority of the strut lies outside of the propwash. This resulted in a negligible change in the strut's pressure coefficients and the lift and drag distributions. The other plots for the pressure distribution on the wing, strut and jury can be found in subsection A.1.2.

3.2.2. Ability to recover swirl from slipstream

To evaluate if the swirl could be effectively recovered from the wing-strut-jury combination, a sensitivity study was performed for the spanwise engine location to analyse the effect on induced drag (Figure 3.6).

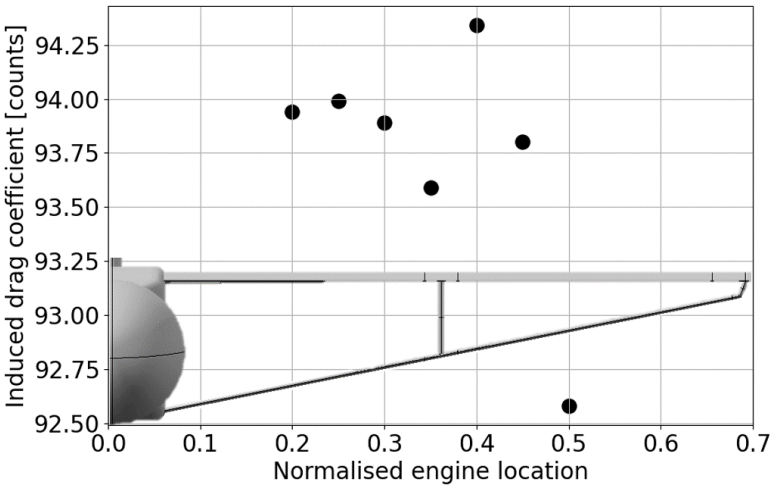

Figure 3.6: Effect of normalised engine location on the induced drag coefficient

Every point in the scatter plot above indicates (Figure 3.6) the centre of rotation of the engine for the inboard-up rotation direction. It can be observed in Figure 3.6 that the induced drag generally reduces when the η_{engine} value is increased from 0.2 to 0.35. At a normalised engine location of 0.35, the induced drag reaches a local minimum due to the increase in the swirl recovery contribution from the jury. As the horizontal separation between the engine and the jury increases, the swirl recovery reduces, thereby increasing the induced drag. However, the contribution of the strut (which initially was outside the slipstream) in swirl recovery is likely to cause a reduction in the induced drag again. The combination of the abovementioned phenomena can be roughly seen in Figure 3.6.

It must be noted that the difference in the induced drag is extremely low (1-2 counts). This also explains why the two SBWs, optimised with and without propeller slipstream effects, converged at similar designs. A possible reason for the smaller difference in drag coefficient could be the smaller gradients in the lift distribution plots for the upgoing and downgoing sides of the propeller(Figure 3.5a). The benefits of swirl recovery on the upgoing side were almost entirely compensated by the downgoing side of the propeller. Since the gradient in the lift distribution curve at η_{engine} value of 0.5 is slightly higher than for the inboard values, the effect of swirl recovery is slightly higher.

As mentioned in Table 2.9, the η_{engine} values considered for the DOE study were 0.2, 0.3 and 0.4. Among these three values, it can be seen in Figure 3.6 that the induced drag is lower by one count for η_{engine} of 0.3 compared to 0.25. Since the induced drag was the only effect that was primarily changing, the fuel burn followed a similar trend, justifying the optimum design in Table 3.1. The skin friction drag for the SBW with propeller effects was higher by one count than that without slipstream effects. Thus, the overall effect on the total drag of the SBW was null. This explains the identical performance of the two SBW designs.

The sudden spike in the induced drag at η_{engine} value of 0.4 was not exactly identified and could be an anomaly. It must be noted that the difference in the induced drag is extremely low (1-2 counts). Hence, the justifications for the observed trends may not be fully reliable. Moreover, the relatively lower fidelity of panel methods and the relatively higher convergence tolerance (Table 2.1) further increase the uncertainty in the results. Finally, although the ability of Flightstream to capture the slipstream effects was qualitatively assessed in Figure 2.3.1, the error margin was not quantified. Due to the abovementioned reasons, the results for the propeller slipstream should be interpreted cautiously.

3.3. Comparison of the optimum design w.r.t MRB

Figure 3.7 compares the MRB w.r.t to the optimised SBW.

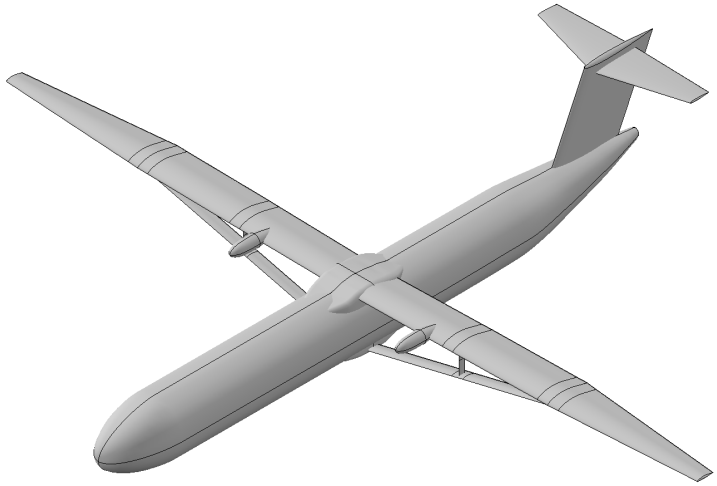

(a) MRB

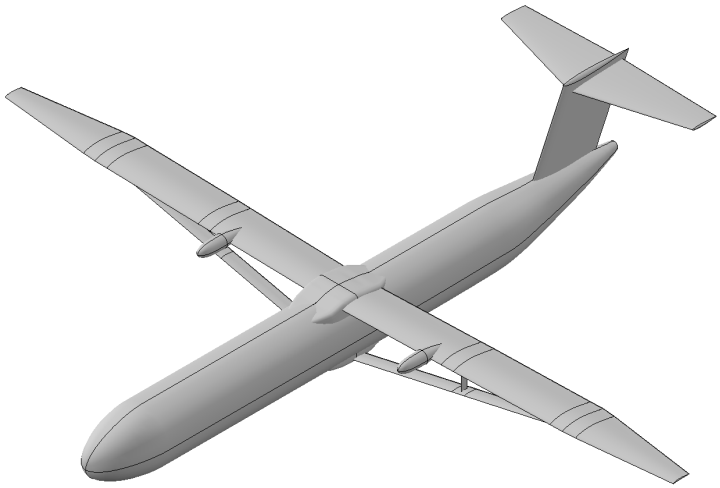

(b) Optimised MRB

Figure 3.7: External geometry comparison of MRB and optimised MRB

The possible reasons and motivation behind the design of the optimised SBW are explained below based on the results in Table 3.1 and Table 3.2. It should be noted that the fuel saving of the optimum design could be on the conservative side. This is because of the discrete nature of the DOE design variables, which can help to point in the direction of the optimum design but may not guarantee the exact values. This can be illustrated in the final sensitivity plots for the root chord and raper ratio (Figure 3.10b and Figure 3.10e), wherein the mission fuel mass is even lower than the baseline (optimised SBW here). A surrogate model based on the DOE results can help provide a better guess. However, the difference in the two designs is not expected to be significant and hence was not considered for this thesis.

1. The optimised SBW design had a slightly smaller wing span and a larger wing chord, because of which the aspect ratio was lower than the baseline. Although the aspect ratio of the wing was not expected to reduce below that of MRB (which was already at its upper limit), it was observed that the high aspect ratio wings typically violated the wing loading criterion. The aspect ratio of 18.3 was in between the typical range of (16-20) for an SBW as observed in previous research works[1], [3], [4], [7].
2. To maintain a relatively high aspect ratio and not violate the wing loading criterion, the optimised design was a trade-off between η_{strut} and the taper ratio. A higher value of η_{strut} resulted in a planform with a higher wing area due to the increase in the area of the untapered section (kink of the semi-tapered wing was placed at η_{strut} as explained in subsection 2.4.1). Similarly, the wing area increased with a higher value of taper ratio. To achieve a compromise between a high aspect ratio and a reasonably high wing area (to meet the wing loading criterion), the η_{strut} value

reached its upper bound, and the taper ratio reached its lower bound. The value of η_{strut} was slightly higher than what was observed in the case of SUGAR[7], FrEACs[1] and AGILE[4] but equal to that of the ALBATROS[3]. The resultant wing area was slightly higher than that of MRB.

3. Due to the greater bending moment relief from the strut, the t/c of the wing could be reduced without a significant weight penalty. The lower value of t/c compared to MRB reduced the pressure drag of the wing. Additionally, the lower frictional drag is due to the lower shear stress in the boundary layer in the case of low t/c wings with less adverse pressure gradients.
4. Despite the lower aspect ratio and the higher bending moment relief from a higher η_{strut} value, the resultant mass of the wing-strut-jury assembly was higher due to a significant 50% reduction in the wing t/c.
5. The mass of the empennage was slightly higher due to the larger area of the horizontal and vertical tail due to the higher wing area and the mean aerodynamic chord.
6. The engine's mass was slightly lower than that of MRB due to the lower wing loading of the optimised design (the engine was sized using the constraint diagram as explained in subsection 2.4.4). This lower wing loading was primarily due to increased wing area.
7. The overall increase in the mass of the wing, empennage and engines resulted in a 1.5% higher structural mass of the aircraft.
8. Due to the higher wing area of the optimised SBW, the lift coefficient (for the nearly identical W_{des}) was lower for the optimal SBW. Although the aspect ratio was also lower, the overall effect was a slight reduction in the induced drag compared to the MRB.
9. As discussed previously, the significantly lower t/c of the wing caused a 13% lowering of the frictional drag coefficient. However, the total frictional drag (in Newtons) reduction is slightly lower than 13% due to the higher wetted area of the wing.
10. The resultant of the lower induced and parasitic drag coefficients increased the overall L/D of the aircraft by 9.7%. This caused a primary reduction in the mission fuel mass by 7% of the optimum SBW. The overall effect of the structural mass of the aircraft and the mission fuel mass resulted in a 0.3% increase in the MTOW.

The mission fuel burn of the optimised MRB was still higher than that of the initially sized RHEA SR-SBW by 15.5%. This was also due to similar reasons that caused a difference in the performance of the MRB and RHEA as explained in section 2.6. Moreover, the optimised SBW had a 17% lower mission fuel mass compared to a conventional ATR 72-600. It must be noted that the fuel mass of the ATR 72-600 was roughly calculated in subsection A.3.2 and may not be fully accurate.

It must be noted that the performance of the optimised SBW (Table 3.2) was evaluated for the SBW geometry with the wing's AOI determined from the condition for equilibrium (Equation 2.10). This required the geometry of the SBW to be re-initialised and simulated in Flightstream multiple times after the base simulation. To avoid this significant increase in the simulation time, the above procedure was not followed for all the DOE points as discussed in step 6 of section 2.5. The overall effect of this assumption resulted in an actual performance which was different compared to the one without these iterations. Figure 3.8 shows the difference in the different performance metrics of the two designs.

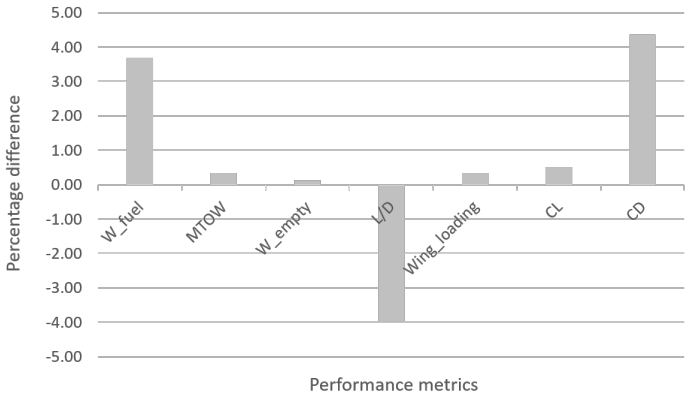

Figure 3.8: Quantification of the error due to the assumption of AOI

Although an error of around 3.5% for fuel burn is significant, given that the optimum SBW had a 7% lower fuel consumption w.r.t the baseline, the assumption in the AOI is likely to give conservative values for the fuel burn due to the slightly higher deviation from an elliptically distributed wing lift. Moreover, this assumption was required to significantly reduce the computation time, allowing a broader design space exploration. Lastly, this difference in the error for the other performance metrics apart from L/D and C_D was negligible.

Figure 3.9 shows the Mach number and pressure coefficient contours normalised with the freestream velocity for the optimised SBW. From Figure 3.9b, it can be observed that the maximum Mach number reached on the wing's upper surface is around 0.6. Moreover, the flow in the junction region is fully subsonic, as seen in Figure 3.9c. As discussed in subsection 2.3.2, Flightstream could not predict the shock-induced separation as expected. However, the prediction of the Mach number was reasonably accurate, as seen in Figure 2.10. The absence of sonic/transonic flow conditions implies that the errors in predicting the aerodynamic coefficients are likely to be less due to the absence of any complex flow phenomena.

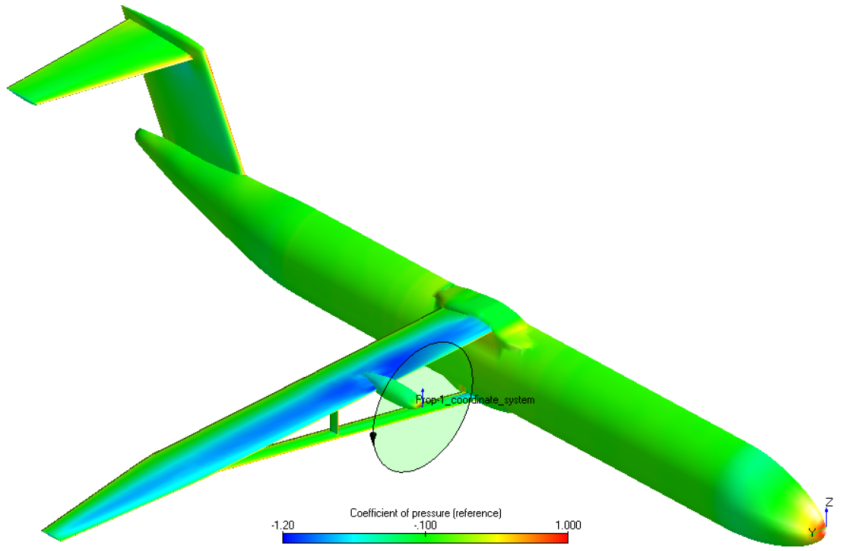

(a) Pressure coefficient contour

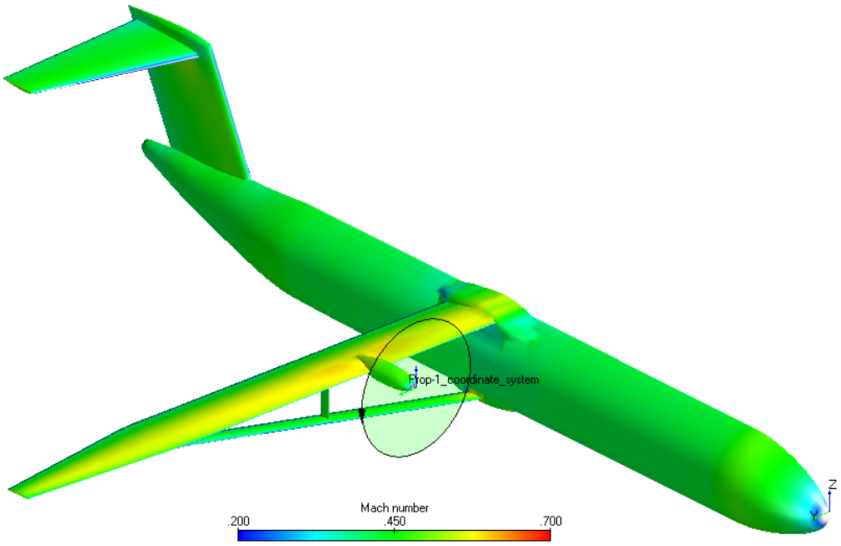

(b) Mach number contour

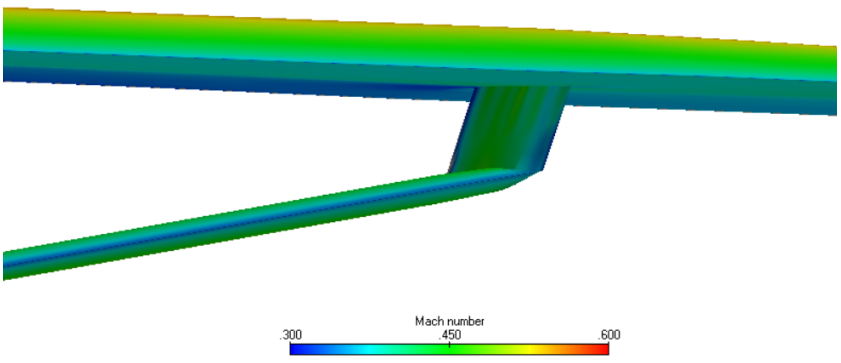

(c) Mach number contour in the junction region

Figure 3.9: Coefficient of pressure and Mach number contours for the optimised SBW

3.4. Final sensitivity study

With the optimum SBW design, a sensitivity study was performed to evaluate the effects of different design variables on the performance of the SBW. The results for the same are plotted in Figure 3.10. To understand the contribution of the other performance parameters on fuel burn, Table 3.3 was created to indicate the general trends observed. The effect of increasing the value of a particular design variable on the performance metrics was qualitatively classified into increasing (Inc), decreasing (Dec), constant (Con), approximately parabolic (Para) or irregular (N/D).

Design variable	**Effect of increasing different design variables on**										
	Wing area	**AR**	**CL**	**CDi**	**CDo**	**CD**	**L/D**	**Wstr**	**MTOW**	**W/S**	**Wing strut mass**
Wing span	Inc	Inc	Dec	Dec	Dec	Dec	Inc	Inc	Inc	Dec	Inc
Root chord	Inc	Dec	Dec	Dec	Dec	Dec	Dec	Dec	Dec	Inc	Dec
Wing t/c	Con	Con	Dec	Dec	Inc	Inc	Dec	Dec	Dec	Dec	Dec
η_{strut}	Inc	Dec	Dec	Dec	Dec	Dec	Para	Dec	Dec	Dec	Dec
Taper ratio	Inc	Dec	Dec	N/D	N/D	N/D	N/D	Inc	Inc	Dec	Inc
Sweep angle	Con	Con	Inc	N/D	Con	Con	Dec	Inc	Inc	Inc	Inc
η_{engine}	Con	Con	Con	N/D	Con	N/D	N/D	Con	Con	Con	Con
C_s/C_w	Con	Con	Dec	Inc	Dec	Dec	N/D	Dec	Dec	Dec	Dec

Table 3.3: Qualitative comparison of the design variable sensitivity on performance metrics at the optimum.

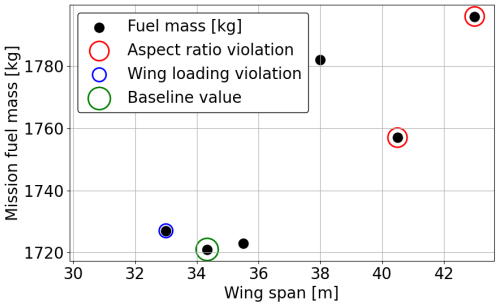

(a) Sensitivity of wing span to fuel burn

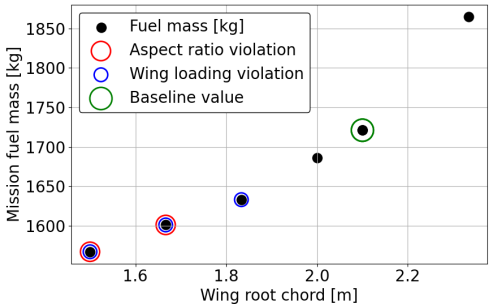

(b) Sensitivity of wing root chord to fuel burn

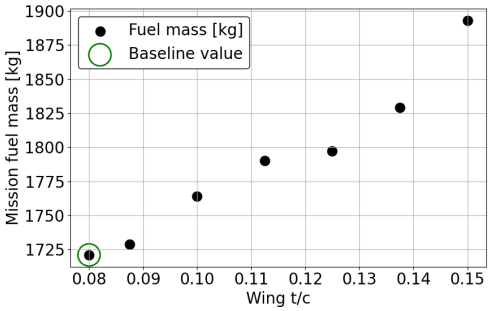

(c) Sensitivity of wing t/c to fuel burn

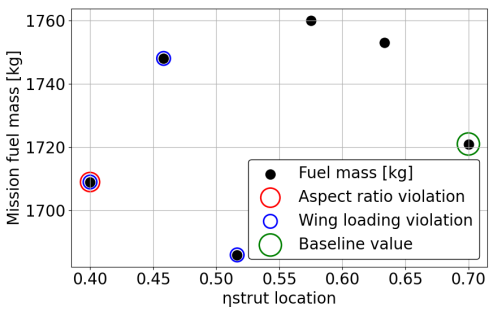

(d) Sensitivity of η_{strut} to fuel burn

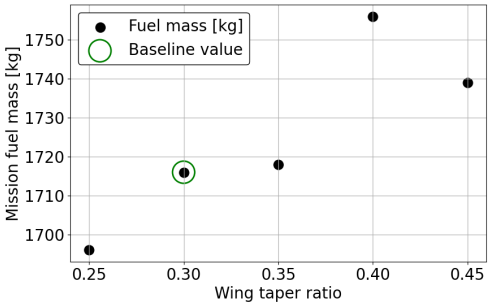

(e) Sensitivity of wing taper ratio to fuel burn

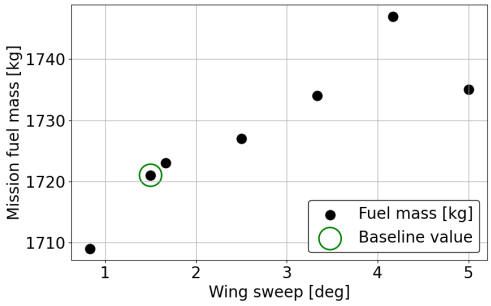

(f) Sensitivity of wing sweep to fuel burn

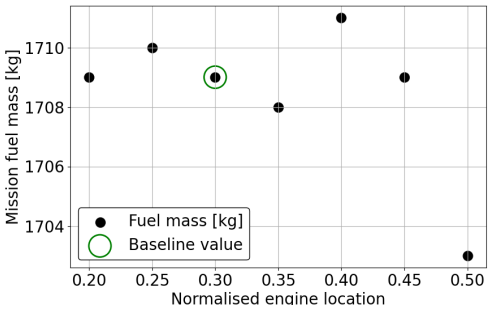

(g) Sensitivity of η_{engine} to fuel burn

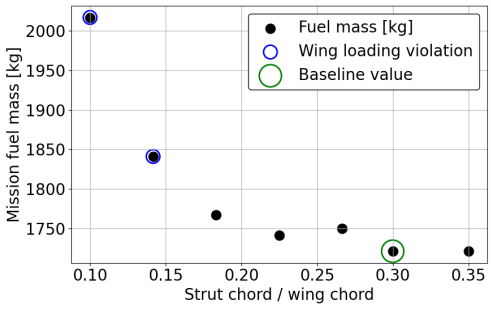

(h) Sensitivity of C_s/C_w to fuel burn

Figure 3.10: Final sensitivity analysis

From Figure 3.10, the following trends can be observed and are explained using Table 3.3 for reference.

1. **Wing span:**
   From Figure 3.10a, it was observed that reducing the wing span violates the wing loading criterion and slightly increases the fuel burn. This increase in the fuel burn is due to the lower aspect ratio and the corresponding induced drag of the resulting wing. Increasing the wing span results in an exponentially increased mission fuel mass. Although the L/D ratio increases due to reduced

induced drag (from a higher aspect ratio), the increase in the MTOW negates the benefits. The optimum balance between reduced induced drag and MTOW was at a wing span of around 34-35m. The fuel prediction for higher values of wing span should be treated with caution due to the lack of WER validation at aspect ratios higher than 20. The maximum violation of the aspect ratio was 23 for a wing span of 42m. The sudden spike in the fuel burn at the wing span of 38m was possibly due to an anomaly.

2. **Wing root chord:**
   The fuel burn continuously increases with root chord length, as seen in Figure 3.10b. This is due to the reduction in the wing's L/D ratio. Due to the higher wing area, the lift coefficient reduces with root chord length. In contrast, the induced drag increases due to the increase in the aspect ratio of the wing. Although the absolute value of skin friction drag increases, the frictional drag coefficient reduces. The lower lift coefficient allowed the wing to fly at a lower AOI to maintain an equilibrium condition at the design point. This reduced the adverse pressure gradient over the wings, reducing the relative increase in the boundary layer growth. The resulting thinner boundary layer resulted in a lower skin friction drag coefficient. However, the overall effect of the lift and the combined drag coefficient resulted in a reduction of the L/D ratio. It must be noted that the lower root chord length values violate the wing loading criterion and the aspect ratio. For the lowest value of the root chord, the corresponding aspect ratio was 25.6. This is quite higher than the upper limit of the WER, and the results are likely to be optimistic.

3. **Wing t/c:**
   From Figure 3.10c, it was observed that the fuel burn uniformly increases with t/c. This was due to a decrease in the L/D ratio of the aircraft. The higher thickness of the wing causes a thicker boundary layer, increasing the skin friction drag. However, the lower structural weight at higher t/c values results in a lower lift coefficient and induced drag. Nevertheless, the overall effect of the two was an increase in the total drag coefficient. This increase was higher than the increase in the lift coefficient, thereby reducing the L/D at higher values of t/c.

4. **Normalised strut location:**
   The η_{strut} plot was more complicated than the other results. Increasing η_{strut} resulted in a higher bending moment relief, thereby reducing the wing's and strut's structural mass. Typically, the higher wetted area of the strut results in an increased frictional drag. The combined effect of lower structural weight and increased drag results in a parabolic distribution for fuel burn with the minimum in between. However, the indirect influence of η_{strut} on the wing area and the planform of the SBW (as discussed in Table 2.6 and subsection 2.4.1) resulted in unexpected trends which can be explained as follows. As discussed above, increasing η_{strut} results in a higher bending moment relief, reducing the MTOW. The resulting lower lift coefficient reduces the wing's induced drag despite the slightly lower aspect ratio. Although the wetted area of the strut is higher, the overall skin friction drag coefficient decreases with η_{strut}. This is because the lower lift coefficient allows the wing to fly at a lower angle of attack. Similar to the effect observed in the case of the root chord, the skin friction drag reduces due to the lower adverse pressure gradient. The overall effect was the reduction in the total drag of the aircraft. Due to the difference in gradients of the lift and drag curves, the resultant L/D ratio was parabolic with a minimum near the centre. Hence, the corresponding fuel consumption resembled an inverted parabola with the maximum at the centre, as seen in Figure 3.10d. The lower wing area violated the wing loading constraints at lower values of η_{strut}. An unexpected drop in the fuel mass was seen at an η_{strut} value of 0.51, likely due to the anomaly. Although the aspect ratio constraint was violated for an η_{strut} value off 0.4 (AR = 20.7), the results are still likely valid due to the smaller margin of violation.

5. **Wing taper ratio:**
   The overall effect of increasing the taper ratio increased the fuel burn. This was likely due to the increase in the tip losses and, hence, the induced drag within the range considered. However, the increased wing area and reduced lift coefficient can cause a reduction in the lift-induced drag. Moreover, the skin friction drag was indirectly affected by the AOI, as mentioned before. Finally, the higher taper ratio increased the wing-strut mass and the MTOW of the aircraft due to

the higher root bending moment at higher taper ratios. The overall effect of these phenomena resulted in an irregular L/D plot, which influenced the nature of the fuel burn in Figure 3.10e.

6. **Wing sweep:**
   The effect of the wing sweep, as seen in Figure 3.10f, was rather straightforward and per expectations. As explained in the initial sensitivity stud, a higher wing sweep increases the wing's and strut's structural weight. However, the contribution of the wing-strut mass to the MTOW was negligible, so the lift and induced drag coefficients remained fairly constant. However, the skin friction drag increased with higher sweep angles due to the thicker boundary layer. This was because increasing wing sweep effectively increases the wing's chord length, allowing the boundary layer to grow over a larger chordwise distance and increase in thickness.

7. **Normalised engine location:**
   As discussed in section 3.2, the skin friction drag remained fairly constant for different values of η_{engine}. However, the induced drag changed depending upon the swirl recovery as seen in Figure 3.6. Since the lift coefficient and MTOW remained unchanged, the fuel burn in Figure 3.10g was a function of the induced drag. However, the marginal difference in the induced drag coefficient may not accurately indicate the actual flow phenomena due to the reasons explained in section 3.2. Additionally, it should be noted that the simulations for this case were run without the engine nacelle, because of which the baseline fuel burn was lower than the others. This was done to reduce the uncertainty in the drag prediction due to the relatively coarse mesh on the nacelle.

8. **Strut chord ratio:**
   From Figure 3.10h, it was observed that the fuel burn exponentially increases for lower values of the strut chord ratio, primarily due to the increase in the MTOW of the SBW. A significant contribution to the MTOW was the mass of the strut, which has to be significantly strengthened to avoid failure in buckling at smaller chord lengths. This was observed by Pinho Chiozzotto [13] and is also explained in section 1.1. The higher MTOW increases the lift and the induced drag coefficient, further increasing fuel burn. It must be noted that the result for a strut chord ratio of 0.35 was evaluated for experimental purposes only and may not be entirely accurate since it exceeds the bounds of the WER (Table 2.3).

Table 3.4 summarizes the impact of different design variables on the fuel burn of a short-range, low-speed SBW aircraft. The table is based on the data from Figure 3.10. The parameters for which the design space was unexplored were marked as 'Unknown'.

Design parameter	Baseline value	Unit	Effect of +10% change on mission fuel mass (kg)	Effect of -10% change on mission fuel mass (kg)
Wing span	34.4	m	+20	+20
Wing root chord	2.1	m	+130	-70
Wing t/c	0.08	-	+(<10)	Unknown
Normalised strut location	0.7	-	Unknown	+40
Wing taper ratio	0.3	-	+(<10)	-(<10)
Wing sweep	1.5	deg	+(<10)	-(<10)
Normalised engine location	0.3	-	-(<10)	+(<10)
Strut chord ratio	0.3	-	-(<10)	Unknown

Table 3.4: Impact of different design parameters on the mission fuel mass.

From Table 3.4, it was observed that the root chord had the highest sensitivity to fuel burn with an impact of around 200kg (11.6% of mission fuel mass) within a range of $\pm$10% deviation w.r.t the baseline value. Although the sensitivity of the strut location to fuel burn beyond the optimum (+10%) value was unknown, reducing it by 10% resulted in a 40kg increase in the fuel burn, accounting for 2.3% of the total mission fuel mass. This was followed by the wing span with an impact of 40kg (2.3% of mission fuel mass) over the entire range ($\pm$10%). Finally, the other design variables, namely the wing t/c, taper ratio,

sweep, engine location and strut chord ratio, had a negligible impact on the fuel burn over the range investigated. Using these numbers, one can get a rough idea of the impact of these design parameters on the fuel burn. These results can be useful in determining whether additional analysis is required if the design parameters have to be modified after the preliminary design stage. However, it must be noted that the values in Table 3.4 and the trends observed in Figure 3.10 may not be generalised. This implies that an alternative design optimised for different conditions can have different sensitivities about its optimum point. However, the order of magnitude is not expected to vary significantly.

4

Conclusions and recommendations

The answers to the research questions have been provided in section 4.1, and the recommendations for future work are provided in section 4.2.

4.1. Conclusion

In this section, the research questions framed in section 1.3 have been answered below.

4.1.1. Comparison of the SBW designs optimised with and without propeller slipstream effects

An SBW design was hypothesised to benefit from swirl recovery from an optimised wing-strut-jury combination. However, the flow acceleration (by the propwash) in the junction region could result in added interference and/or compressibility drag. The first objective of this thesis was to investigate the significance of including the propeller slipstream effects in the preliminary design optimisation of a low-speed, short-range strut-braced wing aircraft. To evaluate this (and to answer the other research questions), a DOE study was conducted in which the relevant design variables were varied to study their effect on the performance with and without the slipstream effects being included. It was observed that the two designs converged at nearly identical designs in terms of external geometry and performance, indicating that the variation in the engine location did not significantly affect the performance. Initially, it was speculated that the lower thrust coefficient and the higher advance ratio at cruise resulted in a lower swirl in the propeller slipstream, due to which there were no significant gains by recovering it. However, it was later confirmed from the lift and drag distributions that there was a non-negligible swirl in the slipstream. The primary reason behind the similarity between the two designs was the marginal change in the aircraft's induced drag (by 2 counts) due to swirl recovery. The reason why the difference in the induced drag was negligible was possibly due to the smaller gradients in the lift distribution plots, as seen in Figure 3.5a. Likewise, a further outboard engine location (with higher gradients in the lift distribution plots) can result in higher swirl recovery. However, the size of the vertical tail will increase (to counter the OEI condition) and could reduce (if not negate) the benefits. However, this change in the drag was less than two counts but should be treated critically due to the lower fidelity of panel methods. Thus, the slipstream effects do not influence the design of a low-speed, short-range SBW aircraft optimised for cruise. Hence, the propeller slipstream effects can be excluded from the preliminary design optimisation procedure to reduce the computational expense.

4.1.2. Crucial design parameters for the design of an SBW with slipstream effects

Since the two designs were quite similar, the second research sub-question regarding the identification of the crucial design variables when an SBW has to be designed with propeller slipstream effects included was no longer applicable. However, it can be roughly stated that the proximity of the engine location to the jury can slightly increase the swirl recovery. A local minimum in the induced drag was observed when the engine was located directly above the jury, as seen in Figure 3.6. Additionally, the induced drag further reduces when the engine is located at more outboard locations. This was possibly

due to the increasing contribution of the strut to swirl recovery

4.1.3. Comparative analysis of the optimised SBW aircraft w.r.t the baseline design

Another objective of the thesis was to compare the performance of the optimised SBW w.r.t the initially sized RHEA and the MRB (the equivalent SBW developed for this thesis). It was observed that there was a 7% reduction in the mission fuel mass of the optimised MRB w.r.t the baseline. The optimised MRB had a lower aspect ratio and a higher wing area w.r.t the baseline. The lower wing area reduced the lift coefficient, because of which the induced drag coefficient was reduced by ten counts. However, the primary reason for the better performance of the optimised design was the reduction in the frictional and pressure drag (30 counts). The significantly lower t/c of the optimised wing reduced the pressure/-form drag. Additionally, the lower t/c reduced the adverse pressure gradients and the shear stress in the boundary layers, decreasing skin friction drag. Although a lower t/c of the wing caused an increase in the wing-strut mass, it was partially compensated by a slightly larger bending moment relief from a more outboard-located strut. The reduction in fuel mass and the slight increase in the structural weight resulted in a negligible change in the MTOW. The performance of the optimised MRB was lower than that of the initially sized RHEA due to the partial violations of the assumptions in their weight estimation methods that resulted in an overprediction of its performance. Thus, the driving design parameters and the underlying physical phenomena that result in the optimal SBW design are understood.

4.1.4. Sensitivity of different design variables to fuel burn at the optimum point

A sensitivity study was performed for different design variables to investigate their impact on fuel burn and other performance metrics when subjected to a unidirectional change in the optimum value by $\pm 10\%$. Table 4.1 explains the trend of fuel burn and the primary reason for the observed effect. Additionally, the impact on the fuel burn is quantified. The values that exceeded the limits of the design space explored are marked with 'Unknown'. It was concluded that the root chord had the highest sensitivity to fuel burn with an impact of 200kg (11.6% of mission fuel mass) within the range of $\pm 10\%$ deviation. This was followed by the normalised strut location with an impact of 2.3% when subjected to a change in just one direction (-10%). This was the same as the wing span but over the entire range of $\pm 10\%$ deviation. The other design variables, namely the wing t/c, taper ratio, sweep, engine location and strut chord ratio, had a negligible impact on the fuel burn at the design point. Thus, if the design of a short-range, low-speed SBW has to be modified after the preliminary design stage, an estimate of the impact on the fuel burn is known. Accordingly, it can be decided if it is worth re-running an optimisation.

Design variable	Effect of Decreasing design variable by 10% w.r.t optimum			Effect of Increasing design variable by 10% w.r.t optimum		
	Mission fuel mass	**Average impact on fuel burn (kg)**	**Primary reason for the observed effect**	**Mission fuel mass**	**Average impact on fuel burn (kg)**	**Primary reason for the observed effect**
Wing span	Increases	+20	Higher induced drag	Increases	+20	Higher MTOW
Wing root chord	Decreases	-70	Lower induced drag	Increases	+130	Higher induced drag
Wing t/c	Decreases*	Unknown (low)	Higher pressure drag	Increases	+(<10)	Lower pressure drag
Normalised strut location	Increases	40	Higher frictional drag	Decreases*	Unknown (high)	Lower frictional drag
Wing taper ratio	Decreases	-(<10)	Lower induced drag	Increases	+(<10)	Higher induced drag
Wing sweep	Decreases	-(<10)	Lower frictional drag	Increases	+(<10)	Higher frictional drag
Normalised engine location	Increases	+(<10)	Higher induced drag	Decreases	-(<10)	Lower induced drag
Strut chord ratio	Increases	Unknown (low)	Higher MTOW	Decreases	-(<10)	Lower MTOW

Table 4.1: Sensitivity of the design variables to fuel burn with explanation

4.2. Recommendations

Based on the limitations of this thesis and the research outcome, a few recommendations are made.

1. Due to the unavailability of open-source physics-based methods for evaluating the structural mass of unconventional configurations like the SBW, regression-based analytical equations (WER) were used to estimate the weights. Since the WER were based on several assumptions (subsection 2.4.2), they indirectly restricted the design space. For instance, the wing planform was assumed to be semi-tapered with the kink at the spanwise strut attachment point. The possible benefits of decoupling the two may result in additional benefits that this thesis could not exploit. If the design space exploration is performed using physics-based methods with fewer assumptions, a further reduction in the fuel burn of the alternative optimum design can be achieved.
2. The scope of this thesis was restricted to optimising the SBW for cruise. For the high-power demanding flight phases like take-off and climb, the SBW optimised with the propeller slipstream effects can result in an alternative optimum design. The effect of different advance ratios and thrust coefficients on the swirl recovery of the SBW was irrelevant for cruise and hence not evaluated in this thesis. However, a properly designed wing-strut-jury assembly may result in non-negligible swirl recovery for particular combinations of advance ratios and thrust coefficients and might be worth investigating.
3. Since the WER could not predict the change in the weight of the wing strut mass for different spanwise engine positioning (inboard of the strut), this thesis evaluated the effect of fuel burn from a purely aerodynamic perspective. However, the weight impact of engine positioning might be crucial while optimising the SBW for other flight phases (which might result in meaningful benefits from swirl recovery). Moreover, the vertical tail sizing should be updated to consider the OEI condition, particularly for outboard engine positioning.
4. In addition to the assumptions in the use of advanced technologies as mentioned in Figure 2.16, the effect of using fully electric or hybrid propulsion architectures can be incorporated, which are likely to be seen in futuristic aircraft instead of the conventional turboprops.
5. While using OpenVSP to generate the geometry and mesh files, the automatic meshing at the intersections occasionally resulted in highly skewed cells, which caused the divergence of the aerodynamic solver. Despite adding refinement in those regions, the mesh-related problems were more case-specific and beyond the user's control. Due to the solver divergence, around 15% of the DOE points had to be discarded, producing small voids in the design space. More sophisticated meshing techniques and/or stabilization in the solver could help solve this problem and are recommended for future researchers.
6. To ensure a level flight, the angle of installation of the wing should ideally be changed to the calculated value. Since generating new models, solver initialization, and running the solver are time-consuming processes, this was avoided by making suitable assumptions to use the computational resources to explore a wider design range. The author recommends using the former approach only if higher accuracy is desired at the cost of a considerable increase in computational time.
7. For this thesis, the NACA 65 series airfoils were used for the wing and the strut. The airfoil family was not changed throughout, leaving scope for future work. Moreover, custom airfoils designed using aerodynamic optimisations can further minimise fuel burn.
8. The propeller's diameter was kept constant and equal to that of the ATR 72-600 for this thesis. However, trade studies on the diameter and number of engines may produce favourable effects regarding swirl recovery. Similarly, the effect of distributed electric propulsion on an SBW may help in further enhancing the performance of an SBW.

Bibliography

[1] E. Moerland, T. Pfeiffer, D. Böhnke, and J. Jepsen, "On the design of a strut-braced wing configuration in a collaborative design environment," *17th AIAA Aviation Technology, Integration, and Operations Conference*, 2017. [Online]. Available: https://arc.aiaa.org/doi/10.2514/6.2017-4397.

[2] N. R. Secco and J. R. Martins, "Rans-based aerodynamic shape optimization of a strut-braced wing with overset meshes," *Journal of Aircraft*, vol. 56, pp. 217–227, 1 2019, ISSN: 15333868. DOI: 10.2514/1.C034934.

[3] G. Carrier, O. Atinault, S. Dequand, *et al.*, "Investigation of a strut-braced wing configuration for future commercial transport," in *28th Congress of the International Council of the Aeronautical Sciences*, ICAS Bonn, 2012, pp. 2012–1.

[4] F. Torrigiani, J. Bussemaker, P. D. Ciampa, *et al.*, "Design of the strut braced wing aircraft in the agile collaborative mdo framework," 2018. [Online]. Available: 11583/2729894.

[5] Y. Ma, S. Karpuk, and A. Elham, "Conceptual design and comparative study of strut-braced wing and twin-fuselage aircraft configurations with ultra-high aspect ratio wings," *Aerospace Science and Technology*, vol. 121, p. 107 395, 2022.

[6] M. K. Bradley and C. K. Droney, "Subsonic ultra green aircraft research: Phase i final report," 2011. [Online]. Available: http://www.sti.nasa.gov.

[7] M. K. Bradley, C. K. Droney, and T. J. Allen, "Subsonic ultra green aircraft research: Phase ii-volume i-truss braced wing design exploration." [Online]. Available: http://www.sti.nasa.gov.

[8] M. K. Bradley and C. K. Droney, "Subsonic ultra green aircraft research: Phase ii-volume ii-hybrid electric design exploration," 2015. [Online]. Available: http://www.sti.nasa.gov.

[9] M. K. Bradley, T. J. Allen, and C. K. Droney, "Subsonic ultra green aircraft research: Phase ii-volume iii-truss braced wing aeroelastic test report," 2014. [Online]. Available: http://www.sti.nasa.gov.

[10] C. K. Droney, A. J. Sclafani, N. A. Harrison, A. D. Grasch, and M. D. Beyar, "Subsonic ultra green aircraft research: Phase iii-mach 0.75 transonic truss-braced wing design." [Online]. Available: http://www.sti.nasa.gov.

[11] N. A. Harrison, G. M. Gatlin, S. A. Viken, *et al.*, "Development of an efficient m= 0.80 transonic truss-braced wing aircraft," in *AIAA Scitech 2020 Forum*, 2020, p. 0011.

[12] M. K. Bradley and C. K. Droney, "Subsonic ultra green aircraft research phaseii: N+4 advanced concept development." [Online]. Available: http://www.sti.nasa.gov.

[13] G. Pinho Chiozzotto, "Improving aircraft conceptual design with methods for wing loads, aeroelasticity and mass estimation," Ph.D. dissertation, Technische Universität Berlin, 2019.

[14] B. De Wit, W. Lammen, J. Vankan, *et al.*, "A collaborative design method for the aircraft supply chain: Multi-level optimization," in *2018 Multidisciplinary Analysis and Optimization Conference*, 2018, p. 3253.

[15] L. Liu and X. Yu, "A study on aerodynamic interference for truss braced wing configuration," *Lecture Notes in Electrical Engineering*, vol. 680 LNEE, pp. 129–152, 2021, ISSN: 18761119. DOI: 10.1007/978-981-33-6060-0_10.

[16] R. K. Duggirala, C. J. Roy, and J. A. Schetz, "Analysis of interference drag for strut-strut interaction in transonic flow," *47th AIAA Aerospace Sciences Meeting including the New Horizons Forum and Aerospace Exposition*, 2009. DOI: 10.2514/6.2009-51.

[17] M. Taflan, H. Smith, and J. Loughlan, "Parametric analysis for structural design and weight estimation of cantilever and strut-braced wing-boxes," in *AIAA SCITECH 2023 Forum*, 2023, p. 1554.

[18] D. Locatelli, B. K. Riggins, R. K. Kapania, J. A. Schetz, and T. Poquet, “A physics-based methodology for cantilever and strut-braced wing weight estimation,” in *54th AIAA Aerospace sciences meeting*, 2016, p. 0780.

[19] R. A. McDonald and J. R. Gloudemans, “Open vehicle sketch pad: An open source parametric geometry and analysis tool for conceptual aircraft design,” in *AIAA SciTech 2022 Forum*, 2022, p. 0004.

[20] DARcorporation, *Flightstream*, Computer software, 2023. [Online]. Available: `https://www.darcorp.com/flightstream`.

[21] T. Sinnige, N. V. Arnhem, T. C. Stokkermans, G. Eitelberg, and L. L. Veldhuis, “Wingtip-mounted propellers: Aerodynamic analysis of interaction effects and comparison with conventional layout,” *Journal of Aircraft*, vol. 56, pp. 295–312, 1 2019, ISSN: 15333868. DOI: `10.2514/1.C034978`.

[22] L. Veldhuis, “Review of propeller-wing,” 2004. DOI: `10.2514/1.C034978`.

[23] L. L. M. Veldhuis, “Propeller wing aerodynamic interference,” 2005.

[24] V. Ahuja, R. J. Hartfield, and D. Ciliberti, “Three-dimensional viscous coupling & flow separation enhancements to an inviscid surface vorticity flow solver,” in *AIAA SciTech 2023 Forum*, 2023, p. 2455.

[25] *Flightstream quick start guide*, Research in Flight, 2023.

[26] E. Torenbeek, *Synthesis of subsonic airplane design: an introduction to the preliminary design of subsonic general aviation and transport aircraft, with emphasis on layout, aerodynamic design, propulsion and performance*. Springer Science & Business Media, 2013.

[27] T. M. Lavelle and B. P. Curlett, “Graphical user interface for the nasa flops aircraft performance and sizing code,” Tech. Rep., 1994.

[28] G. P. Chiozzotto, “Initial weight estimate of advanced transport aircraft concepts considering aeroelastic effects,” in *55th AIAA aerospace sciences meeting*, 2017, p. 0009.

[29] “EASA Type-Certificate Data Sheet for PW100 series engines.” Accessed: 24/08/2023, European Union Aviation Safety Agency (EASA). (), [Online]. Available: `https://www.easa.europa.eu/en/downloads/7725/en`.

[30] O. Gur, M. Bhatia, W. H. Mason, J. A. Schetz, R. K. Kapania, and T. Nam, “Development of a framework for truss-braced wing conceptual mdo,” *Structural and Multidisciplinary optimization*, vol. 44, pp. 277–298, 2011.

[31] *Geometrical properties of cranked and straight-tapered wing planforms*, ESDU Document Number 76003, Engineering Sciences Data Unit, 1976.

[32] R. Nederlof, R. Kooij, L. L. Veldhuis, and T. Sinnige, “Contribution of swirl recovery to the induced drag of a propeller-wing system–a parametric study,” in *AIAA AVIATION 2023 Forum*, 2023, p. 3543.

[33] S. Gudmundsson, *General aviation aircraft design: Applied Methods and Procedures*. Butterworth-Heinemann, 2013.

[34] M. F. Nita, “Aircraft design studies based on the atr 72,” Ph.D. dissertation, 2008.

[35] ATR Aircraft. “Data Summary.” Accessed: 22/09/2023. (n.d), [Online]. Available: `https://www.atr-aircraft.com/wp-content/uploads/2022/06/ATR_Fiche72-600-3.pdf`.

A

Appendix

A.1. Aerodynamics

A.1.1. Mesh sensitivity study

A mesh sensitivity analysis was performed for Flightstream. For this purpose, the number of mesh cells was varied from approximately 17000 to 48000. Since the ultimate goal of this thesis was to evaluate the performance parameters, the effect of mesh sensitivity on W_{fuel} and MTOW was also evaluated in addition to the aerodynamic coefficients (Figure A.1).

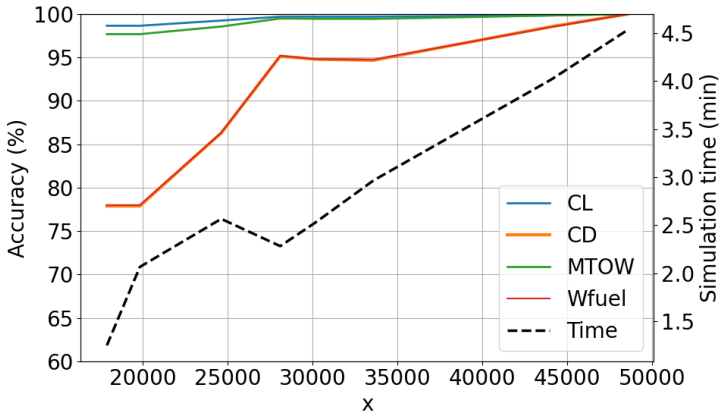

Figure A.1: Mesh sensitivity study of Flightstream

The y-axis represents the deviation from the results obtained with the finest mesh, which had approximately 48,000 cells. This number was considerably higher than the usual refinement required. The accuracy of the drag coefficient (C_D) increased considerably with higher mesh density in contrast to the relatively constant value of the lift coefficient (C_L). Due to this, the L/D ratio and hence, the fuel burn are closely aligned with C_D. Due to the smaller fraction of fuel mass compared to the MTOW, the effect of W_{fuel} was negligible on the MTOW, justifying its relatively constant value. The better prediction of the C_D came at the cost of increased computational time required for running aerodynamic simulations at a given angle of attack. The lift and drag polars for multiple simulations were expected to be run, which would be computationally expensive. Hence, the mesh with around 28000 cells was finalised to get a good compromise between accuracy and computational time. Although there was a 5% error for the mesh size chosen, the relative error w.r.t. a mesh with higher tesselations was less than 2%. This is often used as the convergence criterion; hence, the mesh density can be considered acceptable.

A.1.2. Slipstream effects on wing, strut and jury

The pressure coefficient graphs for the wing, strut and jury were plotted for the cross sections defined in Figure 3.3.

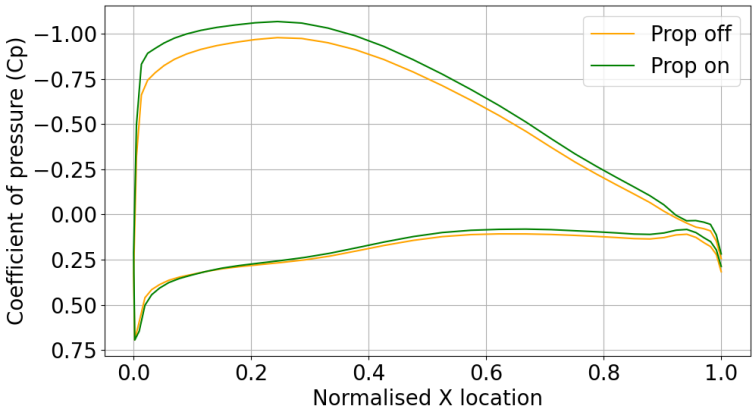

(a) C_P vs x for -0.8D

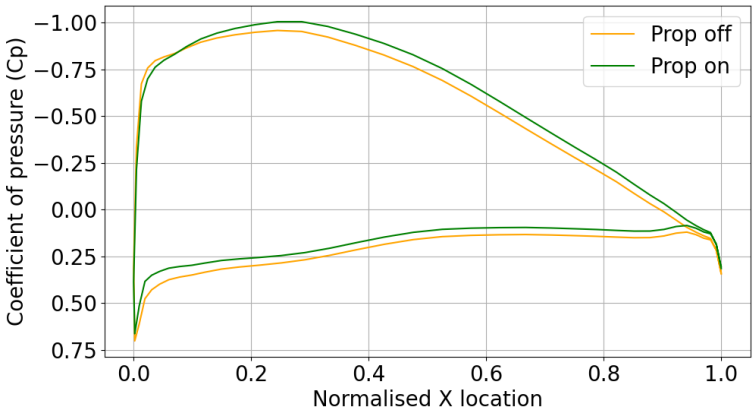

(b) C_P vs x for 0.8D

Figure A.2: Pressure coefficient plots for wing at 80% D

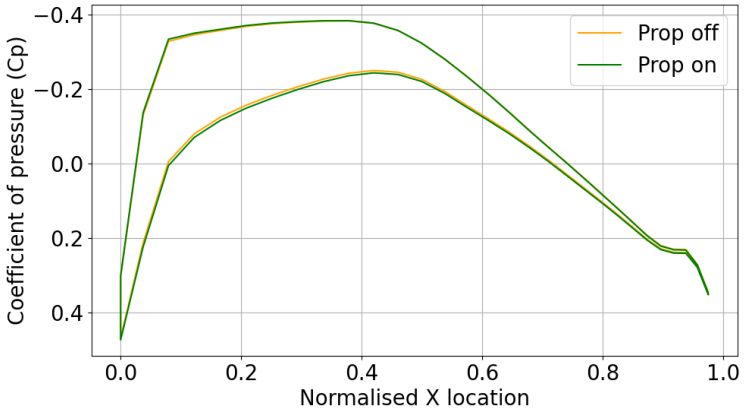

(a) C_P vs x for -0.8D

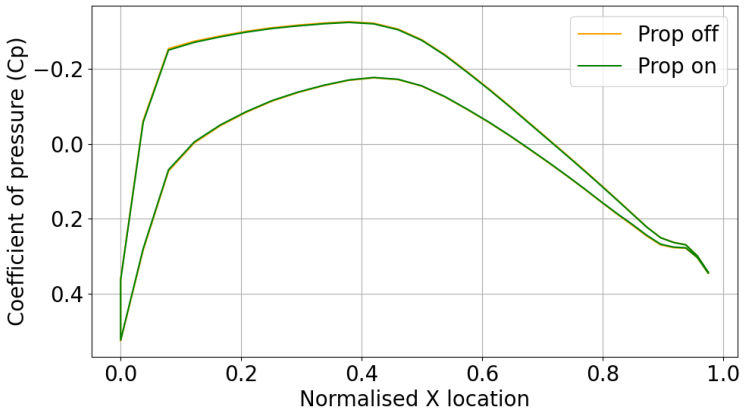

(b) C_P vs x for 0.8D

Figure A.3: Pressure coefficient plots for strut at 80% D

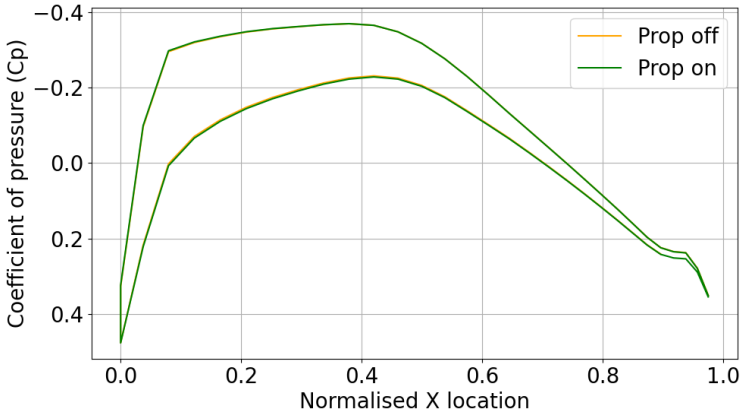

(a) C_P vs x for -0.5D

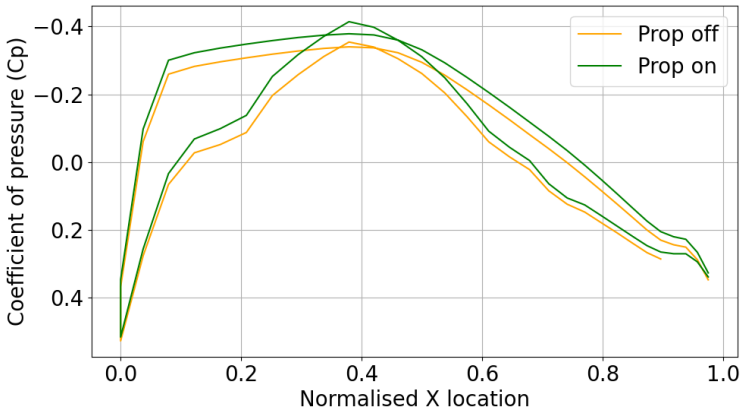

(b) C_P vs x for 0.5D

Figure A.4: Pressure coefficient plots for strut at 50% D

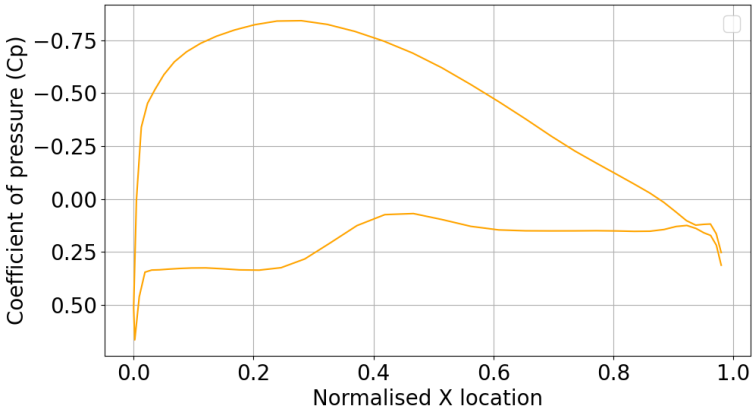

(a) C_P vs x for wing at 0.9*η_{strut}

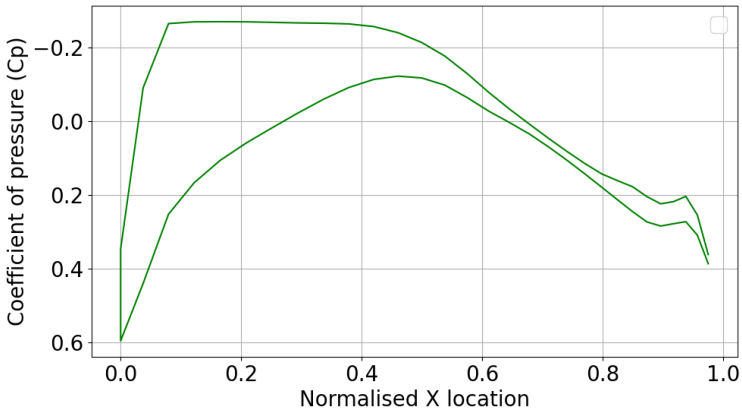

(b) C_P vs x for wing at 0.9*η_{strut}

Figure A.5: Pressure coefficient plots for the wing and strut in the junction region

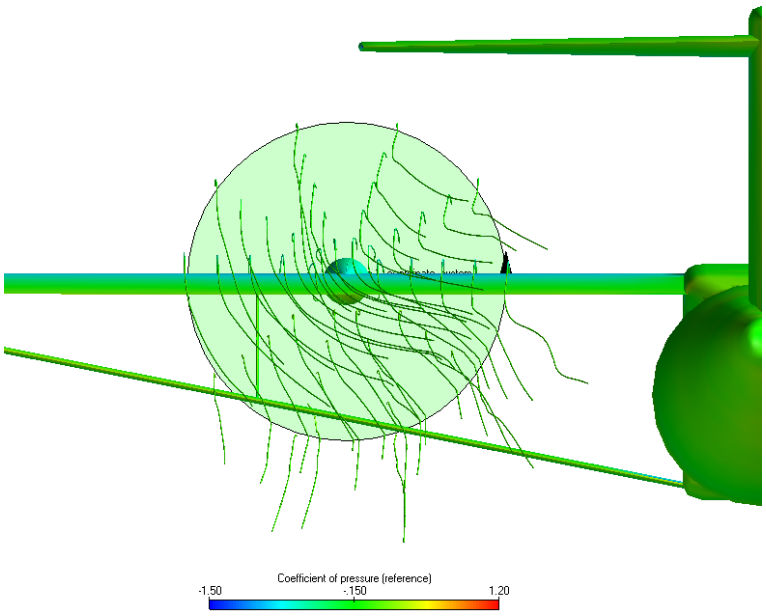

Figure A.6: Visualisation of swirl in Flightstream

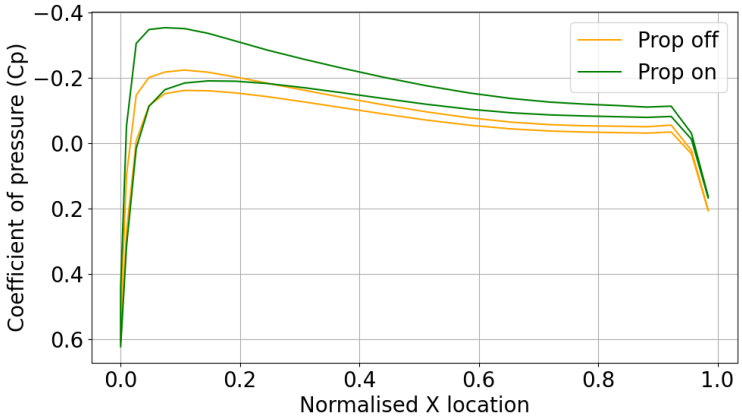

(a) C_P vs x for jury at 15% of jury's height

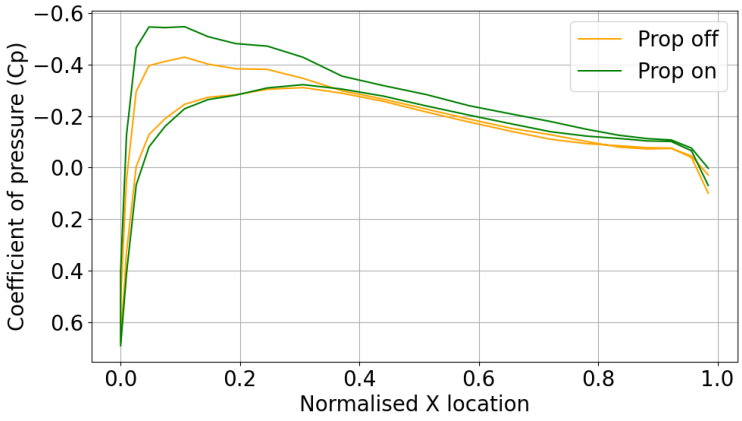

(b) C_P vs x for jury at 15% of jury's height

Figure A.7: Pressure coefficient plots for the jury in the junction region

A.1.3. CFD mesh quality

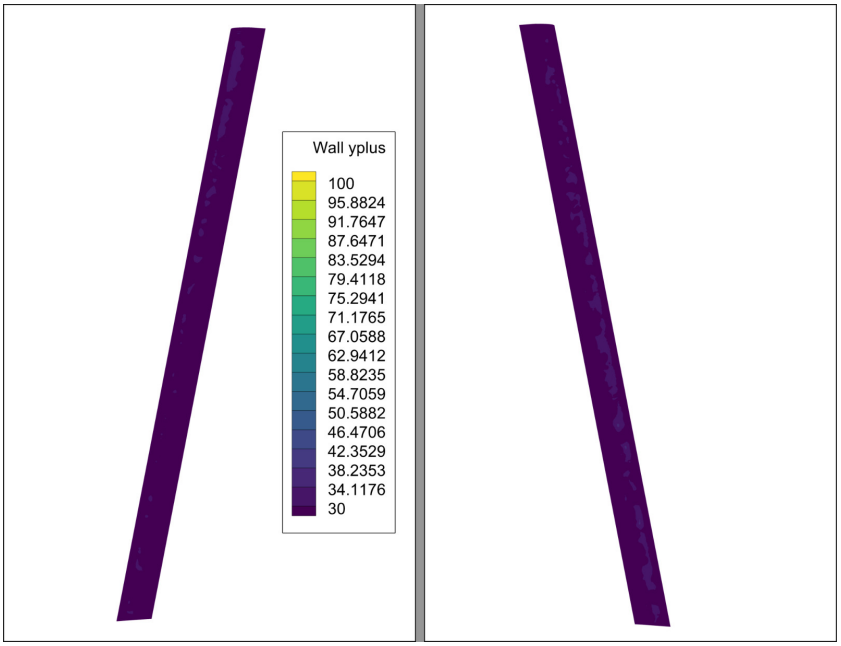

(a) Wing top and bottom surfaces

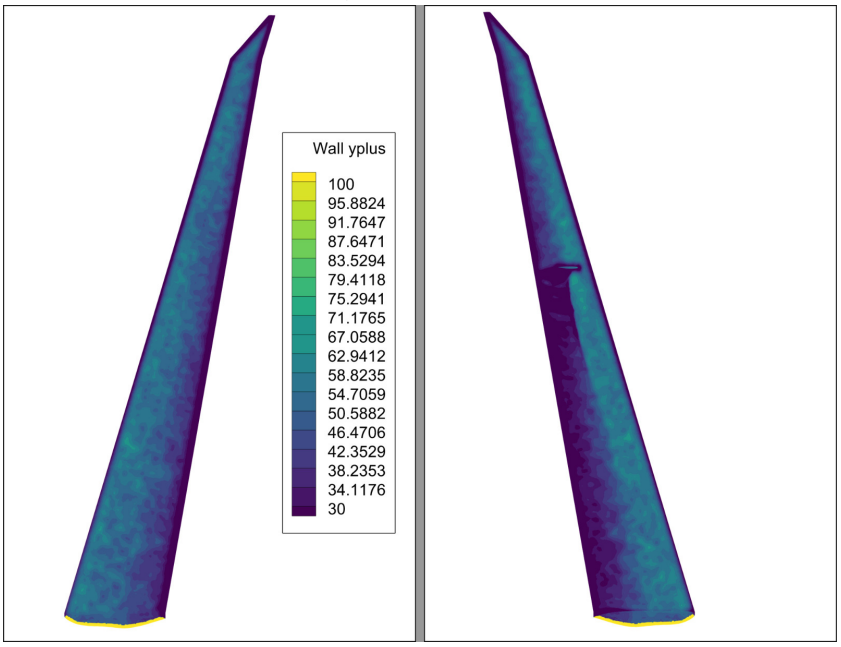

(b) Strut top and bottom surfaces

Figure A.8: y value for PADRI SBW mesh

A.2. Weight estimation

As mentioned in section 2.4, the WER were linear regression-based equations based on a DOE study using the physics-based method. To validate the weight prediction by the WER, the corresponding results from the physics-based method were used and can be seen in Figure A.9.

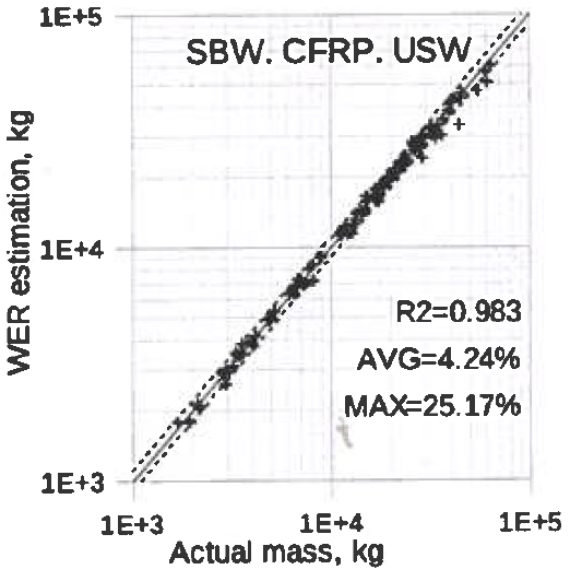

Figure A.9: Validation of WER using the physics based method [13]

The weight breakdown of RHEA SR-SBW is given in Figure A.10

Group	SR-SBW
Max. takeoff weight, kg	22229
Fuel weight, kg	1432
Empty weight, kg	12821
Empty weight breakdown	
Wing, kg	2103
Fuselages, kg	2497
Propulsion, kg	1019
Nacelles, kg	269
Landing gear, kg	643
Horizontal tail, kg	201
Vertical tail, kg	312
Paint, kg	199
Systems, kg	5579

Figure A.10: Weight breakdown of RHEA SR-SBW[5]

A.3. Performance model

A.3.1. Breguet range equation

This section explains the procedure followed to evaluate the value of the constants- f, SFC and η_j used in Equation 2.9. The fraction, 'f' is defined as the ratio of the mass of the aircraft at the start of the cruise to MTOW. The mass of the aircraft at the start of cruise was calculated using Figure A.11

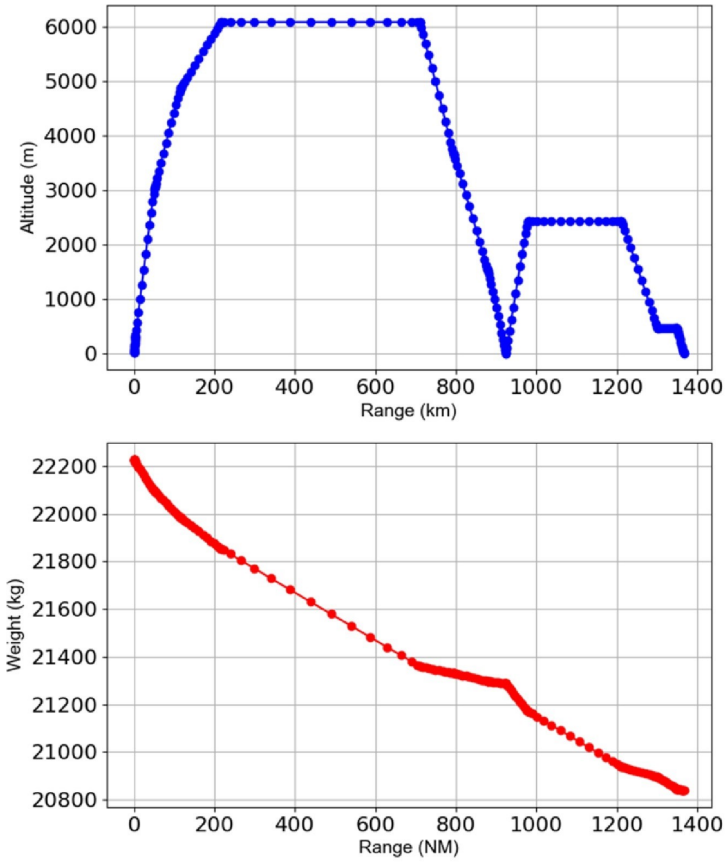

Figure A.11: Mission performance diagram of RHEA SR-SBW [5]

Thus, the weight of the aircraft corresponding to a range of approximately 200 NM (start of cruise) was used to calculate f.

$$f = \frac{22229 - 360}{22229} = 0.9838 \tag{A.1}$$

Table A.1 provides the values of the parameters used in Equation 2.9

Parameter	Value	Unit	Reference
Range	1528000	m	[5]
SFC	$0.76 * 10^{-6}$	kg/Ws	[33]
η_j	0.86	-	[34]

Table A.1: Values of parameters used in Breguet range equation (Equation 2.9)

Parameter		Unit	RHEA
Reference aircraft		–	ATR 72-600
Propulsion concept		–	Turboprop
Cruise Mach number		–	0.42
Max. Mach number		–	0.457
Passengers		–	72
Range		nm	825
Reserves	Contingency fuel	–	3%
	Divert segment	nm	87
	Hold (at 1500 ft)	min	10
Cruise altitude		ft	20000
Service ceiling		ft	25000
Take-off field length		ft	4373
Landing distance		ft	3002
Approach speed		kt	113
Airport category (ICAO C)	Wingspan	m	36
	Main landing gear span	m	9
Certification requirements		–	CS 25

Figure A.12: TLAR of RHEA SR-SBW[5]

A.3.2. Mission fuel mass for ATR 72-600

The fuel burn for the conventional ATR-72 600 aircraft was roughly estimated by extrapolating the mission fuel mass data available onlineATR Aircraft [35]. Assuming the fuel burn is linear, the mission fuel mass for the range assumed for the SBW counterpart (800NM) was estimated to be around 2000 kg. Hence, the optimised MRB with a fuel burn of 1654 kg had more than a 17% reduction in the mission fuel mass.

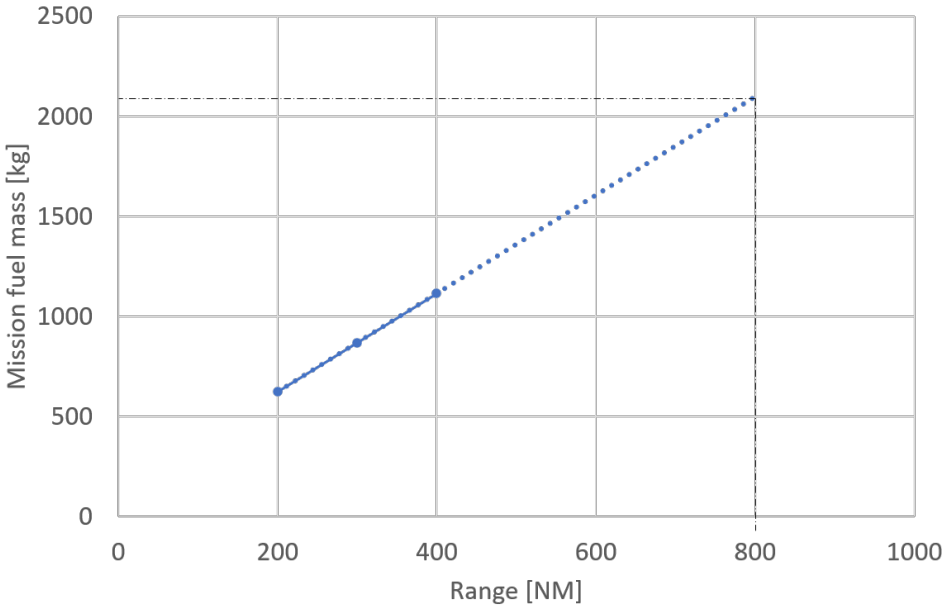

Figure A.13: Fuel burn prediction of ATR 72-600

A.4. Design space exploration

A.4.1. Fuel tank volume calculations

For this thesis, the fuel was assumed to be stored in the wings only. The volume of the fuel tanks was calculated separately for the untapered inboard section (V1) and the tapered outboard section (V2). For the untapered section, the cross-section was assumed to be trapezoidal. The height of the tank was calculated using the relative t/c distribution of the airfoil to decouple the effect of airfoils with different t/c (Figure A.14)

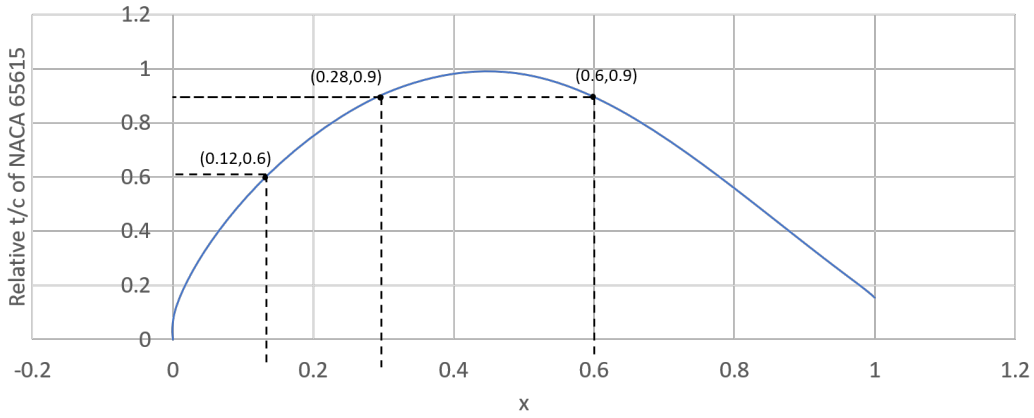

Figure A.14: Relative thickness distribution vs chordwise position for NACA 65615

As discussed previously in subsection 2.4.1 and Figure 2.15, the front spar location was assumed to be at 12% for the untapered section (root and kink) and at 28% for the tip section. The relative t/c corresponding to these values were 0.6 and 0.9 (interpolated from Figure A.14). Thus the cross-section area (S_r) for the inboard section can be calculated in Equation A.2

$$S_r = 0.5 * (0.6 + 0.9) * t/c * C_r * (0.6 - 0.12) * C_r \tag{A.2}$$

where C_r is the root chord. Thus, V1 can be calculated by multiplying it with the length of the untapered section as seen in Equation A.3. The factor of 2 accounts for the fuel tanks stored on the other half of the wing.

$$V1 = 2 * S_r * L_1 \tag{A.3}$$

where

$$L_1 = \eta_{strut} * b/2 \tag{A.4}$$

For the outboard, tapered section, the cross-section at the kink and tip was assumed to be rectangular for simplicity. The area at the kink (S_k) can be calculated using Equation A.5. The height of the tank was calculated corresponding to the lower value of relative t/c among the front (0.6) and rear spar(0.9) to get a conservative estimate.

$$S_k = a_1 * b1 \tag{A.5}$$

where

$$a_1 = (0.6 - 0.12) * C_r \tag{A.6}$$

and

$$b1 = 0.6 * t/c * C_r \tag{A.7}$$

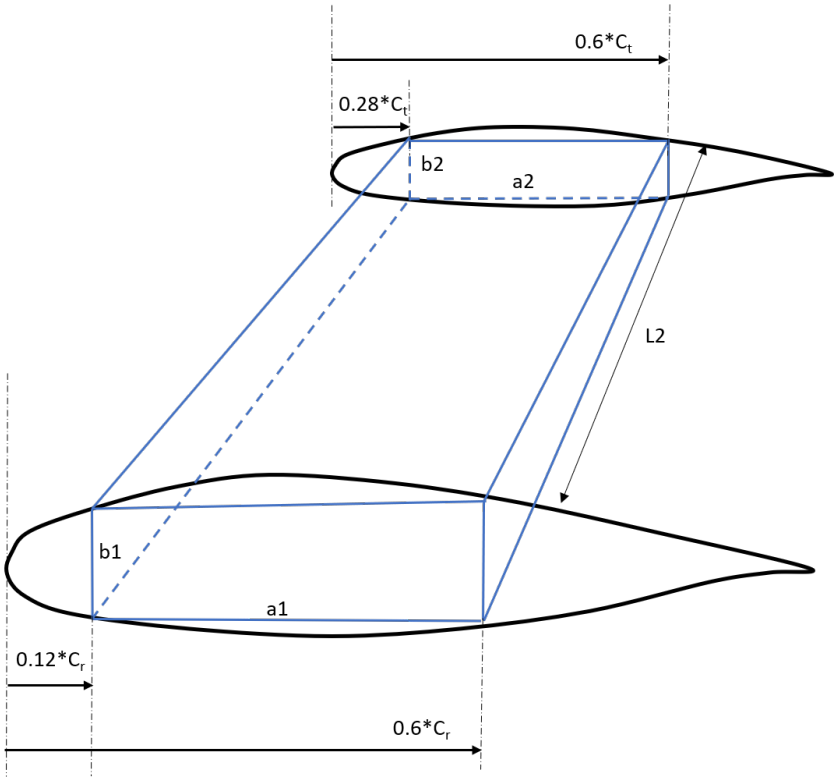

Figure A.15: Schematic for fuel tank of the outboard section

Similarly, the cross-sectional area at the tip was calculated using Equation A.8

$$S_t = a_2 * b_2 \tag{A.8}$$

where

$$a_2 = (0.6 - 0.28) * C_r \tag{A.9}$$

and

$$b_2 = 0.9 * t/c * C_r \tag{A.10}$$

In the above equation, the factor 0.9 comes from the t/c assumptions of the WER as mentioned previously in subsection 2.4.1 Equation A.11 from Torenbeek [26] was used to calculate the value of V2.

$$V2 = \frac{L_2}{3} * (S_k + S_t + a_1 * b_2 + a_2 * b1) \tag{A.11}$$

where L_2 is the spanwise length of the fuel tanks for the outboard section which is assumed to be at 80% of the wing span. Combining Equation A.3 and Equation A.11 gives the equation for the total fuel tank volume (V)

$$V = [2 * S_r * \eta_{strut} * b/2] + [\frac{L_2}{3} * (S_k + S_t + a_1 * b_2 + a_2 * b_1)] \tag{A.12}$$

At the optimum SBW configuration, the values of the relevant design variables have been mentioned in Table A.2

Parameter	Value at Optimum	Unit
Wing span	32	m
Wing root chord	2.4	m
Wing t/c	0.08	-
Wing tip chord	0.36	m
Normalised strut location	0.6	-

Table A.2: Values of design variables at the optimum

Substituting the values from Table A.2 in Equation A.2, Equation A.5 and Equation A.8, we get

$$S_r = 0.5 * (0.6 + 0.9) * 0.08 * 2.4 * (0.6 - 0.12) * 2.4 = 0.1658m^2 \tag{A.13}$$

$$S_k = (0.6 - 0.12) * 2.4 * 0.6 * 0.08 * 2.4 = 0.1327m^2 \tag{A.14}$$

$$S_t = (0.6 - 0.28) * 2.4 * 0.9 * 0.08 * 2.4 = 0.1327m^2 \tag{A.15}$$

Thus, the fuel tank volume can be calculated using Equation A.12

$$V = [2 * 0.1658 * 0.6 * 32/2] + [\frac{6.4}{3} * (0.1327 + 0.1327 + 0.2 + 0.0884)] = 3.185 + 1.184 = 4.37m^3 \tag{A.16}$$

This corresponds to 4370 litres of fuel or 3500kg of aviation fuel (assuming a density of 0.8g/ml).